Internal Report
DESY M 97-10
August 1997

Reports at the PAC 97

May 12 - 16, 1997, in Vancouver, Canada

Deutsches Elektronen-Synchrotron DESY, Hamburg, Germany

CONTENTS

B. Aune, D. Trines, for the TESLA Collaboration	Results from the DESY TESLA Test Facility
M. Clausen, M.R. Kraimer, W. Lupton, C. Watson	Experience with EPICS in a Wide Variety of Applications
D.R.C. Kelly	Dust in Accelerator Vacuum Systems
J. Roßbach, for the TESLA FEL Collaboration	The TESLA Free Electron Laser
R. Bacher, M. Clausen, P. Duval, L. Steffen	The Usage of Transient Recorders in the Daily HERA Machine Operation
M. Bernard, J.C. Bourdon, S. Buhler, R. Chehab, S. Chel, M. Desmon, J. Fusellier, T. Garvey, F. Gougnaud, J.F. Gournay, M. Jablonka, J.M. Joly, M. Juillard, T. Junquera, Y. Lussignol, U. Mencik, A. Mosnier, V. Omeich, B. Phung Ngoc, W. Rodier, M. Taurigna-Quere, A. Variola	First Beam Tests of the TTF Injector
R. Brinkmann, D. Einfeld, M. Plesko, J. Schaper	Design of a Damping Ring for the SB-Linear-Collider Project at DESY
R. Brinkmann, P. Emma	Emittance Dilution through Coherent Energy Spread Generation in Bending Systems
R. Brinkmann, H. Schlarb	Ultra-Short Bunches by Using a Quasi-Continuous Compressor Scheme in a Long Beam Transfer Line
M. Dohlus, A. Kabel, T. Limberg	Wake Fields of a Bunch on a General Trajectory due to Coherent Synchrotron Radiation
W. Ebeling, J.R. Maidment	The Proton Synchrotron DESY III
H.-J. Eckoldt	Failure Statistics of DESY Power Supplies in 1996
N. Holtkamp, G. Jacobs, C.-M. Kleffner, M. Nagl, V. Paramonov, I. Peperkorn, J. Peters, A. Schempp	Upgrade of the H^- - Injection System at the DESY Proton Linac III
W. Kriens	Petra Bunch Rotation

H. Mais, L. Vazquez, M.P. Zorzano	Numerical Solution for Fokker-Planck Equations in Accelerators
D. Proch, J. Sekutowicz, C. Tang	Note on the SC Linear Collider TESLA Cavity Design
S. Reiche, J.B. Rosenzweig, L. Serafini	Experimental Measurement of High-Gradient Standing Wave Accelerator Transport Matrix
M. Schmitz, for the SBLC Study Group	The S-Band Linear Collider Test Facility at DESY
F. Willeke	HERA Status and Upgrade Plans

Results from the DESY TESLA Test Facility

B. Aune, for the TESLA collaboration
Deutsches Elektronen-Synchrotron DESY
D-22603 Hamburg, Germany

Abstract

The TESLA Test Facility (TTF), under construction at DESY by an international collaboration, is an R&D test bed for the superconducting option for future linear e+/e- colliders. It consists of an infrastructure to process and test the cavities and of a 390 MeV linac. The infrastructure has been installed and is fully operational. It includes a complex of clean rooms, an ultraclean water plant, a chemical etching installation and a ultra-high vacuum furnace. The linac will consist of three cryomodules, each containing eight nine-cell cavities operated at 1.3 GHz. The accelerating gradient should be of at least 15 MV/m, with a Q of $3x10^9$. The injector delivers a beam of 10-15 MeV, it has been installed and commissioned. The first module is in place, a 140 MeV beam is expected in June 97. An overview of the facility and results of the tests are given in this paper.

1 INTRODUCTION

The superconducting option for an electron-positron linear collider of 500 GeV center of mass energy (TESLA) is being studied by an international collaboration [1], in parallel with similar efforts by other groups on various technical solutions.

The TESLA approach uses superconducting structures operating at a frequency of 1.3 GHz with a gradient of 25 MV/m and a quality factor of $5x10^9$ at T=2K. This choice presents advantages for the design of the collider, linked to the low rf frequency and the high AC-to-beam power efficiency of a SC linac. Many well-separated bunches are accelerated in a long rf pulse, the tolerances are relaxed compared to other approaches. Another characteristic of this choice is the low peak rf power needed and the availability of klystrons [2].

The technical challenge of TESLA is to operate a large number of cavities (20000) at very high gradient and to design the linac at a reasonable cost.

The TESLA Test Facility (TTF) is under construction at DESY with major components flowing in from the members of the TESLA collaboration. Its aim is to demonstrate the ability to accelerate a beam with proper qualities through a chain of 24 cavities operating at a field level of at least 15 MV/m and to reach an overall design of cavities, cryostats, couplers and auxiliary systems which leads to costs competitive with the other approaches based on conventional structures.

2 INFRASTRUCTURE AND CAVITY PERFORMANCE

2.1 Cavity processing

Obtaining a useable gradient of 25 MV/m or more in 9-cell cavities requires that one can overcome the field limitations: quenches and field emission. The quench limit is due to heat dissipation in local defects, the solution to the problem is to use very high purity Nb with increased thermal conductivity. The field emission, mainly due to the presence of micron sized particules on the surface , requires extreme cleanliness in the processing and installation of the cavities.

The infrastructure for cavity preparation is composed of a complex of clean rooms (from class 10000 to class 10), a chemical etching facility and ultra-clean water supply. A UHV furnace is used to improve the niobium material properties via heat treatment at 1400 C in presence of Ti gettering. High pressure water rinsing (100 bar) is applied at the last step of cavity preparation.

2.2 Cavity performance

The cavities are first tested in a vertical cryostat in which high peak power processing (up to 1 MW in short pulses) can be applied. Temperature mapping is also available.

After welding of the helium tank and mounting of couplers and tuner, a cold test is performed in a special horizontal cryostat, where the complete accelerating system is tested in the TTF pulsed mode (field flat top of 0.8 ms). The behavior of the couplers, the tuning mechanism and other components are checked before the cavity is installed in the linac.

Twenty cavities have been tested in the vertical cryostat, nine of them in the horizontal one. A complete summary of the tests is given in a separate paper [3].

The specifications for TTF have been exceeded in the majority of these tests. In several cases, a field of 25 MV/m has been obtained in cw mode and up to 30 MV/m in pulsed mode. According to the measurements in the horizontal cryostat, the average field in the first module should exceed 15 MV/m.

3 THE TTF LINAC

The experience gained on the TTF linac will feed directly into the TESLA collider design. There are a number of aspects in which both designs are similar. A detailed description of the linac can be found in [4].

The main components of the linac are: the injector, a first cryomodule housing 8 cavities, a 12 m long warm section in which a bunch compressor will be later installed, two cryomodules connected in series and a diagnostic area. The main parameters of the linac are given in table 1.

Table 1 TTF linac parameters

Energy	390 MeV
Beam current	8 mA
rms energy spread	2×10^{-3}
pulse length	0.8 ms
repetition frequency	10 Hz
Accelerating gradient	15 MV/m
Quality factor Qo	3×10^{9}
Heat load at 2 K	86 W
Number of cavities	24
Number of modules	3

3.1 Injectors

The TESLA design values for the beam current will be reached in two stages: the 1st injector delivers 8 mA with a bunch repetition frequency of 216 MHz and a bunch charge of 37 pC, while the 2nd one will give the same current with a frequency of 1 MHz and a bunch charge of 8 nC. In both cases, the rms bunch length is 1 mm.

Injector I delivers a beam of at least 10 MeV. It consists of a thermoionic 250 kV source (40 kV gun followed by an electrostatic column), a 216 MHz (f/6) prebunching cavity and a standard nine-cell SC cavity housed in its own cryostat and powered by a 200 kW klystron. A beam analysis station allows the tuning of the injector linac.

Injector II will be composed of an rf gun followed by the same SC cavity giving a total energy of about 20 MeV. A bunch compressor will be used at this level to obtain the bunch length of 1 mm. Two models of rf gun are under development: one for the full TESLA bunch charge (8 nC) and another one optimized for very low emittance (~1 mm.mr) at reduced charge (1 nC) for FEL experiments. They both use a 1.5 cell 1.3 GHz cavity powered by a 5 MW klystron and a Cs_2Te photocathode. The installation will permit the use of injector I or injector II alternatively.

3.2 Cryomodules

Three cryomodules, each 12.2 m in length, constitute the main body of the linac. Each one contains eight cavities, and a 4 K package including a superferric quadrupole doublet, steerers, a beam position monitor (cylindrical RF cavity, TM110 mode) and a HOM absorber. The liquid helium distribution and cold gas recovery system are incorporated into the cryostat. The cryostat design principle is to make the individual accelerating modules as long as possible and combine them to strings fed by a single cold box. This should result in low static losses (typically 0.2 W/m at 2K) and important cost reduction. The cavities are suspended from the helium gas return pipe which serves as a reference girder. Each cavity is equipped with its own Ti helium vessel welded around it, the beam tubes and the connections for couplers being inside the insulating vacuum.

3.3 Cavities

The 9-cell cavities are made of 2.8 mm, high RRR niobium. In addition to the standard fabrication technique, stiffening rings between adjacent cells have been added in order to reduce the detuning due to radiation pressure. With this technique a detuning parameter of ~1 $Hz/(MV/m)^2$ is obtained. The main parameters of the accelerating cavity are given in table 2.

A tuning mechanism acts on the overall length of the cavity, driven by a stepping motor located in the isolation vacuum. The tuning range is 800 kHz, corresponding to about 10^6 motor steps.

Table 2 Parameters of the TTF cavity

Frequency	1.3 GHz
Number of cells	9
Active length	1.036 m
Cell to cell coupling	1.87 %
Iris diameter	70 mm
Epeak/Eacc	2
R/Q	1010 Ohms
long. loss factor (σ=1mm)	8.5 V/pC
RF power at 25 MV/m	206 kW
External Q	3×10^6

3.4 Couplers

Two versions of coaxial input coupler have been developed. The coupler consists of a cold part mounted on the cavity in the clean room and closed by a 70 K ceramic window, and a warm part mounted after the installation of the cavity in the cryomodule. This part contains a coaxial to wave-guide transition and a second ceramic window at room temperature. An adjustment of the coupling by a

factor of 3 around the design value is provided by moving the inner conductor. Flexibility for axial displacement during cooldown of up to 15 mm is achieved via inner and outer conductor bellows.

The HOM couplers are mounted at both ends of the cavity with a nearly perpendicular orientation. A notch filter is incorporated for the fundamental mode rejection. Two types have been developed, a welded version and a demountable one. Both have been tested at high field level during the horizontal cryostat tests and the damping of the most dangerous modes has been measured. The Q's of the dipole modes are sufficiently low for the designed multibunch instability in TESLA.

3.5 RF system

RF power is provided by a 5 MW klystron which can feed 16 cavities. The power distribution is a linear system branching off identical amounts of power for each cavity from a single line by means of directional couplers. Individual three stub wave guide tuners for impedance and phase matching of each cavity provide the possibility of adjustment of phase by ± 30 deg. Individual low power circulators are installed on each cavity.

The low level RF control system must keep the fluctuations of the accelerating field (vector-sum of 16 cavities) to a low level to reduce the uncorrelated contributions to energy spread. The major sources of field perturbations are caused by fluctuations of the resonance frequency of the cavity and by fluctuations of the beam current. A digital feedback system will provide control of the accelerating field [5].

4 STATUS AND RESULTS

All the components for beam acceleration through the first cryomodule (140 MeV) are installed, the first beam is expected at the beginning of June 97.

4.1 Injector

The complete injector has been installed and tested [6]. During this first experiment the accelerating field in the capture 9-cell cavity was limited to 14 MV/m by strong field emission, although in the previous horizontal test a field of 18 MV/m was obtained. High power processing will be applied during the next run. The designed characteristics for the beam have been obtained (table 3) with a very good stability and reproducibility. The analog RF control system has been extensively tested with and without beam [7]. The expected values for amplitude and phase stability have been demonstrated: ± 4.10^{-4} and ± 0.1° peak to peak.

In addition the 12 MeV beam has been used for beam monitors developments: profile and emittance using an OTR station associated with an intensified gated camera, calibration of BPM, beam current measurement and loss monitoring system using toroid transformers.

Table 3 Injector Test Results

	Design	Measured
Beam current	8 mA	8 mA
Energy	> 10 MeV	12 MeV
rms energy spread	100 keV	< 100 keV
pulse length	0.8 ms	0.8 ms
bunch rep rate	216 Mhz	216 Mhz
bunch width (gun)	640 ps	600 ps
rms norm emitt.	5 mm.mr	3-4 mm.mr

4.2 Cryomodule and cryogenic system

The connection and pre-alignment of the string of 8 cavities and the SC quadrupole doublet has been made inside the clean room. The string is then moved on a rail outside the clean room. The complete mounting of the cryomodule has been achieved in 8 weeks, as scheduled. This first module has been equipped with a large number of temperature sensors as well as vibration sensors. Particular care has been taken in the alignment procedure. It has been found that with the present design, an accuracy better than 0.5 mm can be achieved for the cavities, as required from the TESLA specifications. Some improvements will be made for the following cryostat which will permit an accuracy of 0.2 mm. The position of the cavities will be monitored during cool-down and steady state operation with a system of stretched wires and wire position monitors [8], each cavity being equiped with 4 monitors.

The cryogenic system is fully operational, it has been used in routine operation during the injector tests.

4.3 RF system

The existing 5 MW klystron and modulator will be used to power the 8 cavities of the first cryomodule. A new multi-beam klystron is under development by Thomson which will deliver a power of 10 MW with an efficiency of 70%. The first tube is expected by the end of 97, it will be used to power the 24 cavities.

The digital low level RF control system has been extensively tested during experiments in the horizontal cryostat. The design performances of the system have been demonstrated under high field operation where the detuning of the cavity due to Lorentz forces is important. The data acquisition system for amplitude and phase of RF signals based on a 1 MHz sampling, digital in-phase and quadrature detection system has been used during the injector tests to monitor the field stability.

4.4 Beam lines and monitors

The complete beam line from the injector to the high energy beam analysis station is installed and under vacuum. All the components have been vacuum fired and carefully cleaned, the connections in the tunnel being

made under the protection of a local clean room. The pressure in these lines is in the range of 10^{-10} mbar.

The complete beam monitoring system, including data acquisition is installed, some monitors have been tested using the 12 MeV beam from the injector.

5 SCHEDULE AND EXPERIMENTS

5.1 First module, injector I

Starting in June 97 the experimental program with the beam accelerated through the first module includes:

- Measurements of cavity performance in linac environment.
- Cryostat behavior: losses, alignment of cavities.
- RF to beam power transfer: test of the rf control system.
- RF steering effect of couplers by measuring the beam displacement for various rf phases.
- Measurement of dark current.

5.2 Modules 2 and 3, injector II

In 98 will be installed the high charge injector and two more modules, giving an energy of at least 400 MeV. This equipment will permit to evaluate some of the key parameters for the collider design, like:

- HOM power deposited at T=2 K and choice of absorber at intermediate temperature.
- Cavity offset measurement with HOM power on dipole modes.
- short range and long range wakefields evaluation, damping of HOM with beam on axis and off axis.

In 99 an ondulator will be installed to demonstrate the feasibility of a free electron laser operating in the SASE mode. A bunch compressor after the 1st module will reduce the bunch length to 0.2 mm.

5.2 Future plans

For the longer term future, it is planned to double the length of the linac to 1 GeV and to operate a VUV light source yielding a coherent, very bright beam of photons with wavelength tuneable between 20 nm and 6 nm.

The linac extension would be composed of optimized versions of the components of TESLA.

6 CONCLUSION

The first stage of the TTF linac is now finished, the injector has delivered a 12 MeV beam, the beam experiments at the level of 140 MeV will start in June 97. A test set up for the FEL gun will be operated at DESY starting in September 97, the final tests for the TESLA gun are being accomplished at Fermilab. Experiments on free electron laser are schedule for 99.

REFERENCES

[1] The TESLA R&D effort is carried out by a number of institutions which includes IHEP Beijing, TU Berlin, Max Born Institute Berlin, Cornell Univ., Cracow Univ., TH Darmstadt, DESY, TU Dresden, DSM/DAPNIA Saclay, JINR Dubna, Fermilab, Frankfurt Univ., IN2P3/LAL Orsay, IN2P3/IPN Orsay, INFN Frascati, INFN Roma II, INFN Milano, FZ Karlsruhe, INP Novosibirsk, Polish Acad. of Science, IHEP Protvino, SEFT Finland, UCLA Dep. of Physics, Warsaw Univ., Wuppertal Univ.

[2] R. Brinkmann, "Status of the design for the TESLA linear collider", PAC 95, Dallas.

[3] M. Pekeler: "Test results on the 9-cell 1.3 GHz superconducting RF cavities for the TESLA Test Facility Linac", this conference.

[4] D.A. Edwards ed, "TESLA Test Facility Linac Design Report", DESY Print TESLA Rep. 95-01

[5] S. Simrock et al. "Design of the digital RF control system for the TESLA Test Facility", EPAC 96, Sitges

[6] T. Garvey et al., "First beam tests of the TTF injector", this conference.

[7] A. Mosnier et al., "RF control system for the SC cavity of the TTF injector", this conference

[8] A. Bosotti et al., "A Wire Position Monitor System to Control the Cold Mass Movements inside the TTF Cryomodule", this conference

EXPERIENCE WITH EPICS IN A WIDE VARIETY OF APPLICATIONS

Martin R. Kraimer
Argonne National Laboratory, 9700 South Cass Ave., Argonne, Illinois 60439
Matthias Clausen
Deutsches Elektronen Synchrotron (DESY), 85 Notkestrasse, Hamburg, 22603, Germany
William Lupton
W. M. Keck Observatory, 65-1120 Mamalahoa Highway, Kamuela, Hawaii 96743
Chip Watson
Thos. Jefferson National Accelerator Facility, 12000 Jefferson Ave., Newport News, Virginia 23606

Abstract

Currently more than 70 organizations have obtained permission to use EPICS, a set of software packages for building real-time control systems. In this paper representatives from four of these sites discuss the reasons their sites chose EPICS, provide a brief discussion of their control system development, and discuss additional control system tools obtained elsewhere or developed locally.

1 INTRODUCTION

The Experimental Physics and Industrial Control System (EPICS) [1] is currently in use at over 70 sites in Asia, Europe, and North America. It is used in accelerator facilities, astronomy, commercial industry, and industrial research. EPICS is the successor to the Ground Test Accelerator Control System (GTACS) that was developed at Los Alamos National Laboratory (LANL). EPICS resulted from a collaborative effort between the GTA controls group and the APS controls group. Over the last few years other sites have started using EPICS and contributing to its development.

Since EPICS is a collection of software components that can be used to develop a control system rather than a "turnkey" system, each site normally extends EPICS at the low level—i.e., custom record, device, and driver support—and adds support for high-level applications. This paper describes how four sites have used and extended EPICS.

2 ADVANCED PHOTON SOURCE

The Advanced Photon Source (APS) is a third-generation synchrotron light source located at Argonne National Laboratory. With regards to APS, this paper discusses the following: 1) APS/LANL cooperative development on input/output controller (IOC) software, 2) APS/LANL cooperative development on general-purpose high-level tools, 3) implementation of the APS accelerator control system, and 4) high-level applications developed by the APS accelerator physicists.

2.1 APS/LANL Cooperative IOC Software Development

During the last three months of 1989, APS evaluated GTACS by having a member of the controls group study the code and give tutorials explaining what he was learning. Most of the time was spent evaluating both the code which runs in the IOCs and Channel Access [2], the code which provides network-independent access to the IOCs. The result was a decision to use GTACS to build the APS control system. APS and LANL agreed to start cooperative development on improvements and on new general-purpose high-level tools [3].

While studying the GTACS code, APS identified many places where improvements could be made. The most important was the ability to add new record, device, and driver support without modifying core software. Although LANL also wanted the same or nearly the same improvements, GTA had already started commissioning and the GTA developers did not have time to implement these improvements. At that point the LANL and the APS staffs met and agreed on a design. APS then implemented the changes with input from LANL.

During the early years a lot of new hardware support was developed. If support for a device was developed at one site it was normally used at the other site. Improvements were folded into the common system. A VXI resource manager was implemented at LANL and used extensively at both sites. GPIB support was developed at APS and used at both sites. There was almost no duplication of effort in any area from Channel Access down to the device/driver software.

2.2 APS/LANL Cooperative Development on General-Purpose High-Level Tools

APS and LANL jointly decided on high-level tools which were needed but not yet available. The first tools to be developed were a general-purpose display manager/editor, an alarm handler, and an archive tool.

At that time a display manager/editor already existed but it ran only on VAX/VMS using a proprietary windowing system. LANL had already started design of an X-based replacement. When LANL/APS agreed to cooperate, the one point on which agreement could not be reached was whether this tool should be built directly on Xlib or on Motif. LANL, for performance reasons, wanted just Xlib. APS, for ease of development, wanted Motif. The end result is that two display managers/ editors were developed and are being used successfully. Each EPICS site normally chooses only one.

The alarm handler tool was proposed and designed by APS, LANL reviewed it before development was started, and APS developed the tool. It is used at most EPICS sites.

The archiver was designed and implemented at LANL, reviewed at APS before development began, and implemented at LANL. It is used at many EPICS sites. Archiving is a difficult and many-faceted subject. Some EPICS sites use the LANL-developed archiver but many sites use other archive tools. New archive tools are currently being considered by several EPICS sites.

2.3 Implementation of the APS Accelerator Control System

The accelerator control system currently has 165 IOCs containing approximately 160,000 records. The main control room (MCR) has 10 Ultra Sparc workstations each equipped with two video monitors. The control system network has ten satellite hubs which are dual connected to a central hub using FDDI. Each IOC is connected to two hubs using a redundant fiber Ethernet transceiver. Each MCR workstation is connected via FDDI to a network hub.

The APS accelerator control system was developed by control engineers using the EPICS-supplied toolkit. The controls group assigned engineers to subsystems based on the APS technical groups, i.e. linac, rf, diagnostics, power supplies, and vacuum. For each subsystem one engineer was assigned overall responsibility for all controls-related activities, i.e., hardware and software. This engineer interacted closely with the group responsible for the subsystem itself. For example, the engineer discussed requirements with the people in the group, attended group meetings, etc. Controls group engineers are responsible for all controls-related activities from engineering-related display screens to the hardware that interfaces to the equipment.

In addition to EPICS-supplied support, the control engineers needed custom record, device, and driver support for their IOCs. Although they sometimes asked the APS EPICS developers for help, they developed most of the support themselves, implementing 13 special record types, 48 device support modules, and 2 drivers. In addition, a number of sequence programs and subroutines for the subroutine record were written.

The APS controls system makes extensive use of GPIB devices. BITBUS is used as a low-level subnet. Many of the special record and device support modules were created for GPIB and BITBUS devices. One of the EPICS tools developers created general-purpose GPIB support and helped with the BITBUS driver, but the rest of the support was developed by the control engineers.

An APS-developed event system, consisting of VME event generators and event receivers interconnected with 100-Mbaud fiber optic links, provides the means of distributing medium resolution/accuracy timing events throughout the facility. Special record support was developed to integrate the event system with EPICS, including the ability to synchronize time stamps across IOCs.

Other major APS control applications developed using the EPICS toolkit include fast timing, BPM control and monitoring, charge and current monitors, and the orbit feedback system.

2.4 High-Level Applications Developed by the APS Accelerator Physicists

The APS accelerator physicists have developed a set of high-level tools grouped under the collective name of Self Describing Data Sets (SDDS). The SDDS toolkit can read and write data in EPICS database records. Though most of the applications do rather simple operations, the combination of these and others from the SDDS postprocessing toolkit allow arbitrarily complicated analysis of data and control of the accelerators at the Advanced Photon Source. These tools are general and can be applied to devices other than accelerators under control of EPICS.

Initially adopted for complex physics simulation programs, it was clear that the SDDS file protocol would excel in data-collecting software as well. Typically, an EPICS tool would write EPICS data to an SDDS file with each readback written to a column of names corresponding to the EPICS database record name. Single value data that describe the experimental conditions might be written to the file as parameters. Once collected, the EPICS data can be further analyzed and plotted with any of the SDDS tools. One can regard the SDDS tools as the layer between the EPICS control system and more functional analyzing tools and scripts, with SDDS protocol files as an intermediary.

The various tools are joined together via a scripting language, originally C shell, now Tcl/Tk. Most of the accelerator physicists can write Tcl/Tk scripts to diagnose problems or to solve new controls problems. Before new control strategies become operational, a Tcl/Tk-based tool is prepared for use by operations.

3 DEUTSCHES ELEKTRONEN SYNCHROTRON (DESY)

Shortly after commissioning the HERA (Hadron-Electron Ring Accelerator) storage ring it was obvious that some of the components developed for the cryogenic control system needed immediate performance and reliability improvements (the MKS-2 group is responsible for the cryogenic systems). One major problem was related to random crashes of one of the subsystems responsible for transfer and conversion of data between the in-house fieldbus called SEDAC and the cryogenic process control system. It was obvious that the replacement component should not only match the requirements for this special application but also open the door to a new standard of control applications tools. In 1993 EPICS was chosen because of its process control and record-oriented structure.

3.1 *Conversion of Cryogenic System to EPICS*

Along with EPICS, a new UNIX operating system environment (replacing VMS) and VxWorks real-time kernels (instead of iRMX) had to be learned within six months in order to replace the existing subsystem. From installation of the various software packages to the start of the first running period of an EPICS system at DESY took about eight months. The HERA cryogenic controls system must be extremely reliable because the superconducting magnets run 24 hours a day, every day for at least six months at a time. The first EPICS system met these stringent requirements and was considered an unqualified success.

Once the EPICS IOCs were in operation, it was possible to make use of the new freedom these systems provided the system designers and the operators. Online access to all the individual data was now possible as well as the chance to establish new ways of archiving process data for long-term storage. This led to the first new development for the EPICS system. An archive record, the archiver (still under VMS), and a viewer (based on IDL) were programmed to improve the quality of the archived data, storing on significant change instead of at a fixed time (i.e., every 60 sec). The analysis of problems was now possible with a much higher resolution than before. In addition, other EPICS tools such as display managers (first edd/dm, later medm) became so popular that the operators became involved in the process.

3.2 *DESY Utilities*

The next major use of EPICS at DESY was for monitoring utilities. The installed system of Siemans program logic controllers (PLCs) had improved the stability of HERA operations; however, it lacked adequate operator interfaces and tools like an archiver and alarm handler. In addition, the distributed nature of the installation necessitated that displays be distributed throughout the DESY site and into the halls of the 6.3-km-long HERA tunnel. EPICS was chosen to provide these services. The initial goal was to provide tools to the utilities group that would enable them to create their own environment for supervisory control. Students were trained to create hundreds of graphic screens. Special tools (scripts) were prepared to create EPICS databases from the PLC configuration databases. But the most difficult job was preparing the interface to the H1 network of the PLCs. Nearly half a man-year was spent writing the software to interface H1 and the common driver interface (CDI), which is DESY-developed software that provides an easy-to-use EPICS interface to various fieldbuses.

This system has grown continuously since it began operation. Even more important than this growth is the acceptance of the new control environment by the operators who, until EPICS arrived, had not had any contact with computer-based controls. The HERA water system is now monitored by engineers who use the archive viewer to supervise their water pumps and to tune their control loops.

Recently new systems went into operation to monitor the quality of DESY's main power supply. Three 10-kV transformers are monitored to catch any power glitch and freeze the current reading into an EPICS waveform record, which is then read by an archive process and stored in a raid array for later analysis.

In addition to the supervisory controls for the HERA water systems (based on H1 communication) another fieldbus, Profibus, is supported. Profibus is a German standard widely used for small- and medium-sized PLC applications. At DESY the Profibus-based PLCs control the air condition systems and small general-purpose systems. An EPICS interface was quickly implemented due to experience gained on the previous work.

3.3 *Collaboration with Other Institutes*

In addition to the utilities group, the machine controls and process controls groups were demanding more support from the MKS-2 group. The modular nature of the EPICS toolkit made it possible to distribute the various jobs to collaborators outside DESY like the Institutes of High Energy Physics in Protvino, Russia and Beijing. China. DESY staff trained the new collaborators in order to coordinate the work and reintegrate the new software into EPICS. Thanks to their excellent collaborative efforts, many new features were developed and are now in operation. One of these areas was the controls for the magnet power supplies for the Tesla Test Facility (TTF) which is the test bench for the next generation of linear colliders at DESY based on superconducting cavities.

To implement the TTF cryogenics controls, several functions necessary for process controls, such as the PID algorithm, had to be added or modified in the EPICS toolkit. All these modifications have been in operation for several months and are providing stable operations for TTF cryogenics.

3.4 *ORACLE*

The need to handle EPICS databases for multiple IOCs and different versions of databases for different EPICS releases was the driving force behind creation of a relational database for configuring and storing record information. An ORACLE database was designed to support both the old report structure and the new ASCII type of EPICS databases. The interface to configure individual records as well as record prototypes and prototype record groups was written in ORACLE-Forms to facilitate configuration of complete databases without requiring in-depth knowledge of the record structures. New records are created by merely supplying default values.

In operation since February 1997, this tool is the basis for a new phase of database generation at DESY since it is now possible to train people quickly. The database functionality was recently expanded to integrate configuration data for the alarm tools and the global database structure

following the idea that a record belongs to a *device* within a *location* of a *facility*. This type of information can also help generate information for the CDEV API from Jefferson Lab (see section 4), a feature that is attracting growing interest at DESY.

Cryogenic operators without any knowledge of the EPICS control architecture are now preparing the EPICS database, creating graphics, and providing the information to create sequence programs. This would not have been possible without the ORACLE-based record configuration tools.

3.5 Current and Future EPICS Projects

Another project that is nearly finished is providing EPICS services to PC-based fast ADC boards. This will allow access to PC-based information from any X-terminal or PC. In addition, the data stored in the ADC boards will be written to the central raid-array so that everyone can retrieve the data.

While the above-mentioned projects are relatively small, the next big project is in the planning phase: The original process control system for the HERA refrigerator will be phased out within the next two to three years. The replacement time schedule will be very tight. Thousands of lines of sequence programs will be converted into the native EPICS language of the sequencer; the internal structures of the DDC controls will be converted into EPICS records; and the functionality of the partly redundant processors will be analyzed and, if necessary, implemented for the IOCs.

The network is based on distributed Ethernet switches on an FDDI backbone. The Ethernet workstation connections are evolving towards switched 100baseT connections, again on the FDDI backbone.

EPICS installations at DESY are still growing because of the reliability and rich functionality of its software. The software distributed to the collaborators is very stable and can be used for production after making local modifications, and the collaboration provides help and support for all installed software. Common development efforts, such as the joint Argonne-DESY- CERN improvements to the medm graphical user interface, are made known to a wide audience.

4 THOMAS JEFFERSON NATIONAL ACCELERATOR FACILITY

Thomas Jefferson National Accelerator Facility (Jefferson Lab, formerly CEBAF) made a decision to adopt EPICS, following an extensive review of its control system, in 1993. At that time it was recognized that the in-house-developed TACL control system would have difficulty scaling up to full machine operation without extensive work, and it was decided that there would be immediate and long-range advantages in joining the EPICS collaboration [4]. Conversion began in the midst of accelerator commissioning.

As much of the existing control system (over 90%) was CAMAC-based, Jefferson Lab quickly implemented support for CAMAC based I/O devices, using the IEEE standard 758-1979 to define the interface between EPICS and an arbitrary CAMAC interface. This allowed the use of existing IEEE-compliant software device drivers available for parallel crate controllers. Further development of IEEE routines for a CAMAC serial highway interface allowed integration of the remaining I/O.

In migrating from TACL to EPICS, much of the design of the original system was preserved, and support for CAMAC interrupts was not needed (i.e., not used in the original system and not implemented in the conversion). The following year, LANL modified the CAMAC driver for the serial highway to add support for interrupts and for multiple serial highways (controllers). Jefferson Lab further extended CAMAC capability by adding support for multiple processors sharing a single serial highway for compute-bound configurations.

Over the past three years, a wide variety of hardware has been integrated into the control system, including GPIB, VME, and RS-232 devices. In most cases this has required writing additional device drivers; in approximately 15-20% of the cases device drivers were obtained from the EPICS community. EPICS has proved very flexible in this regard.

Because CEBAF was further into its commissioning schedule than APS, it was the first site to scale EPICS up to a single integrated system with tens of thousands of database records, hitting the 100,000 mark in 1994. With only a few minor problems, this more than tenfold increase in the size of the largest system was accomplished smoothly, giving every indication that an additional order of magnitude is achievable.

The current configuration of the control system contains 70 IOCs and 160,000 records providing an interface to 50,000 hardware I/O points. Compared with APS, Jefferson Lab has fewer single-board computers (by more than a factor of 2), and has consequently had to deal more with loading issues (this is partly budget driven, as this is the second control system for a relatively young site). Many problems were encountered in the first two years related to poor behavior of the EPICS software under low memory conditions. This has been solved with additional memory and some software improvements. Some remaining problems still under investigation may be related to CPU loading and/or network loading.

4.1 Accelerator Controls

The EPICS toolkit is quite flexible and is not specific to accelerator operations. It provides extremely flexible name-based control of a wide variety of hardware I/O points. Much of the work done by the controls group at Jefferson Lab has been in adding accelerator-specific software on top of, and alongside of, EPICS.

Due to the time pressure of ongoing accelerator commissioning in 1994-1995, it was necessary to rapidly pro-

duce a handful of accelerator applications to provide high-level accelerator setup and control. In particular, beam steering, linac optics setup, cavity phase cresting, and machine settings management were urgently needed. In order to provide operator-friendly tools, the Tcl/Tk scripting language and its graphics library were adopted. An interface between Tcl and the EPICS channel access network library was implemented, and this provided the basis for a rapid prototyping environment with name-based I/O and full graphics support [5].

Experience with this environment is extremely positive. While some of the more demanding applications, such as beam feedback and an online accelerator model, have been rewritten in C++ to improve performance and capability, additional Tcl- based tools continue to be written. The most recent work includes an automated turn on of the entire injector, written by the accelerator operations group (not software engineers), and an accelerator optics tuning package which looks at the Courant-Snyder invariant as a function of beam pathlength.

In creating these accelerator control applications, it was unavoidable that work done at other laboratories was to some extent duplicated. Several attempts were made to port software from other systems to Jefferson Lab, but most online applications had too many dependencies upon the other laboratories' control systems (non-EPICS). This was one of several motivations in creating a new framework for control system applications called CDEV [6]. Additional motivations include isolating high-level applications from the details of the low-level control system implementation, and organizing named I/O points into devices.

CDEV is a C++ and Java framework for developing device control applications and provides a definition of a virtual control system which is independent of local implementation. It allows applications to be shared between EPICS sites like Jefferson Lab and APS, and non-EPICS systems such as SLAC and CERN. One unique feature of CDEV is that it supports multiple protocols (concurrently, if desired), and in particular it includes support for the EPICS channel access protocol, allowing CDEV applications to access EPICS-named variables through a device-oriented API. CDEV has also been shown to map well onto the SLAC and CERN/PS control systems.

A small number of new CDEV applications have been written at Jefferson Lab (e.g., beam steering, a correlation measurement package), and a few of the EPICS applications have already been modified to call CDEV instead of Channel Access (stripTool converted at Jefferson Lab, alarm handler at APS, display manager an ongoing joint project between LANL and Jefferson Lab). As these tools are finished, they may be used immediately at CERN and other non-EPICS sites which have implemented the CDEV adapter.

It is hoped that as this suite of control system-independent accelerator applications grows, additional non-EPICS sites will contribute to creating a reusable suite of high-level accelerator control software [7].

For some of the non-hardware portions of the control system (e.g., on-line accelerator model, error log, and archive data log query processing), the "software bus" used in EPICS does not provide a sufficiently rich protocol, and Jefferson Lab has implemented an additional message oriented protocol under CDEV for these applications. The protocol is also implemented in Java, allowing Web-based applets full live access (typically restricted to read-only) to all control system data through a gateway program on the Web server.

A final significant area of accelerator-specific developments is a fast feedback system for beam energy and orbit corrections [8]. This system may eventually provide feedback at more than 2 kHz to fully suppress observed 60-Hz and 180-Hz noise. Feedforward is also under investigation. A prototype state space formalism-based tool has been implemented which executes at 60 Hz, with plans to scale this to 540 Hz in the next six months. These speeds are outside of the range at which EPICS is an appropriate solution, and the current implementation uses separate tasks running on the same processor as EPICS (a separate processor may be used for highest rates). These tasks are controlled and monitored through EPICS, allowing a uniform view of this mixed system. Early performance results are quite encouraging.

4.2 Physics Controls

EPICS is also being used in the control of the three major physics detectors at Jefferson Lab. The data acquisition system CODA is also accessible through CDEV, and joint development projects between the accelerator and physics divisions on the use of EPICS and CDEV are further improving software reuse within the extended EPICS community. The most recent development in this area is a new error message logging facility co-developed by these two teams.

5 KECK OBSERVATORY

The W. M. Keck Observatory operates the twin Keck 10-meter optical telescopes on the summit of Mauna Kea in Hawaii. Both telescopes have identical control systems, entirely implemented using EPICS [10].

The Keck I telescope was commissioned in 1992 using an in-house control system. This system was functional but had various problems and was hard to extend. When the Keck II telescope was funded in early 1994, it was decided not to propagate the Keck I system to the new telescope but instead to produce a new control system that would scale to the planned future use of the two telescopes for optical interferometry. Since EPICS had already been selected by the Gemini 8-meter telescopes project, and there was already interest in EPICS throughout the astronomical community, it made sense to consider it for the Keck II control system.

Various low-level design studies were carried out in 1994 and the formal decision to use EPICS was made at a design review in March 1995. Development proceeded rapidly (with much help from LANL staff) and Keck II saw "first light" in January 1996, becoming fully operational in October 1996. Keck I was retrofitted with the new control system in March 1997 and both telescopes are now (independently) running identical software versions.

Unlike the accelerators described elsewhere in this paper, the Keck EPICS systems have relatively small numbers of IOCs, records, and I/O points. Each telescope currently has three IOCs, with about 2000 records total per telescope, of which about 850 are attached to hardware. In contrast to many accelerator systems, there is little duplicated hardware and a lot of algorithmic code runs on the IOCs, both in subroutine records (including two extended versions of the subroutine record supplied by the Gemini project) and in custom records (thirteen custom records have been implemented in-house).

In addition, EPICS is being used for the Keck adaptive optics program, which will add two or three IOCs per telescope. Looking further into the future, it will also be used for coordinating the two telescopes and several outrigger telescopes as an optical interferometer.

5.1 EPICS for Telescope Control

The main telescope control servo runs at 40 Hz, a low enough frequency to permit standard EPICS record processing to be used for reading hardware and performing the necessary encoder and servo processing. This processing has many inputs and outputs and it was decided early on that it would be necessary to write custom records with many fields. (Even if the new genSub record had been available at the time, it is probable that the same number of custom records would need to have been written.)

The time interval between the timing pulse that latches the telescope encoders (and triggers EPICS record processing) and the velocity demand being written to the drives is termed the critical region. This critical region is required to be less than 1 ms. In order to achieve this specification, the custom records use precalculated coefficients to perform critical processing as fast as possible and then forward link to the next record in the chain. Once critical processing is complete, the coefficients for the next iteration are calculated. As downstream records finish processing, the records that forward linked to them continue with their noncritical processing.

The main telescope control described above accounts for five of the thirteen custom records. Five more are used for the "pointing code," the rigorous astrometry that determines where the telescope should be at a given time. The three remaining records handle some standard conversions that, while logically appropriate for subroutine records, require more inputs and outputs than can be handled by such records.

In the early days, several LANL contractors wrote EPICS device and driver support for devices not already supported by EPICS. One generally-applicable product which has resulted is drvAscii/sioSup, which uses a C printf()-like format string in a record's PARM field to describe a prompt and an expected response. This allows control of many serial devices without having to write any C code (and is similar in concept to the ANL generic GPIB support).

5.2 Use of Standard EPICS Tools

Nearly all databases are generated using Capfast; there are still one or two snippets that use the LANL DCT tool or which are hand-edited in the ANL .db format. Experience with Capfast has in general been positive: the end result is wonderful but the drawing tool causes some gnashing of teeth.

At first, the LANL display manager was used extensively. However, use of Tcl/Tk and the commercial dataViews package—interfaced via the Keck-specific KTL library (described below) to Channel Access—for user interface screens is increasing. DM continues to be used primarily for engineering screens.

The EPICS alarm handler and archiver have been used extensively, and both have been invaluable. There have been some user acceptance problems with the alarm handler but this is probably due to insufficient attention being given to the configuration files. The m4 macro processor is used to combine subsystem alarm handler configuration files into a single telescope-wide file.

5.3 Locally-Developed Tools

Keck is only partially an EPICS shop. Owing to the freedom afforded the university groups who build its instruments, several different messaging systems and control APIs are in use. In order to alleviate this problem, the Keck Task Library (KTL) [11] API was defined in 1991. KTL shares some features with CDEV in that the API is independent of the underlying services and an internal API permits run-time activation of shareable libraries containing service-specific code. Like CDEV and Channel Access, all I/O is name-based, an object being identified by a service name (which identifies the shareable library) and a service-specific keyword name. Keck requires all telescope and instrument subsystems to provide a KTL library; as with CDEV, this permits KTL applications (mostly GUIs) to use a single API to control multiple heterogeneous underlying systems. Recent GUI development has used a Tcl/Tk/KTL extension called KTCL.

The EPICS archiver can log binary data at high rates and is used for collecting 40-Hz servo data. This data is imported using arrIDL (described below) and analyzed using IDL. The archiver can also log ASCII data at specified intervals but this produces files which are verbose and hard to handle. To address these difficulties, a simple archiver (EZAR) was written. EZAR can log both events and periodically sampled data in a comma-separated ASCII format. It is useful where ease of access to archived data is more important than efficient collection of the data.

The ANL BURT tool was evaluated as a means of loading and restoring calibration data. However, it seemed more sophisticated than warranted by Keck requirements and instead a simple PVLOAD tool was written. PVLOAD parses a file of EPICS channel assignments (including support for array-valued fields) and then uses Channel Access to set the values. A complementary PVSAVE tool is planned but has not yet been implemented.

Sequence programs are used for managing complex interactions such as subsystem initialization and fault handling. They are also used, at a higher level, for managing groups of subsystems. When implementing the latter, it was necessary to add a feature to the sequencer program to permit queueing of Channel Access monitors. This change will be made available to the EPICS Consortium.

Finally, IDL is used extensively for the analysis of engineering data. Accordingly, an EPICS extension to import EPICS archiver data into IDL has been written. This extension, arrIDL, is based on the C code from the LANL arrtk extension.

6 CONCLUSIONS

As shown in Table 1, EPICS has been successfully used to implement controls for medium to large facilities. APS, TJNAF, and Keck are using EPICS for most of their controls. DESY is using it mainly for cryogenic controls and facility monitoring.

Each site uses the same EPICS core, but has implemented special low-level software to communicate with hardware and/or fieldbuses connected to other control systems. The EPICS design makes it easy to add such support without having to modify the EPICS core.

Similarly, each site has developed high-level software that exists above the EPICS core software; the existence of the Channel Access client library has made this possible.

Table 1: Control System Sizes

	APS	DESY	TJNAF	Keck
# of Workstations	~10	~8	~10	~6
# of IOCs	165	31	70	6

7 ACKNOWLEDGMENTS

The work at Argonne was supported by the U.S. Department of Energy, Office of Basic Energy Sciences, under Contract No. W-31-109-ENG-38.

The W. M. Keck Observatory is operated as a scientific partnership between the California Institute of Technology and the University of California. The observatory is made possible by the generous financial support of the W. M. Keck Foundation.

The work at TJNAF was supported by the U.S. Department of Energy, under Contract No. DE-AC05-84ER40150.

8 REFERENCES

[1] L. R. Dalesio et al., "The experimental physics and industrial control system architecture: past, present, and future," Proc. of ICALEPCS '93, Berlin, Germany, *NIM A* **352**, pp. 179-184, (1994).

[2] J. O. Hill, "Channel Access: A Software Bus for the LAACS," Proc. of ICALEPCS '89, Vancouver, British Columbia, Canada, *NIM A* **293**, pp. 352-355 (1990).

[3] L. R. Dalesio et al., "Distributed Software Development in the EPICS Collaboration," Proc. of ICALEPCS '95, Chicago, Illinois, pp. 360-366 (1997).

[4] W. A. Watson et al., "The CEBAF accelerator control system: migrating from a TACL to an EPICS based system," Proc. of ICALEPCS '93, Berlin, Germany, *NIM A* **352**, pp. 118-121 (1994).

[5] J. van Zeijts, "Rapid Application Development Using the Tcl/Tk Language," Proc. of the 1995 PAC, pp. 2241-2243 (1996).

[6] J. Chen et al., "CDEV: An Object-Oriented Class Library for Developing Device Control Applications," Proc of ICALEPCS '95, Chicago, Illinois, pp. 97-104 (1997).

[7] W. Watson, "A Portable Accelerator Control Toolkit," these proceedings.

[8] M. Chowdhary et al., "A Fast Feedback System for CEBAF," Proc. of ICALEPCS '95, Chicago, Illinois, pp. 429-434 (1997).

[9] W. Lupton, "Software Infrastructure for the Keck II Telescope," in Telescope Control Systems, Proc. of SPIE, Vol. **2479**, pp. 140-151 (1995).

[10] W. Lupton, H. Lewis, K. Tsubota, A. Honey, S. Quady, "The Keck II Telescope Control System," Optical Telescopes of Today and Tomorrow, Proc of SPIE 1996 (to be published).

[11] W. Lupton, A. Conrad, "The Keck Task Library (KTL)," ADASS '92, PASP Conference Series **52**, pp. 315-319 (1993).

DUST IN ACCELERATOR VACUUM SYSTEMS

Darren R.C. Kelly, DESY, Notkestr.85, 22603 Hamburg, Germany

Abstract

Many accelerators of electron beams are susceptible to persistent beam lifetime disruptions, with correspondingly reduced performance. One distinguishes between three prevailing explanations of these disruptions: (1) trapping of positive atomic ions in the negatively charged beam; (2) trapping of small highly positively ionised micro-objects ("dust") in the negatively charged beam; (3) disruptions due to stray magnetic objects trapped in the magnetic field of undulators.

The lifetime disruption of certain electron storage rings that employ ion-getter pump systems are attributed by most researchers to explanation (2), the trapped dust hypothesis. Systematic experimental studies of HERA, PETRA and DORIS reinforce the suspicion that specifically this type of pump system is the culprit.

Examples of beam lifetime disruptions are presented, together with a summary of observations and experiments performed at various afflicted storage rings to investigate dust trapping and the connection between ion getter pumps and dust particle release. Observations of the disrupted beam are found to agree with the dust trapping hypothesis.

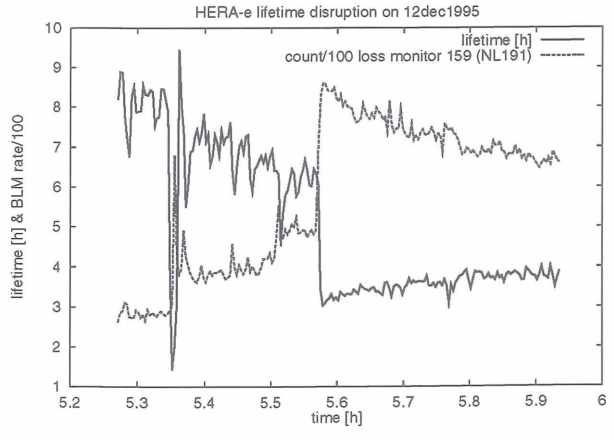

Figure 1: Example of the reaction of a beam loss monitor during a lifetime disruption in HERA-e at injection energy 12 GeV on 12 Dec 1995. The beam loss monitor count $R_{i,j}$ divided by 100 for monitor NL191 (number j=159) and the lifetime τ in hours are shown against time t_i. Reductions in the lifetime coincide with local loss rate increases.

1 INTRODUCTION

Various electron storage rings are afflicted by a spurious reduction of the beam lifetime – apparently caused by the deflection of beam electrons by positively charged dust particles of size order 1μm trapped in the electric field potential of the negatively charged beam: Super-ACO [1], TRISTAN AR [2], CESR [3], HERA-e, PETRAII, DORISIII [4, 5], PF [6]. The complementary experience at these machines has built a consistent picture of the symptoms of macroparticle lifetime disruptions, and this picture agrees quantitatively with the dust trapping model detailed in [3, 4].

This *electron beam lifetime problem* is beam charge dependent, i.e. it only occurs with electron beams, as evidenced by the problem-free switch to positron operation in HERA and DORIS.

Observations confirm that the ion getter pumps of all above-mentioned machines are implicated in casting dust particles into the beam pipe. The lifetime disruption can be provoked by switching an ion getter pump on and off, or by abruptly increasing the pump voltage, when a discharge within the pump can be sometimes be observed.

Such lifetime disruptions are not observed in the non-evaporative getter (NEG) pump based storage ring LEP or at ESRF (with NEG pumps and auxilliary lumped ion pumps), with the exception of the possible capture of magnetic dust in undulators [7]. Trials over a limited region of HERA with NEG pumps indicate a strong if not complete reduction of the release of disrupting particles within this NEG pump region.

It will be illustrated in this report that the extensive observations of beam lifetime disruptions in a number of accelerators are well described by the trapped dust hypothesis. However, the formation or liberation of dust particles within the complicated environment of the ion-getter pump chamber is poorly understood. Relatively few direct observations of the processes within these pumps systems are available, whereas many observations of pump configurations and operating conditions conducive to the onset of beam lifetime disruptions have been performed, in particular with HERA, PETRA and DORIS. Such observations are however not sufficient to form a causal model of dust particle release into the beam pipe; our knowledge of the processes on the pump side of the vacuum chamber gas conduction slits is as poor as the available diagnostics. A number of interesting observations and experiments of dust-like disruptions at other

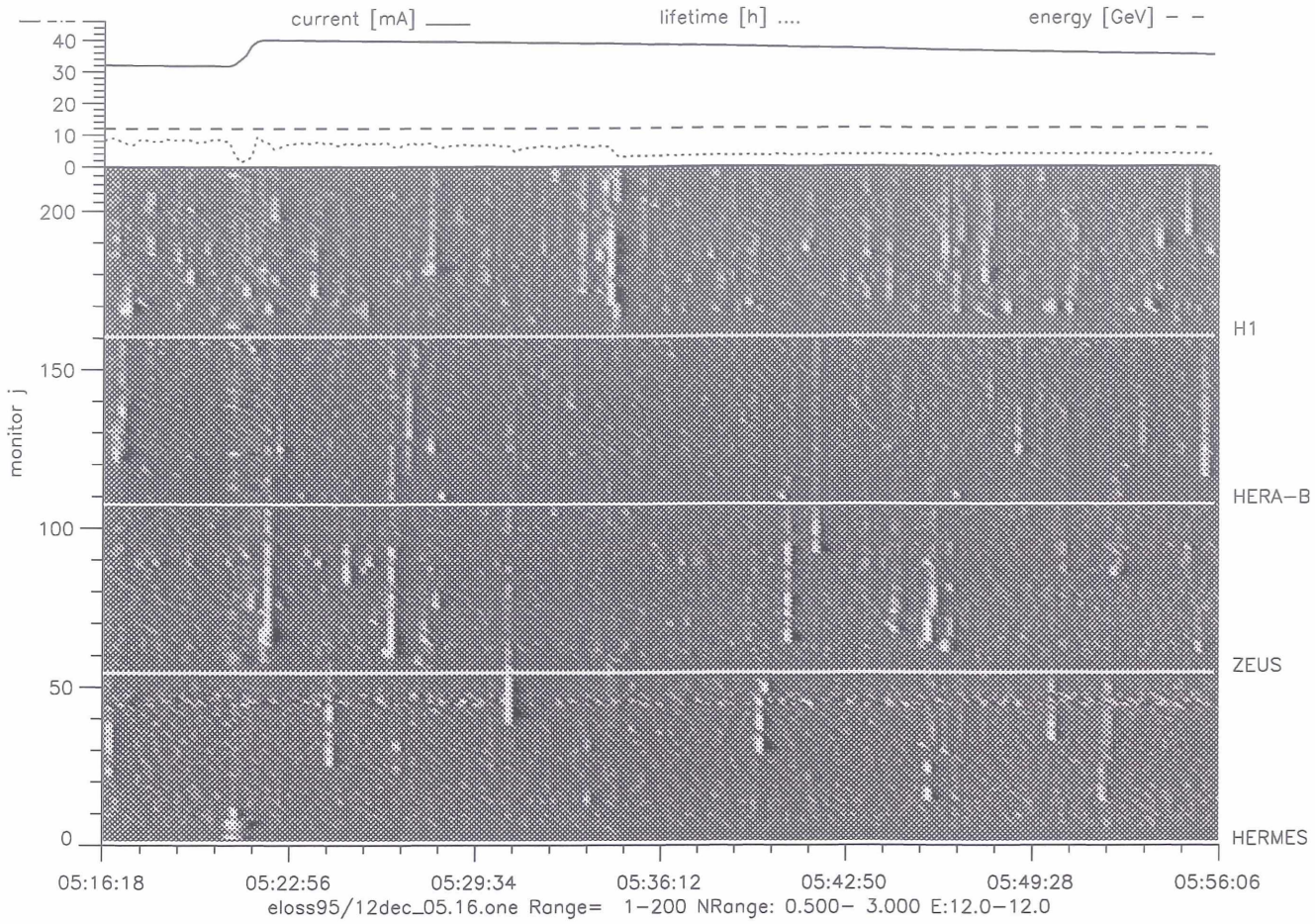

Figure 2: The beam loss monitor count ratio $N_{i,j} = R_{i,j}/R_{i-1,j}$ reveals the influence of dust particles moving longitudinally around the HERA electron ring. The grayscale corresponds to a range 0.5...3 in $N_{i,j}$ at 12 GeV, where 1 represents background (no change). The ratios are plotted over the (i, j)-plane of BLM monitor numbers $j = 1 \ldots 214$ for the entire machine against time t_i. Current in mA, energy 12 GeV and lifetime in h are shown on an extended scale

afflicted storage rings will also be discussed.

2 AN EXAMPLE OF LIFETIME DISRUPTIONS IN HERA-E

Of all available diagnostics of the disrupted beam, the 214 beam loss monitors of HERA [8] are perhaps the most revealing. In Fig. 1 we see an example of a typical lifetime disruption in HERA-e at injection energy 12 GeV[1]. In this particular HERA-e run a number of abrupt beam lifetime reductions seemed to correlate with increases in the rate $R_{i,j}$ of beam loss monitor number j=159 at position NL191 over times t_i.

More global insight into the dust trappings is obtained when the time development of the beam loss monitor count ratio $N_{i,j} = R_{i,j}/R_{i-1,j}$ of all monitors $j = 1 \ldots 214$ around the machine is displayed simultaneously in one diagram for a range of times t_i. Thus *changes* in the reaction of each monitor are reflected by departure from $N_{i,j} = 1$, which value then represents predominantly the synchrotron radiation background and beam electron losses due to deflection from residual gas molecules in the vacuum chamber. In Fig. 2 the count ratio is associated with grey shades for a range 0.5 – 3 in $N_{i,j}$ for the same HERA-e run on 12 Dec 1995 at 12 GeV . *The reader will be rewarded by taking a few minutes to peruse and understand this somewhat overwhelming diagram, which illustrates most of the important aspects of the dust trapping problem.* A number of features of the disrupting particles can be identified in this diagram:

- The longitudinal flight of many particles can be easily discerned as bright flight trails, and their

[1] In HERA-e at 12 GeV the beam loss monitor reaction to scattered electrons dominates over the loss monitor's reaction to synchrotron radiation, permitting easy recognition of events, whereas at e-p luminosity energy 27.5 GeV transient reactions *can* be identified but at 3% of the count are difficult to resolve against the dominant synchrotron radiation background, so examples in this paper are restricted to injection energy 12 GeV .

velocities can be measured to be around 10 to 100 m/s (in HERA-e at beam energy 12 GeV and current 30-40 mA).

- Both transient and instransient disruptions of the lifetime can be seen to correspond with particles entering the beam. The lifetime is plotted against time on the extended axis.
- It can be seen that there are hundreds to thousands of particles passing through the beam per hour, only a handful of which are permanently trapped. Many particles do not survive their flights along an arc, perhaps due to thermal, structural or dynamic instability. There is clearly a narrow stability window.
- The reaction of monitor number 159 (position NL191) shown individually in Fig. 1 can be identified at the instant of lifetime reduction (extended axis).

3 THE TRAPPED DUST HYPOTHESIS

Most if not all symptoms of the electron beam lifetime disruption can be quantitatively explained by the prevailing *dust trapping model* as detailed in [3, 4], which I summarise briefly. Macroparticles, perhaps of SiO_2 or metallic oxides from the beam pipe and ion pump surfaces, are cast into the beam pipe by numerous ion pumps at frequent intervals, where they are rapidly ionised and drawn into the electron beam by the beam's strong electric field. The particles are transversely trapped and rapidly reach an equilibrium charge determined by competition between ionisation by beam electrons and deionisation through field evaporation and photoelectron capture. The equilibrium charge obtained by SiO_2 particles of sizes $0.1 - 1$ μm – as computed by integration of a trapped particle's equation of motion [12] with charge development after [4] – is listed in Table 1 for current 20 mA and energy 27.5 GeV in HERA-e. The particles oscillate transversely at frequencies of a few kHz. Particles of low mass-to-charge ratio, i.e. of radius $\ll 0.1\mu$m are transversely unstable.

The macroparticles are driven downstream by Mœller scattering at about 12 ms^{-2} [4] until they are possibly trapped in horizontally defocussing quadrupoles by restoring kicks due to the longitudinal asymmetry of the beam bunches from the β-function gradient there [3]. In HERA particles of radius $< 1\mu$m achieve an equilibrium charge meeting this longitudinal trapping criterion.

Particles of size $0.1 - 1$ μm should be thermally stable in HERA-e at typical current 40 mA and energy 27.5 GeV , although [4] has predicted that these particle might be thermally unstable at very high electron currents $\gg$ 40 mA.

In view of this model the myriad of activity in the beam loss monitor diagram Fig. 2 becomes understandable. A large number of dust particles with a distribution of sizes are cast into the beam pipe at many locations in the machine. Only the handfull of particles per hour meeting the transverse, longitudinal and thermal stability conditions survive to cause intransient lifetime disruptions, the others leaving merely brief trails of losses as they are swept downstream before melting, falling out of the beam, or becoming structurally unstable.

Table 1: Charge number Q, mass number to charge number ratio Q/A, and and transverse oscillation frequencies obtained by particles of different radii R trapped in the core of the HERA electron beam at 20 mA current at 27.5 GeV.

R [μm]	Q	A/Q	f_x [Hz]	f_z [Hz]
1.0	5.81E+06	1.04E+06	1510.88	3152.41
0.5	4.75E+06	1.58E+05	3863.99	8062.09
0.3	4.04E+06	4.02E+04	7668.93	16001
0.1	2.72E+06	2.23E+03	32576.5	67969.8

4 EXPERIMENTAL INVESTIGATIONS

A number of chance observations and machine studies at various institutes have added greatly to our knowledge of the lifetime disruption problem, some of which are now briefly described.

Since the inception of CESR sudden lifetime drops have been observed and by comparison of the magnitude of the observed lifetime drops with a model of a trapped macroparticle's equilibrium charge as a function of particle mass the typical particle size was estimated to be of order 1 μm [3].

At TRISTAN AR dust particles were dropped into the beam pipe via a 1 mm nozzle to see whether macroparticles could indeed be trapped in an electron beam [14]. Metal particles consisting of Cu, Al, Ti (sizes 0.1-8 μm) were not trapped, whereas metallic oxides such as Cu0 (0.35 μm), TiO_2 (0.3 μm), and the NEG compound Zr-V-Fe ($\sim$ 1 μm) were trapped for many minutes at currents order 10 mA and energy 6.5 GeV. Particles of diameter 0.5 μm consisting of C (diamond), SiC and Al_2O_3 were trapped even at very low currents (less than 0.1 mA).

Surprisingly, the TRISTAN AR beam lifetime was found to be poor *after* dumping and refilling, and bremsstrahlung signals and electron losses typical of trapped particles were still observed. This "hysteresis" effect has also been observed at HERA, and is not yet understood. Simple considerations predict that the image charge force on a dust particle exceeds the beam electric field force within a few mm of the vacuum chamber wall for both HERA and TRISTAN AR

[3, 15].

During dust trapping investigations at TRISTAN AR bremsstrahlung observations with γ-ray detectors [15] suggested both longitudinal motion and transverse oscillations of dust particles.

At CERN a troublesome ion pump installed above an electrostatic separator was reported [7]. The pump was found to arc frequently. When the pump was moved below the separator and around a 90^o elbow the problem disappeared.

At Super-ACO a CCD camera 10 m from an ion pump in a beam-line from Super-ACO was found to be "sand-blasted" with titanium and stainless steel after an accidental gas inlet [7].

The degree and frequency of beam lifetime disruptions seems to increase with higher beam energy and beam current. This correlation has been systematically studied in HERA-e [9]. Analysis of the correlation reveals that dozens of particles of radius 0.3 μm are typically trapped in HERA at current 20 mA and energy 27.5 GeV resulting in a total lifetime reduction from 10 h to about 3 h.

It has been suggested [16] that the likelihood of spontaneous ion pump discharge and consequent macroparticle release is related to the number of photoelectrons released per metre from the vacuum chamber surface, a quantity approximately proportional to the product $E \times I$ where E and I are the beam energy and current respectively. This defines a locus for onset of the disruptions, although clearly one is dealing with a stochastic phenomenon not a sharp threshold. There were no indications of lifetime disruptions due to macroparticles at the NEG-pump based LEP storage ring with beam current 8 mA at 45 GeV[19], whereas lifetime disruptions are prevalent at HERA at current 30 mA at 12 GeV and at current 13 mA at 27.5 GeV.

Investigations in PETRA showed that a range of adapted ion pumps were capable of causing lifetime disruptions [17], either spontaneously or by abrupt switching of the pump high-voltage. These pump variations included: (1) a regular PETRA ion pump where many cylindrical Penning cells share a common cathode; (2) a regular HERA ion pump where perforated anode foils offer an open discharge region to the side; (3) a HERA ion pump with a baffle between the gas conduction slits and the pump anode, blocking the direct route to the beam pipe; (4) an "inverted" pump with high negative voltage attached to the cathode instead of the anode. A "dummy" pump with a closed, inactive rectangular tube replacing the cylindrical Penning cells did not give rise to lifetime disruptions.

A possible mechanism for dust particle release from ion pumps is the liberation of pump material such as titanium by strong discharges known to occur spontaneously within the pump cells, and provokable by abrupt switching of the pump high voltage. Resistors of strength 100 MΩ were installed before integrated dipole pumps in HERA in the hope of dissipating the energy of the discharge sufficiently to prevent liberation of particles [18]. However beam lifetime disruptions where found nevertheless to occur frequently and analysis of beam loss monitor responses did not show a reduction in the frequency of particle release into the beam pipe.

It has been shown that both strong repeated beam kicks and a carefully tuned beam excitation sweep with a feedback kicker can restore the disrupted beam lifetime of PETRA and HERA [17, 11, 12]. In HERA, where the lifetime is "multiply-disrupted", presumably by dozens of disrupting particles, the lifetime and the rates in particular beam loss monitors and experiment detectors could be seen to improve in discrete steps as the parameters of the beam excitation were scanned, providing strong support for the dust trapping model. Bremsstrahlung detector observations at PETRA likewise indicated discrete beam disruption.

A clearing field constructed using beam position monitors button electrodes immediately downstream from HERA's horizontally defocussing quadrupoles was shown to deflect the longitudinal flights of particles travelling sufficiently slowly past the clearing field [13]. The location of the BPMs is not suitable for construction of a clearing field capable of improving the beam lifetime in HERA by removing particles trapped within horizontally defocussing quadrupoles, but the experiment provides further support for the dust trapping model. The installation of general clearing-field electrodes to improve the HERA-e beam lifetime is a technically cumbersome option.

5 CONCLUSION

A wealth of experimental and observational information has been gathered by researchers at many electron storage rings afflicted by spontaneous beam lifetime disruptions, most of which is consistent with the model of macroparticles (dust) of size order 1 μm being trapped in the electron beam.

Yet despite this consistent picture of the symptoms, the cause is not fully understood. As researchers of viral infections know, the tiniest creatures can be responsible for the greatest grievances and warrant the most extensive combat. An elegant, inexpensive solution to the electron beam lifetime problem compatible with general machine operation in HERA is not yet available. Trials indicate that replacing the ion getter pump system with NEG pumps will likely restore good electron beam lifetime. But a deeper understanding of dust generation/liberation in accelerator *pump* systems would be welcome now that so much is known about dust in electron accelerator beam pipes.

6 ACKNOWLEDGEMENTS

Thanks to DESY colleagues and other electron storage ring colleagues too numerous to list for discussions and communications.

7 REFERENCES

[1] P. Marin. 'Microlosses of beam current on Super-ACO operated with electrons', *LURE, ORSAY* RT/90-01 (1990)

[2] H. Saeki, T. Momose, and H. Ishimaru. 'Observations of dust trapping phenomena in the TRISTAN accumulation ring and study of dust removal in a beam chamber', *Rev. Sci. Instrum.* **62**, 874 (1991)

[3] D. Sagan. 'Mass and charge measurement of trapped dust in the CESR storage ring', *Nucl. Instrum. Methods.* **A330** 371 (1993)

[4] F. Zimmerman. 'Trapped dust in HERA and prospects for PEP-II', *Technical Report PEP-II AP* Note No.: 8-94, (Stanford Linear Accelerator Center, 1994).

[5] D. R. C. Kelly. 'Characterisation of lepton beam lifetime behaviour in HERA', *Technical Report DESY HERA 95-01*', (Deutsches Elektronen Synchrotron, 1995).

[6] K. Fuke 'Photon Factory activity report #6',R-1, 1988

[7] P. Marin. 'Problems encountered with stray micro-objects in various ultra-high vacuum systems', *LURE, ORSAY* RT/93-04 (1993)

[8] Bialowons, W., Ridoutt, F., and Wittenburg, K. (1994), 'Electron beam loss monitors for HERA', in *Fourth European Particle Accelerator Conference (EPAC94)*, Vol. 2, p. 1628, World Scientific

[9] D. R. C. Kelly. 'Many-event lifetime disruption in HERA and DORIS', *Technical Report DESY HERA* 95-02, (Deutsches Elektronen Synchrotron, 1995).

[10] D. Sagan. 'Some aspects of longitudinal motion of ions in electron storage rings', Nucl.Instrum.Meth.**A307** 171 (1991)

[11] D. R. C. Kelly. 'The effect of beam excitation on the HERA electron beam lifetime disruption'. In *Fifth European Particle Accelerator Conference (EPAC96).*

[12] D. R. C. Kelly. 'The effect of transverse beam excitation and kicking on the HERA electron beam lifetime disruption'. To be submitted to *Nucl. Instrum. Methods.A* (1997)

[13] D. R. C. Kelly. 'The effect of a static clearing field on trapped dust particles in the HERA electron ring', To be submitted to *Nucl. Instrum. Methods.A* (1997)

[14] K. Kanazawa, (TRISTAN) pers.communication, (1995)

[15] H. Saeki, T. Momose, and H. Ishimaru. 'Motions of trapped dust particles around the electron beam in the TRISTAN accumulation ring', *Rev. Sci. Instrum.* **62**, 11 (1991)

[16] J. Kouptsidis,'Lebensdauerprobleme in Elektronenspeicherringen', in *HERA Seminar, Bad Lauterberg* DESY (1995)

[17] H. Ehrlichmann,'Untersuchung zur Elektronenlebensdauer in PETRA', in *HERA Seminar, St.Englmar* DESY (1996)

[18] W. Bialowons,'HERA Betrieb mit Elektronen', in *HERA Seminar, Hamburg* DESY (1997)

[19] CERN, LEP machine study 10 June 1995: S. Myers, F. Willeke, J. Kouptsidis, W. Bialowons, H. Ehrlichmann, K. Wittenburg, D. Kelly.

The TESLA Free Electron Laser

J. Rossbach, for the TESLA FEL collaboration
DESY, Notkestrasse 85, D22603 Hamburg, Germany

Abstract

The TESLA Free Electron Laser (FEL) makes use of the high electron beam quality that can be provided by the superconducting TESLA linac to drive a single pass FEL at wavelengths far below the visible. To reach a wavelength of 6 nanometers, the TESLA Test Facility (TTF) currently under construction at DESY will be extended to 1 GeV beam energy. Because there are no mirrors and seed-lasers in this wavelength regime, the principle of Self-Amplified-Spontaneous-Emission (SASE) will be employed. A first test of both the principle and technical components is foreseen at a photon wavelength larger than 42 nanometers.

With respect to linac technology, the key prerequisite for such single-pass, high-gain FELs is a high intensity, diffraction limited, electron beam to be generated and accelerated without degradation. Key components are RF guns with photocathodes, bunch compressors, and undulators. The status of design and construction as well as both electron and photon beam properties are discussed.

Once proven in the micrometer to nanometer regime, the SASE FEL scheme is considered applicable down to Angstrom wavelengths. This latter option is particularly of interest in context with the construction of a linear collider, which requires very similar beam parameters. The status of conceptual design work on a coherent X-ray user facility integrated into the TESLA Linear Collider design is briefly sketched.

1 INTRODUCTION

Most of the information humans receive from their environment are provided by photons. Thus it is not surprising that also for research in natural sciences photons, ranging from radio frequencies to hard γ-rays, provide the most important tool to study nature. For the photon range beyond the narrow optical spectral window up to the hundred keV γ-regime synchrotron radiation has provided over the past thirty years an increase in flux and brightness by more than ten orders of magnitude. The development of storage ring designs with special magnetic components, called wigglers and undulators, over the past twenty years has led to third generation machines specially designed for synchrotron radiation research.

Most recent successes in accelerator development concerning linear accelerators have opened the route to a new jump in photon source quality. X-ray lasers coupled to linear accelerators can possibly provide coherent X-rays with true laser properties through very long undulators. Although such a source of coherent laser-like X-rays would have many applications and the search for such a device has occupied many scientists, a practical solution to this problem has not yet been realized. To be an efficient research tool, such a source would have to provide stable intensities with short pulses and repetition frequencies similar to what is found in optical lasers. Exactly this seems to be possible by using the so-called self amplified spontaneous emission process SASE.

The basic principle [1] makes use of the fact that an electron beam of sufficient quality, passing a long undulator magnet, exponentially amplifies an initially existing radiation field, if the photon wavelength λ_{ph} matches a resonance condition determined by undulator parameters and the beam energy:

$$\lambda_{ph} = \frac{\lambda_u}{2\gamma^2}(1 + K^2) \qquad (1)$$

Here, γ is the electron energy in units of its rest mass, λ_u is the undulator period, K is the undulator parameter, and a helical undulator is assumed. Coherent, stimulated emission is achieved because a bunch density modulation of the electron beam at the optical wavelength builds up during the passage of the bunch through the undulator.

If the desired wavelength is very short, one can, instead of providing the "initially existing radiation field" by a conventional laser, consider the undulator radiation radiated spontaneously in the first part of the undulator as an input signal, see Fig. 1. This principle of Self-Amplified-

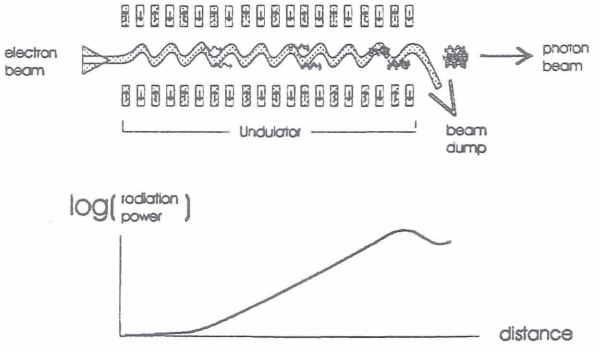

Figure 1: Schematic Diagram of a Single-Pass Free Electron Laser (FEL) operating in the Self-Amplified-Spontaneous-Emission (SASE) mode.

Spontaneous-Emission (=SASE) [2], [3] also does not require the optical cavity resonator normally used in multi-pass, longer wavelength FELs and can hence, in principle, deliver light with wavelength in the Angstrom regime. Compared to state-of-the-art synchrotron radiation sources, one expects a transversely fully coherent beam, larger average brilliance, and, in particular, a pulse length of about

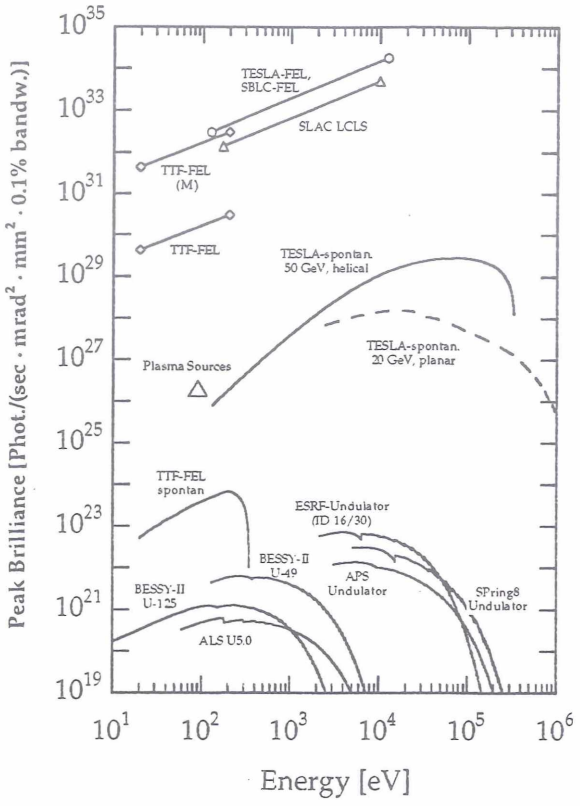

Figure 2: Spectral peak brilliance of X-ray FELs based on SBLC and TESLA linear colliders, together with that of third generation synchrotron radiation sources and the LCLS Free Electron Laser project discussed at SLAC, Stanford, USA [8]. For comparison, also the spontaneous spectra of two XFEL undulators are shown. The peak brilliance of state-of-the-art plasma lasers is also noted.

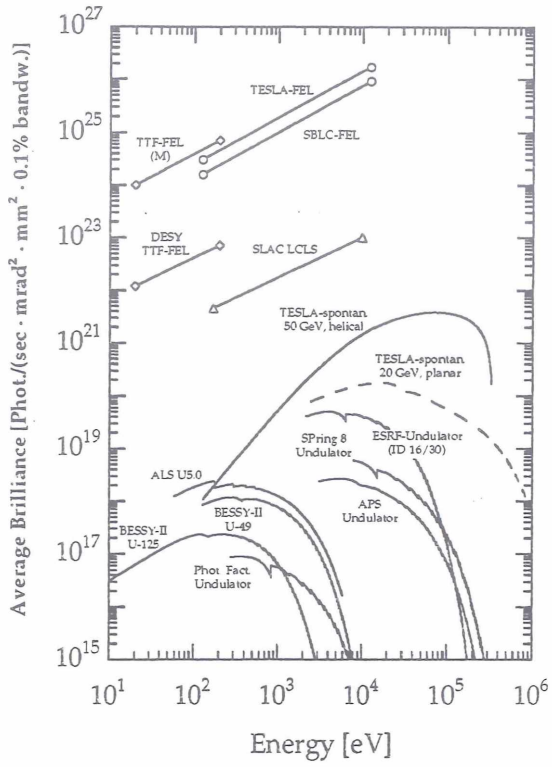

Figure 3: See Fig. 2, but spectral *average* brilliance values are shown.

200 fs FWHM with eight or more orders of magnitude larger peak brilliance, see Figs. 2 and 3. The peak power is in the range 1 – 100 GW. The average brilliance is significantly larger than for the LCLS device proposed earlier[8] mainly because TESLA accelerates a bunch train of ~10000 bunches at a rate of 5 Hz, i.e. the mean repetition rate is much higher. As the SASE FEL is completely independent of atomic excitation levels, it can be tuned over a wide range of wavelengths.

If, according to technical restrictions, undulator periods in the order of few centimeters are assumed, Eq.1 indicates that multi-GeV electron energies are required to achieve photon wavelengths in the Angstrom regime. This goes in parallel with the large energy gain needed in order to sufficiently reduce the beam emittance provided by the injector. Therefore, the electron accelerator required for an X-ray FEL will be a major investment. Also, construction, commissioning and operation of such a device needs a considerable staff of well-trained experts. Last but not least, a large laboratory site will be needed to accommodate the various user facilities. It was concluded, that it will be most attractive to combine an X-ray FEL facility into a linear collider installation [4], and that this will be possible without serious mutual interference.

2 THE TESLA CONCEPT

The different linac concepts considered by linear collider study groups mainly differ with respect to the choice of RF frequency [5]. Roughly speaking, higher RF frequencies offer a higher accelerating gradient, i.e. a shorter tunnel length, at the price of reduced power efficiency and larger beam energy spread. In contrast, low frequency linacs (down to 1.3 GHz for the superconducting TESLA linac) promise very good beam quality, because each electron bunch extracts only a small fraction of the large energy stored in the big cavity volume (small wakefield effects, see section 5). For an X-ray FEL, the highest priority is electron beam quality and large average beam current, while high accelerating gradient might be of minor importance. Finally, it is attractive for many users if a large variability in pulse timing can be offered. In this respect, the TESLA linac again offers an advantage, because a large variety of timing patterns can be realised due to the very large duty cycle of 1%. Thus, for FELs there is a clear preference for low frequency linacs. A Conceptual Design Report on such a combined laboratory has been worked out by the international TESLA collaboration [9]. This paper also discusses

a normal-conducting linac version based on conventional S-band technology (3 GHz), called SBLC.

It is understood that the challenging goal of an 1 Å FEL cannot be achieved within a single step. Thus, a SASE proof-of-principle experiment will be installed at the TESLA Test Facility (TTF), called TTF FEL Phase 1, see Fig. 4. Based on three TESLA accelerating modules, 390 MeV beam energy will allow to reach a photon wavelength of λ_{ph}=42 nm. First operation is scheduled for 1999. A more detailed description and the status is given in Ref. [6].

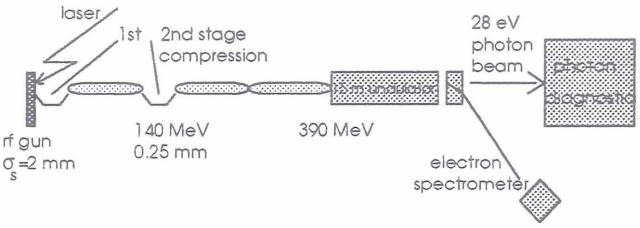

Figure 4: Schematic diagram of the TESLA Test Facility installation including the Phase 1 SASE FEL components.

As a second phase, an energy upgrade to 1 GeV has been approved which will bring the wavelength down to 6 nm in the first harmonic. Besides testing SASE in the soft X-ray regime, an attractive physics program has been identified for this installation [7], covering applications ranging from magnetic materials research and various pump-and-probe experiments to photochemistry and X-ray microscopy of biological samples. In the following sections, design and status of key TTF FEL components are discussed.

3 ELECTRON SOURCE

The transverse coherence condition imposes a tight requirement on the transverse emittance ε_t of the electron beam [10]:

$$\varepsilon_t^n \leq \frac{\gamma \lambda_{ph}}{4\pi} \quad , \tag{2}$$

ε_t^n is the normalized emittance. For λ_{ph}=6 nm, γ=2000, Eq.2 requires $\varepsilon_t^n < 1\pi$mm mrad. Actually, this condition is not very strict, but the saturation length significantly increases if ε_t^n is larger. Thus, we aim at $\varepsilon_t^n = 1\pi$mm mrad for the rms electron emittance of a 1 nC bunch charge from an RF electron gun [11], and we allow for a factor of 2 in emittance dilution during longitudinal bunch compression and acceleration up to 1 GeV, see Table 1.

Compared to state-of-the-art, space-charge compensated, RF photoinjectors [12], the TESLA gun has to provide a longer bunch train and smaller emittance. The laser developed [13] provides an intensity stability of a few % and will be delivered to DESY in summer 1997. Neodymium doped Yttrium-Lithium Fluorid (Nd:YLF) has been chosen as the active medium since it combines a small thermal lensing effect with a high induced emission cross section and a relatively long fluorescence lifetime (480 μs). A pulse train with the desired spacing is selected from the bunches in a pulse train oscillator working at 36 MHz by means of Pockels cells. The light pulses are amplified in a linear low gain amplifier chain and then quadrupled in frequency. Relay imaging techniques in combination with spatial filtering is used to produce a radially uniform intensity profile.

To gain in emittance, any asymmetries in the RF field have been avoided in the design. Since previous calculations have revealed an emittance contribution of more than 1 π mrad mm for a conventional asymmetric input coupler, a symmetric input coupler has been developed. Fig. 5 shows a schematic layout of the gun and the coupler. At present, most components have been built or are under construction. An Aluminum model has successfully been tested to verify the coupler and cavity geometry.

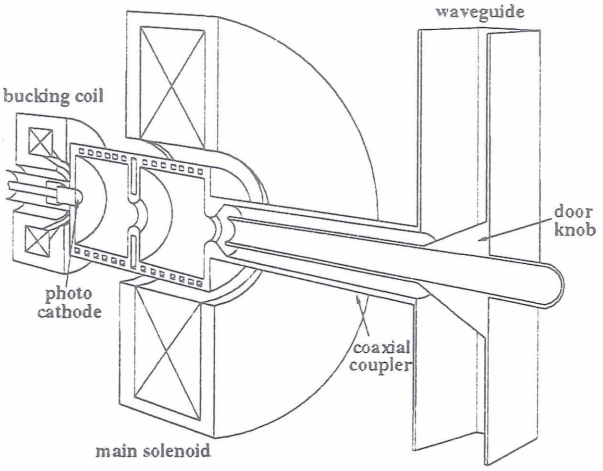

Figure 5: Cross sectional view of the RF gun (schematic) with the gun cavity, the cathode plug, the main solenoid and the bucking coil, and the coaxial input coupler. The RF is coupled from the rectangular waveguide via a door knob transition into the coaxial line and the cavity. The electrons leave the gun through the inner conductor.

4 BUNCH COMPRESSION

In order to achieve laser saturation within a single passage, XFELs require electron pulse currents of few kiloamperes. Because of space charge effects, such high currents cannot be generated directly from the RF gun cathode without blowing up the transverse emittance. Instead, a 7 ps long, 120 A beam is produced, accelerated, and longitudinally compressed by a factor of 20. This compression takes place in several steps at different energies. Bunch compressors are beamline sections which longitudinally compress the bunch using path length differences in a magnetic chicane. This is a well established technique, but has not yet been realized with extremely brilliant electron beams. Although simple in first-order theory, the physics of bunch compression becomes very challenging if collective effects like space charge forces [14],[15] and wakefields (see next section) are taken into account. Especially emittance conservation is then a critical issue [16].

Linac Parameters	Unit	TTF FEL Phase 1	TTF FEL Phase 2	TESLA X-ray FEL
gradient for XFEL operation	MV/m	10-15	10-15	10-25
linac repetition rate f_{rep} for XFEL	Hz	10	10	5
bunch length (rms)	fs	800	160	80
bunch spacing	ns	93	93	93
number of bunches per train		11315	11315	11315
bunch train length	μs	1050	1050	1050
bunch charge	nC	1	1	1
normalized emittance at undul. entrance	π mrad mm	2	2	1
longitudinal emittance	keV mm	166	50	27
RF duty cycle	%	1	1	0.5
FEL Parameters				
typical saturation length	m	<14	<27	50 - 100
undulator period length	mm	27.3	27.3	5 - 7
undulator K-parameter (planar)		1.27	1.27	4.1 - 5.6
photon wavelength range (1st harmon.)	nm	> 42	> 6	0.1 - 10
peak photon beam power	GW	0.2	3	60 - 280
number of photons per bunch	10^{12}	100	40	10 - 500
typical photon beam divergence (rms)	μrad	100	30	1
typical photon beam diameter (rms)	μm	70	55	20

Table 1: Parameters of the FEL at the TESLA Test Facility (TTF) (phases 1 and 2) and at the TESLA Linear Collider.

5 ACCELERATION

Each of the superconducting acceleration modules of the TESLA Test Facility provides a nominal acceleration of 120 MeV. For a more detailed desciption and the status, see Ref. [6]. With respect to FEL performance, a specific issue are the wakefields, because even for TESLA with its big cavity volume, the energy distribution inside each bunch is distorted or even dominated by longitudinal wakefields if the bunches are compressed to 50 μm rms bunchlength (phase 2). Analytical and numerical investigations have shown that the longitudinal wake potential accumulated over one TESLA module is close to the analytic solution of a point charge in an infinitely long periodic structure [18], see Fig. 6.

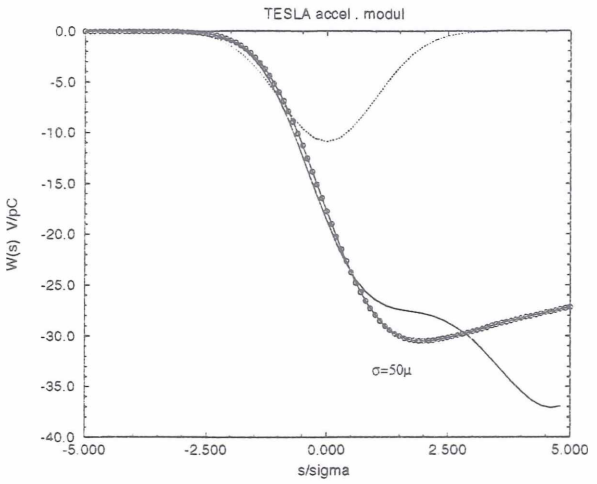

Figure 6: Wake potentials in the 8th cavity of a TESLA cryo-module for an rms bunch length of 0.05 mm and analytical approximation (circles). From Ref. [18].

6 UNDULATOR

The undulator is the most prominent FEL specific component. It has two functions: It has to provide the sinusoidal magnetic field so that the FEL process can take place, and, in order to keep the beam-size small over the whole undulator length, the undulator has to be combined with a superimposed periodic quadrupole lattice. The design for the TTF FEL is based on a planar hybrid permanent magnet undulator [19], see Table 1. It will be fabricated in modules 4.5 m long each, see Fig. 7. Between these modules and inside the 12 mm undulator gap a number of high resolution beam position monitors will be placed to ensure that the overlap between electron beam and photon beam stays within the specified tolerance of approx. 10 μm [20]. The undulator is using four additional magnets per halfperiod to provide focusing, see Fig. 8. A 220 mm long prototype has been built and tested, and two 1 m long prototypes are presently under construction.

7 PHOTON BEAM PROPERTIES

The prediction of photon beam parameters of short wavelength FELs is based on both an elaborate theory and various computer codes (for references, see [7] - [10]). Table 1 contains only few numbers on the expected FEL performance. The values quoted should be used as a guideline only, since there is no experimental experience yet in this wavelength regime. There is a radiation property that is specific to SASE FELs called superradiant spik-

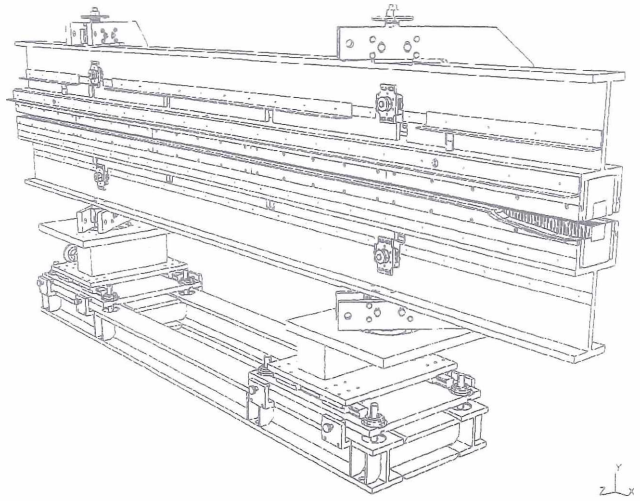

Figure 7: 3-D view of one undulator module for the VUV-FEL at the TTF. From Ref. [9].

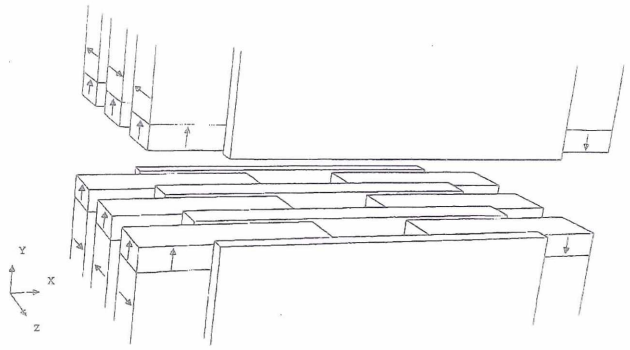

Figure 8: Perspective view of $1\frac{1}{2}$ periods of the TTF FEL undulator which combines undulator field and strong focusing. From Ref. [19]. The small pole pieces with magnetization perpendicular to the gap plane provide the focusing field.

ing [21]. Due to the statistical character of the start-up from noise, the FEL radiation intensity is not homogeneously distributed along the pulse length but concentrated within ultrashort pulses as long as the cooperation length. This length is typically about 1000 times the photon wavelength, i.e. much shorter than the bunch length. There is no phase correlation between these spikes, so the spike length reflects the longitudinal coherence of the radiation. The photon statistics has been shown to be that of completely chaotic polarized radiation [22]. A two-stage FEL scheme has been devised to considerably reduce the bandwidth [23]. In Figs. 2, 3 its performance is referred to by the index (M).

8 REFERENCES

[1] J.M.J. Madey, *Stimulated Emission of Bremsstrahlung in a Periodic Magnetic Field*, J. Appl. Phys. **42** 1906, 1971

[2] A. M. Kondratenko, E. L. Saldin, *Generation of Coherent Radiation by a Relativistic Electron Beam in an Ondulator*, Part. Accelerators, **10**, 207, 1980.

[3] R. Bonifacio, C. Pellegrini, L.M. Narducci, *Collective Instabilities and High-Gain Regime in a Free Electron Laser*, Opt. Cummun. **50**, No. 6 , 373, 1984.

[4] R. Brinkmann, et al., *An X-Ray FEL Laboratory as Part of a Linear Collider Design*, Proc. 1996 FEL Conf., to be Published in Nucl. Instr. Meth. A , 1997.

[5] G. A. Loew (ed.), *International Linear Collider Technical Review Committee Report*, SLAC-R-95-471, 1995.

[6] B. Aune, *Results from the DESY TESLA Test Facility, this conference*

[7] T. Åberg, et al., *A VUV Free-Electron Laser at the TESLA Test Facility at DESY, Conceptual Design Report*, DESY Print TESLA-FEL 95-03, 1995.

[8] H. Winick, et al., *A 2-nm - 4-nm Linac Coherent Light Source (LCLS) Using the SLAC Linac*. SLAC-PUB-6185, May 1993. 3pp. Presented at 1993 Particle Accelerator Conference (PAC 93), Washington, DC, 17-20 May 1993.

[9] R. Brinkmann, G. Materlik, J. Rossbach, A. Wagner (eds.), *Conceptual Design of a 500 GeV e+e- Linear Collider with Integrated X-ray Laser Facility*, DESY 1997-048 and ECFA 1997-182

[10] See e.g.: W.B. Colson, C. Pellegrini and R. Renieri (eds.), *Laser Handbook*, Vol.6, North-Holland, 1990

[11] J. Fraser and R. Sheffield, NIM **A 250** 71, 1986

[12] J.E. Clendenin, Proc. 18th Linac Conf., 298, Geneva, 1996

[13] I. Will, P. Nickles, W. Sandner, *A Laser System for the TESLA Photo-Injector*, internal design study, Max-Born-Institut, Berlin 1994.

[14] Ya. S. Derbenev, et al., DESY Print TESLA-FEL 95-05, 1995.

[15] E. L. Saldin, E. A. Schneidmiller, M. V. Yurkov, DESY Print TESLA-FEL 96-14, 1996.

[16] M. Dohlus, T. Limberg, *Wake Fields of a Bunch on a General Trajectory Due to Coherent Synchrotron Radiation*, this conference

[17] R. Tatchyn, et al. , Proc. PAC93, Washington, 1993.

[18] A.N.Novokhatski and A.Mosnier, *Short Bunch Wake Potentials for a Chain of TESLA cavities*, DAPNIA/SEA-96-08, 1996.

[19] J. Pflüger, Y. M. Nikitina, B. Faatz, T. Teichmann, *The undulator system for the VUV-FEL at the TESLA Test Facility*, Proc. 1996 Intl. FEL Conference, Rome, 1996, to be published.

[20] B. Faatz, J. Pflüger, Y.M. Nikitina, *Study of the Undulator Specification for the VUV-FEL at the TESLA Test Facility*, Proc. 1996 Intl. FEL Conference, Rome, 1996, to be published.

[21] R. Bonifacio, et al., Phys. Rev. Lett. **73** 70, 1994.

[22] E. L. Saldin, E. A. Schneidmiller, M. V. Yurkov, DESY Print TESLA-FEL 97-02, 1997.

[23] J. Feldhaus, et al., *Possible Application of X-ray Optical Elements for Reducing the Spectral Bandwidth of an X-ray SASE FEL*, Proc. 1996 Intl. FEL Conference, Rome, 1996, to be published.

The Usage of Transient Recorders in the Daily HERA Machine Operation

R. Bacher, M. Clausen, P. Duval and L. Steffen, DESY, Hamburg, Germany

Abstract

Many parameters of HERA machine components such as RF systems or quench protection as well as important beam parameters are continuously measured using transient recorders. In general, these recorders are not synchronized among one another and sample the data with very different rates ranging from 200 Hz to 50 MHz. At present, work is going on to integrate the different existing transient recorders into a global system. The article reviews the transient recorder hardware in operation at HERA. In addition, the proposed trigger distribution based on the HERA Integrated Timing system as well as the software concept to archive, retrieve and display the data will be described.

1 INTRODUCTION

The HERA accelerator complex is a proton-electron collider. A proton beam of more than 70 mA is injected at an energy of 40 GeV into a ring of superconducting magnets and accelerated to 820 GeV. Electrons are transferred to HERA at 12 GeV and ramped to 27 GeV using conventional magnets. Typical electron currents are about 40 mA. A successful fill remains stored in HERA about half a day. Less than 50 % of the time scheduled for physics experiments can be used for data taking. The remaining fraction is mainly dominated by the filling, ramping and tuning processes. In particular, the filling of protons takes a long time. Therefore, the most unfavourable situation in the daily operation of HERA is the loss of one or even both circulating beams. If the origin of the beam loss can be uniquely identified, improvements of the machine operation or the technical components can be performed. However, a loss not understood contains the risk of a new loss during the following run. Besides a reduction of the running efficiency, losses can generate dangerous situations for the superconducting magnets and radiation-sensitive components close to the beam pipe of the physics detectors.

To identify the reasons for beam losses, many parameters of HERA machine components like RF systems or quench protection as well as important beam parameters are continuously measured using transient recorders. In general, these recorders are not synchronized among one another and sample the data with very different rates ranging from 200 Hz to 50 MHz. This lack of synchronization often does not allow us to disentangle the temporal or causal development of a beam loss. At present, work is going on to integrate the different existing transient recorders into a global system. In addition, a new universally usable recorder is currently being developed. This article reviews the transient recorder hardware in operation at HERA. The proposed trigger distribution based on the HERA Integrated Timing system as well as the software concept to archive, retrieve and display the data will be described.

2 EXISTING TRANSIENT RECORDER SYSTEMS

At present, more than 100 parameters such as phase and amplitude of the different electron RF transmitters as well as of the feeding HV power supplies are recorded at different locations along with the electron current. Commercially available PC boards (Bakker BE 490) with 8 inputs each are used. The sampling rate and the storage capacity per channel are 100 kHz and 20k byte, respectively. The analog signals are converted by a 12-bit ADC. The data recording can be stopped by an external or an internal trigger. The software runs on top of Windows 3.1 and has no networking functionality. The different PC's can be remotely controlled via PCAnyWhere. Only a couple of parameters of the proton RF system are continuously measured. The system is controlled and operated by a front-end DOS-PC sampling the data every some milliseconds. An external trigger is not implemented.

The HERA quench protection system for the superconducting magnets is the most prominent user of transient recorders. For diagnostic purposes more than 1400 voltages measured across the magnets and with respect to ground are stored in case of a quench. The transient recorder boards used have been developed at DESY as dedicated measuring devices. The boards are distributed in the HERA tunnel along the magnets. The sampling rate and the number of data samples per channel are 250 Hz and 1k, respectively. A 12-bit ADC measures the voltages between +5 V and -200 V or +25 V and -1000 V. A cluster of about 20 boards is read out by a VME-CPU via a commercial field bus (CAN). The data taking is stopped one second after the corresponding CAN broadcast message. The control, archiving and display software has been written at DESY using C and Visual Basic.

The proton beam diagnostics makes extensive usage of dedicated post-mortem memories. The proton beam loss rates are measured at about 250 locations every 5 ms. A history of 128 data samples is stored as well as 128 average loss rates integrating over 128 measurements. At almost the same locations, the proton

beam orbit is recorded. Horizontally and vertically, the last 1024 turns are stored as well 256 closed orbit data samples gained by averageing over 128 turns. In each case, data taking is stopped by a common hardware trigger released from the beam loss detection or the quench protection system. The data are read out via DESY standard field bus lines (SEDAC) by a DOS-PC belonging to the HERA control network. Front-end control and display application software are written in C and VisualBasic, respectively.

The current pulses of the 12 kickers and septum magnets necessary to eject the beams from the booster accelerator PETRA and to inject the beams into HERA are recorded at every transfer process. Standard HP digital scopes and PC ADC boards from National Instruments are used. The sampling rates differ from 250 kHz for septum pulses to 5 MHz and 50 MHz for kicker pulses. Per pulse 512 data samples are taken. The Scopes are controlled by PC's via GPIB. A LabView application displays the traces.

3 DEVELOPMENTS FOR FUTURE USAGE OF TRANSIENT RECORDER SYSTEMS

At present, work is going on in order to enhance the profit which can be gained from the usage of transient recorder systems.

- Improved functionality of the power supply controllers to store permanently with 12-bit resolution the set value of the current as well as the actual values of current and voltage. The sampling rate will be less than 1kHz. More than 1000 data samples per channel can be stored. The data stored in about 680 controllers will be read out via SEDAC lines by a server responsible for all magnets and currently under development.
- Enlarging the number of measured parameters. A couple of signals from the electron and proton multi-bunch feedback and the electron tune controller will be recorded in the future. In addition, the currents of the electron and proton reference bunches as well as more parameters of the HV power supplies for the electron RF transmitters will measured continuously.
- Implementation of networking capability into the software of the Bakker BE 490 boards. The software has been completely re-written at DESY to support the VxWorks operating system on PC hardware. This allows us to integrate the boards into the HERA control system keeping the same flexibility as in the original Windows 3.1 environment
- Development of a low-cost multi-purpose transient recorder at DESY with moderate sampling rate. A cluster of 8 or 16 channels will share the same clock and memory. The probes with the ADC's can be configured according to the dedicated measuring requirements (isolation to ground, amplitude and band width of input signals). Analog and digital electronics can be separated by about 20 m. In addition, 12 digital input ports are offered per cluster, which can be logically combined to generate stop trigger conditions. Also a simple threshold as well as a software trigger functionality will be foreseen. The sampling rate will be about 100 kHz which is twice the revolution frequency of HERA. The sampling process can be synchrozid to the HERA clock system if requested. It is proposed to connect the clusters to a field bus e.g. CAN or to an Ethernet line.
- HERA-wide trigger distribution for a simultaneous stopping of data tating of all or a subset of all transient recorder systems. The HERA Integrated Timing (HIT) system offers the possibility of distributing events along HERA. Independent of location at HERA, the HIT system guarantees the synchronization of the events. Two trigger conditions are foreseen: (1) proton beam loss and (2) electron beam loss. The generation of triggers can be inhibited by additional conditions like beam energy or beam current thresholds as well as by a operator or control system request. In addition, triggers can be released by software events.
- Integration of all different transient recorder and post-mortem systems into the HERA control system which will be described in the following section.

4 SOFTWARE ARCHITECTURE FOR AN INTEGRATED ARCHIVE SYSTEM

A common application to remotely operate the various transient recorders and post-mortem systems e.g. to set a trigger threshold is not practicable. The systems are mostly part of complex technical systems and will be operated by dedicated applications.
However, starting the archiving of the data after a freeze trigger and the retrieving of the data for display and analysis puposes must be handled in a common way. Due to the very different hardware and software concepts a heterogeneous software architecture as shown in Fig. 1 with the following specifications has been chosen:

- client-server prinicple,
- modularity, distribution of functionality over 3 software layers (front-end, middle and application layer) reflecting the different needs of the different systems, easily adding of components in all layers,
- distributed archiving, shared usage of all archives, no standard data base format,
- standardized interface to the network using in-house Remote Procedure Calls (RPC) based on IP sockets,
- open for a wide range of platforms (UNIX-like systems, Windows NT),
- open to add commercial data bases such as Oracle or future software standards like JAVA applets.

Attached to each Archive Server is a set of Device Servers reflecting different transient recorders. If

the data taking of any transient recorder channel (Device) is stopped by an external or internal trigger the corresponding Archive Server will ask an Event Server for a unique event number (Unix time stamp). All requests even from different Archive Servers within a short time interval are tagged by the same event number. The Archive Servers start their archive processes locally and store all data delivered from the Device Servers in a unique way. A standardized gobal data header is added to each archive and a local header is added to the data set of each device which has stopped sampling. The global header contains all information to characterize and select the archive event, e.g. the event number, the number of stored data sets or a comment. The local header consists of individual information such as sampling rate, number of data samples or number of pre-trigger values which are necessary to display the data. During the archiving the Archive Server does not accept any other event number. After the completion of an archiving process the corresponding Archive Server reports to the Event Server the names of the Device Servers which have delivered data for this particular event.

The Event Server stores a list of all event numbers and the additional information obtained from the various Archive Servers. It creates automatically an event code which contains encoded information to be used by filtering routines. A similar event code is generated at the Archive Server level.

All triggers distributed by the HIT system are marked with the current HIT time stamp (Trigger Server), i.e. the actual value of the revolution counter. This time information allow us to correlate data sets generated even by different trigger sources.

To display data by an application client, first a query is sent to the Event Server to obtain the event numbers and the contents of the archives stored within a certain time interval. In a second step the Archive Servers are asked to provide more specific informations about the data sets stored as available from the global and local data headers. Finally, the application requests the measured data to be displayed.

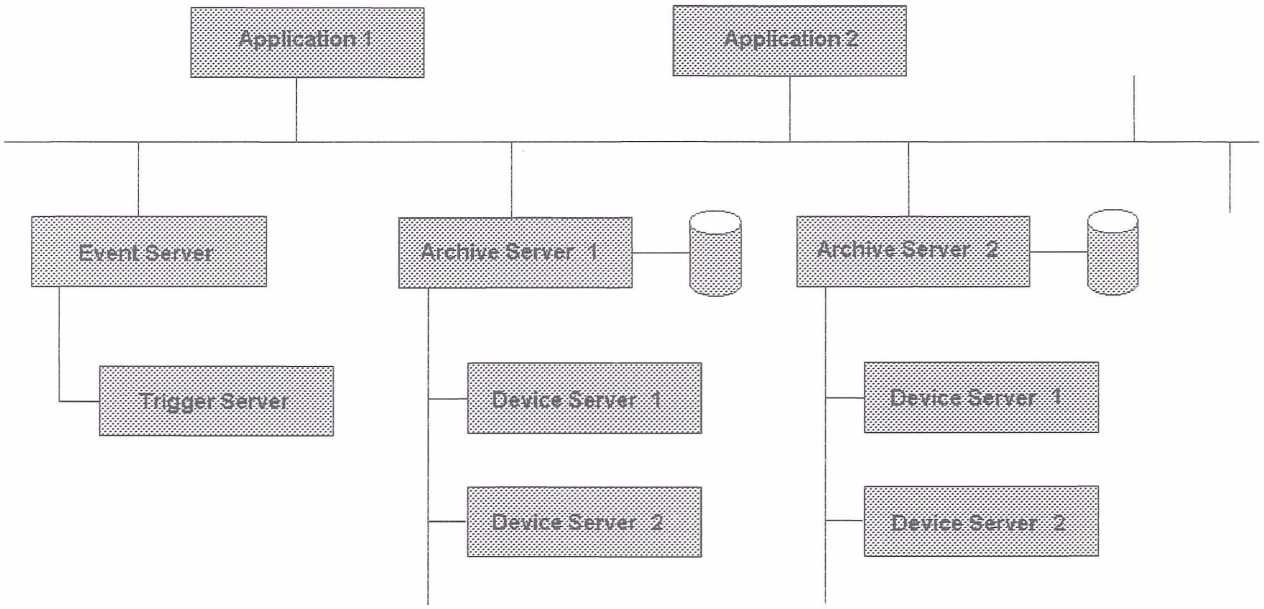

Figure 1: Software Architecture for an Integrated Transient Recorder Archive System

5 STATUS AND OUTLOOK

The software modules described in sections 3 and 4 are currently developed. The production of the hardware to distribute triggers via the HIT system is almost finished. The design work for the low-cost multi-purpose transient recorders has been started. It is expected that all transient recorder and post-mortem systems already existing will be integrated into a common system at the beginning of the 1998 running period of HERA. Additional systems will be added in the future according to the availability of the new hardware components.

6 ACKNOWLEDGEMENTS

The encouraging help and engagement of K.-H. Meß (low-cost multi-purpose transient recorder) and S. Pätzold and H.-T. Duhme (trigger distribution) is gratefully acknowledged.

FIRST BEAM TESTS OF THE TTF INJECTOR

T. Garvey, M. Bernard, J.C. Bourdon, R. Chehab, M. Mencik, M. Omeich, J. Rodier,
M. Taurigna-Quere and A. Variola.
Laboratoire de l'Accélérateur Linéaire, IN2P3 - CNRS, Orsay, France.

S. Chel, M. Desmon, J. Fusellier, F. Gougnaud, J.F. Gournay, M. Jablonka, J.M. Joly,
M. Juillard, Y. Lussignol, A. Mosnier and B. Phung Ngoc.
CEA, DSM/DAPNIA, Saclay, France.

S. Buhler and T. Junquera.
Institut de Physique Nucléaire, IN2P3-CNRS, Orsay, France.

Abstract

Following tests of the various sub-assemblies at Saclay and Orsay, installation of the entire TESLA Test Facility Injector was completed in Hall 3 at DESY in December 1996. The first phase of operation employs a 250 kV thermionic electron source providing an 800 μs train of bunches, each containing 37 pC, and followed by a 216.7 MHz pre-bunching cavity. Subsequent bunching and acceleration is achieved using a standard 1.3 GHz superconducting 9 cell TESLA cavity operated in pulsed mode (10 Hz). Prior to injection in the main linac, the beam parameters are verified using a spectrometer consisting of a dipole magnet and SEM profile monitor. Once the beam is adjusted it is transported to the linac using an optical matching system employing two triplets. We present results of the first beam tests of the completed injector which took place early in 1997.

1 INTRODUCTION

The TESLA Test Facility (TTF) is a high duty cycle superconducting (SC) electron linac and its associated infrastructure. The L-band (1.3 GHz) linac will be used as a test bed to validate the principle of a SC e^+e^- linear collider (TESLA). TTF is currently under construction by an international collaboration at the DESY laboratory (Hamburg). Within the collaboration the three French laboratories named above have undertaken the task of constructing a pulsed SC injector for the linac. Descriptions of the linac and its injector can be found elsewhere [1,2] and here we will restrict ourselves to a report of the first beam tests with the complete injector which took place in January/February of this year. Tight scheduling of the installation of the first linac cryomodule meant that only four weeks of operation were available for these tests.

2 THE CAPTURE CAVITY

The capture cavity is a standard 9 cell TESLA cavity fabricated by CERCA. Its cryostat (CRYOCAP) was built and tested by the IPN-Orsay. Cryogenic tests and tests of the analogue feedback loops were performed at Orsay and Saclay. The feedback system is described in a companion paper [3]. It allows the cavity to operate with an amplitude stability better than 0.1% and a phase stability of less than 1 degree. Although the cavity has operated at 18 MV/m without field emission (FE) in a horizontal cryostat, we restricted our tests to 14 MV/m. This was due to the FE now seen at the latter gradient which results in a reduction of the Q factor to 5×10^8 and a high X-ray level around the cryostat. No high power RF processing was applied following the installation. During operation at 14.8 MV/m we measured a dark current level of 300 nA on a Faraday cup (ϕ = 25 mm) placed 1.15 m upstream of the first cavity iris.

3 BEAM ACCELERATION TESTS

The "pre-injector" consists of a 250 keV electron source, a 216.7 MHz sub-harmonic buncher (SHB) and four solenoidal focusing elements. Tests of the pre-injector have been reported previously [4]. The SC 'capture cavity' is used to provide further longitudinal bunching and to accelerate the beam to the desired energy (typically 8 to 12 MeV). Tuning of the injector is achieved by varying the amplitudes and phases of the SHB and capture cavity. The criteria for correct tuning during these tests has been the achievement of a minimum in the beam energy spread while ensuring maximum current transmission along the injector. The energy spread is measured using a spectrometer arm consisting of a magnetic dipole and an SEM-grid to measure the horizontally dispersed beam profile [5]. The current is measured with the use of toroidal current monitors. Four such monitors are mounted on the injector. Toroids #1 and #2 are at the entrance and exit respectively of CRYOCAP, #3 is on the spectrometer arm (upstream of the SEM-grid) and #4 is at the end of the injector.

3.1 *Beam transmission measurements*

The required current for TTF is 8 mA during an 800 μs macropulse at 10 Hz repetition rate. As the average beam power in the TTF linac is high, a differential protection system, based on the toroidal current monitors, is used to protect the machine against beam losses [6]. This system cuts off the gun if an integrated charge loss of 80 nC is detected between successive toroids during the macropulse. This corresponds to an average current loss of 0.1 mA during an 800 μs pulse (or 1.25% of the 8 mA beam). The same system is employed on the injector and

thus setting up the injector requires careful adjustment of the RF cavities and magnetic elements. Consequently, the injector is tuned using a "short pulse mode" of 30 μs duration. For the commissioning tests the loss threshold for the long pulse or "un-restricted mode" was increased to 200 nC between toroids #2 and #3.

With the beam well centred at the entrance to CRYOCAP one quickly obtains 100% transmission of 8 mA through the capture cavity and upto the end of the injector. The beam energy is measured using the spectrometer while the cavity gradient can be estimated from the incident power. The ratio of the energy gain to field gradient is consistent with calculations [7]. Typically we obtain 11 MeV for 12.5 MV/m. Figure 1 shows signals from the first three toroid monitors superimposed. The SHB uses a feedback loop to correct the phase and amplitude changes induced by beam loading. Left uncorrected, an 8 mA beam would induce a phase shift of 18° of the 216.7 MHz. In practice, the feedback system is capable of compensating for the beam loading with the exception of the first 8 μs during which a residual phase shift of < 5° is present. This effect explains the difference in current level between the first two toroids and the dispersed beam on toroid #3 during the pulse rise time (Fig. 1, left). This can be cancelled by applying a "phase-jump" to the cavity with a sense opposed to that induced by the beam (Fig. 1, right).

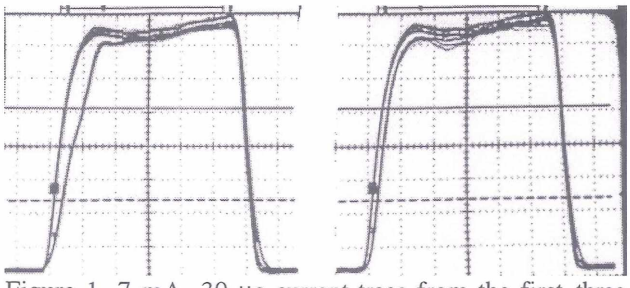

Figure 1. 7 mA, 30 μs current trace from the first three toroids; (left) without phase jump, (right) with phase jump (see text for details).

3.2 *Energy spread measurements*

The spectrometer dipole produces a dispersion of 16 mm/% of energy spread at the location of the SEM-grid. The grid contains tungsten wires of 20 μm diameter spaced at 2 mm intervals and is intended for use with the full pulse width. The first tests with 8 mA of accelerated beam showed that the transmission to the beam analysis line was only 90%, insufficient for switching to the long pulse mode. In view of the limited time available for injector tests, rather than investigating this loss in detail, we reduced the current to 6 mA for which the transmission to the analysis line was 97%, just enough to operate in long pulse mode and thus to investigate the distribution in energy. Figure 2 shows the output of the grid for an 11 MeV beam. The RMS energy spread is 68 keV. Several measurements made for different current levels (from 2 to 6 mA) show that the fractional RMS energy spread is always inferior to 0.8% when the injector is properly adjusted.

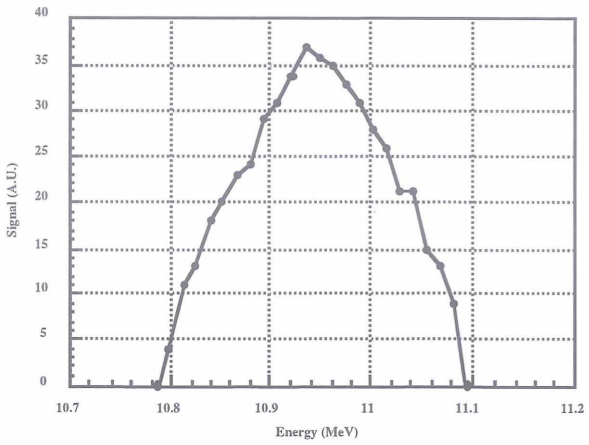

Figure 2. Beam energy distribution obtained on the SEM-grid.

4 EMITTANCE MEASUREMENTS

The transverse emittance has been obtained from measurements of the transverse beam profile using optical transition radiation (OTR). An aluminium foil of 20 μm thickness is employed as the radiator. Light from the OTR foil is focused onto a gated, intensified CCD camera using a telescope composed of two achromatic lenses with a magnification of 0.5. Data acquisition is obtained by means of a CPU operating in a VxWorks environment. A frame grabber and the camera record signals with an 8 bit resolution. The camera is synchronised to the master oscillator of the injector and the gain and shutter time are contolled by a serial port of the CPU. Acquisition, image processing and statistical analysis are performed using an "in-house" computer program so allowing on-line calculation of the emittance. Fig. 3 shows a typical example of an acquired profile. Emittance measurements are taken with a macropulse of 30 μs width to avoid damage to the aluminium foil.

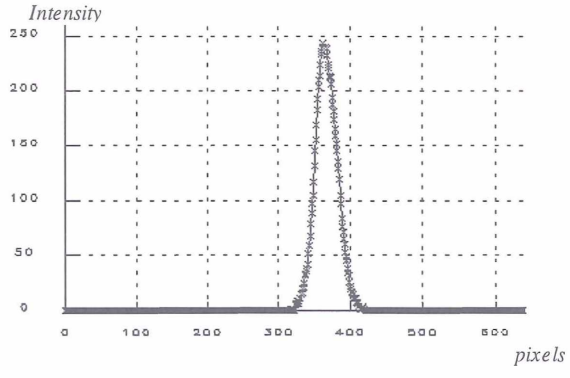

Figure 3. Horizontal profile of the beam from the OTR image. The scale is 37 μm/pixel.

To obtain the Twiss parameters of the beam we have used the method of "three gradients". The focusing of the beam is varied by means of a magnetic triplet placed

upstream of the OTR foil and the beam profile recorded for each setting. To improve the reliability of the fit between the beam radii and the triplet strengths, ten images are recorded for each of eleven different settings of the triplet. Statistical analysis of the image sets allows the beam radii and the related standard errors to be calculated. The radii are calculated for 50% and 90% intensity contours as well as for the FWHM. These calculations are performed both for the integrated profiles and for the horizontal and vertical profiles through the centre of charge of the beam. All these data are then fitted using an "in-house" chi-square minimisation routine. At our energy and with our experimental layout the approximation of a thin lens for the triplet is not valid. Consequently, we use the real transport matrix values. As well as the emittance, we also calculate the error to the fit, the covariance matrix, the beam matrix coefficients and the chi-square value as a measure of the statistical degree of confidence of the measurement [8].

Emittance measurements have been performed for various beam energies and linac optics. At 10.6 MeV, and with correct setting of the injector optics, the 90% contours give normalised emittances of ε_x = 16.5 mm-mrad and ε_y = 18 mm-mrad for the horizontal and vertical planes respectively. During the triplet scan, the beam centroid was seen to displace in the verical direction and so the larger emittance values in the this plane may be due to an imperfect vertical alignement of the beam in the triplet. The corresponding figures for the 50% contour are 2.4 mm-mrad and 2.8 mm-mrad. Similar values were obtained for a beam energy of 8.7 MeV. In varying the trigger time and acquisition period of the camera, time resolved measurements of the emittance were also obtained by recording profiles for 1 μs slices within the macro-pulse. These data show slightly smaller values for the "slice" emittance during the pulse rise-time with stable values found during the flat-top.

5 CONTROLS

The control system for the injector has been described elsewhere [9]. The system is based on EPICS with VME crates for equipment interface and SUN workstations as operator consoles. During the entire commisioning period the controls have been very reliable. Extensive use has been made of the EPICS task to 'save' and 'restore' machine parameters. The operator can create special "parameter' pages which can be assigned to eight encoder 'knobs' allowing analog control of eight parameters and making visible useful information. Binary control, such as the insertion of diagnostics or ON/OFF control of power supplies, is also permitted with these pages.

6 CONCLUSIONS

We have presented results of the first operation of a high field gradient (> 10 MeV/m), pulsed mode, superconducting linac. These tests show that the linac performs as foreseen and that certain specified beam parameters have been met (table 1). The emittance values are consistent with measurements made on the gun and pre-injector [4,10]. Injector tests will resume in May of this year and the transmission of 8 mA onto the spectrometer arm will be investigated further. In addition, the measurement of the micropulse length will be performed by streak camera analysis of the OTR.

Table 1. Comparison of achieved and specified parameters.

	Specified	Achieved
Energy	> 8 MeV	8 - 13.5 MeV
Current	8 mA	8 mA
Pulse width	800 μs	800 μs
RMS energy spread	< 100 keV	~ 70 keV*
RMS emittance	< 5 mm-mrad	< 4 mm-mrad

(* at 6 mA)

7 ACKNOWLEDGEMENTS

We are indebted to the technicians from Saclay and Orsay for their efficient installation of the injector on the DESY site. The participation of K. Honkavaara (SEFT, Helsinki) in the tests is gratefully acknowledged. We are pleased to acknowledge the enthusiastic participation of DESY personnel during the commisioning period of the injector, especially to B. Aune, A. Gamp, K. Rehlich, T. Schilcher and H. Weise. The injector uses a timing system that was built by M. Shea and M. Kucera of Fermilab.

REFERENCES

[1] The TESLA Collaboration, "TESLA Test Facility Linac - Design Report", (Ed. D.A. Edwards), DESY print TESLA 95-01.

[2] R. Chehab et al., "Progress in the Study and Construction of the TESLA Test Facility Injector", Proc. of the 1995 Particle Accelerator Conference, pp 998-1000, (Dallas), 1995.

[3] A. Mosnier et al., " RF Control System for the SC cavity of the TESLA Test facility", these proceedings.

[4] J. Fusellier et al., " First Tests of the 250 keV Electron Source and Beamline for the TESLA Test Facility Injector", Proc. of the 1996 European Particle Accelerator Conference (Sitges), pp 1541-43.

[5] M.Bernard et al., "Secondary Emission Grids for Low Energy and High Energy Electron Beams", Proc. of the 1996 European Particle Accelerator Conference (Sitges), pp 1690-02.

[6] J. Fusellier and J.M. Joly, "Beam Intensity Monitoring and Machine Protection by Toroidal Transformers on the TESLA Test Facility", Proc. of the 1996 European Particle Accelerator Conference (Sitges), pp 1591-93.

[7] M. Ferrario et al., "Multi-bunch energy spread induced by beam loading in a standing wave structure", Particle Accelerators, Vol 52, pp1-30, 1996.

[8] A. Variola, Ph.D. thesis in preparation.

[9] F. Gougnaud et al., "The TESLA Test Facility Controls" presented at the International Conference on Accelerator and Large Experimental Physics Control Systems (Chicago), 1995.

[10] T. Garvey et al., "Simulations and Measurements of the TTF phase I injector gun", Proc. of the 1995 Particle Accelerator Conference, pp 935-37.

Design of a Damping Ring for the SB-Linear-Collider Project at DESY

R.Brinkmann[1],D.Einfeld[2],M.Plesko[3],J.Schaper[2]
[1] DESY, Notkestr. 85, D-22607 Hamburg, Germany
[2] Fachhochschule Ostfriesland, Constantiapl. 4, D-26723 Emden,Germany
[3] J.Stefan Institute, Jamova 39, SLO-1001 Ljubljana,Slovenia

Abstract

For the SB-Linear-Collider project (SBLC) at DESY a redesign of the damping ring has been performed, mainly in order to optimise the dynamic aperture. The lattice of the proposed damping ring has a DBA structure, similar to the 3rd generation light sources ESRF, APS and SPRING-8. The damping ring is build up with 6 superperiods. The straight sections between these periods are used for the injection, ejection and rf-cavities. In turn, each superperiod consists of 6 DBA cells. The straight sections of these cells are used for the installation of the wigglers, which are needed for the damping. With the installation of overall 150 m of wigglers (B_0 = 2 T and λ_0 = 0.2 m) the equilibrium emittances are $\varepsilon_{x,0} = 6.5 \cdot 10^{-10}\ m \cdot rad$ and $\varepsilon_{y,0} = 1.3 \cdot 10^{-11}\ m \cdot rad$ (the corresponding normalised emittances are : $\varepsilon_{x,n} = 3.8 \cdot 10^{-6}\ m \cdot rad$ and $\varepsilon_{y,0} = 7.6 \cdot 10^{-8}\ m \cdot rad$. The damping time results in $\tau_y \leq$ 3.4 ms. The dynamic acceptance including misalignment and magnet errors is in the range of $A_x \leq 72\ mm \cdot mrad$ and $A_y \leq 80\ mm \cdot mrad$.

1 INTRODUCTION

1.1 General

High luminosity in linear colliders can only be reached by damping the beam in a so called damping ring before it is accelerated to high energies. For the S-Band-Linear-Collider project (SBLC) at DESY [1] the beam has to be damped to normalised emittances $\varepsilon_{x,n} < 5{\cdot}10^{-6}\ m{\cdot}rad$ and $\varepsilon_{y,n} < 2.5{\cdot}10^{-7}\ m{\cdot}rad$ within a time of 19.6 ms corresponding to the repetition frequency of 50 Hz. According to the pulse structure within the linacs (2 μs) the circumference of the damping ring has to be larger than 600 m. The current within one pulse should be 300 mA. In order to reach these parameters the damping ring must have a sufficient dynamic aperture for the injection process and a sufficient lifetime. To meet the requirements on the damping time, damping wigglers have to be introduced. Conventionally, such a ring is realized by a racetrack structure [2] [3][4]: two arcs with bends and two long straight sections that accommodate the damping wigglers, injection, extraction and the RF-system. In such a scheme the dynamic aperture is drastically reduced by introducing the long straight sections for the damping wigglers.

In comparison to these design the 3rd generation light sources like ESRF, APS, ALS, ELETTRA [5] etc. have a relatively large dynamic aperture. Investigations at these projects have shown that the installation of insertion devices doesn't reduce the dynamic aperture very much.

1.2 Damping Ring Requirements

The damping of the emittance within a storage ring is,

$$\varepsilon_f = \varepsilon_{inj} \cdot e^{-2t/\tau_D} + \varepsilon_{equ} \cdot (1 - e^{-2t/\tau_D}) \qquad (1)$$

where ε_f is the final emittance, ε_{inj} that one of the injected beam and ε_{equ} is the equilibrium emittance of the damping ring. τ_D is the damping time of the ring and t is the accumulation time within the ring, t = 19.6 ms.

The evaluation of eq.(1) gives for the damping ring the following requirements : $\varepsilon_{x,n} = 4 \cdot 10^{-6}\ m \cdot rad$, $\varepsilon_{y,n} = 2 \cdot 10^{-7}\ m \cdot rad$, $\tau_D \leq 3.5$ ms.

Here, an emittance dilution budget of 25 % from the damping ring to the IP is taken into account. The energy of the damping ring should be in the range between 2.5 and 3.5 GeV. At an energy of 3 GeV the normalised emittance of $4 \cdot 10^{-6}\ m \cdot rad$ translates into an absolute horizontal emittance of $6.7 \cdot 10^{-10}$ $m \cdot rad$ which is the domain for a fourth generation light source, about an order of magnitude below existing third generation light sources.

The small emittance of the injected electron beam ($\varepsilon_{x,n} = 1 \cdot 10^{-4}\ m \cdot rad$) results in a relaxed dynamic aperture ($\approx 10\ \pi \cdot mm \cdot mrad$ for the electron damping ring (DR). Quite different is the situation for the positron DR. The emittance of $1 \cdot 10^{-2}\ \pi \cdot mm \cdot rad$ results in a beam size at injection of 5 mm. According to the fast damping ($\tau_D \leq 3.5$ ms) this value will be damped within 3.5 ms down to 1.8 mm. We assume that an aperture of 3 $\sigma_{x,inj}$ = 15 mm should be enough for the positron damping ring, resulting in an acceptance of 20...30 $\pi \cdot mm \cdot mrad$.

2 LATTICE

2.1 Lattice of the base ring

We took as the base of the redesign the lattice of the ESRF [6] and performed the following alterations : 1.) Reduction of the circumference from 880 m to 660 m. 2.) Decreasing the radius of curvature of the bending magnets in order to enhance the damping. 3.) Changing of the deflection angle from 5.625 degree to 5.0 degree in order to reduce the emittance and increase the number of straight sections from 32 to 36.

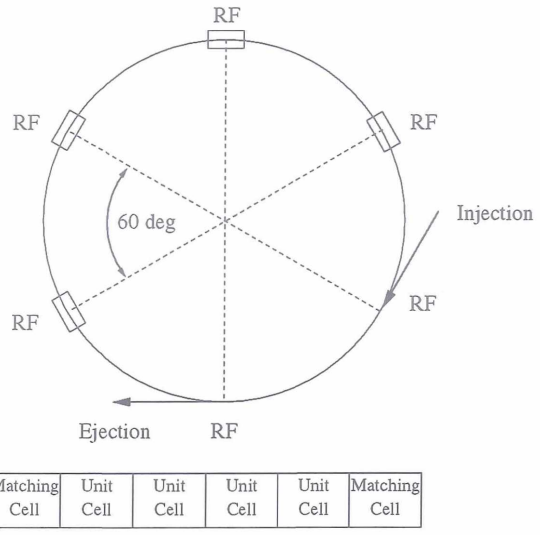

Figure 1: Schematic layout of the SBLC-DR. With a sixfold symmetry. each superperiod consists of five unit cells and two matching sections.

2.2 Introduction of damping wigglers

Six straight sections are needed for injection, extraction and the rf-system. With an equal distribution of them around the ring we have a sixfold symmetry. The length of a straight section - from quadrupole to quadrupole - is 6 m. With 5 m long wigglers an overall length of 150 m of wigglers can be installed. The maximum magnetic field within the wiggler has been set to 2.0 T and the period length to 0.2 m.

The wigglers have an effect on the damping time, the energy spread and the emittance. The emittance is reduced five-fold, the damping time by a factor of 7.5 and the energy spread increases by 3.1. Including the wigglers the ring has the following parameters : $\varepsilon_{x,0} = 6.5 \cdot 10^{-10}\ m \cdot rad$, $\varepsilon_{y,0} = 0.13 \cdot 10^{-10}\ m \cdot rad$, $\tau_\varepsilon = 1.67$ ms,$\tau_x = 3.34$ ms, $\tau_y = 3.34$ ms.

2.3 Damping Ring Layout

The schematic layout of the SBLC-DR is presented in fig. 1. The DR has a sixfold symmetry and each superperiod consists of five unit cells with two matching sections. The unit cells are the normal DBA-structures with a damping wiggler in the straight section. The matching sections are the places for the injection, ejection and the rf-system. The lattice functions of the superperiod are presented in fig. 2.

In order to have within the matching sections the same phase advance as within the unit cell one has to introduce in the straight section of the matching section some extra quadrupoles because the wigglers within the straight section of the unit cell perform a focusing in the vertical direction. The dynamic aperture including misalignment and some magnet errors is given in fig. 3. At injection the aperture is a factor 5 larger as the positron beam size. This is sufficient.

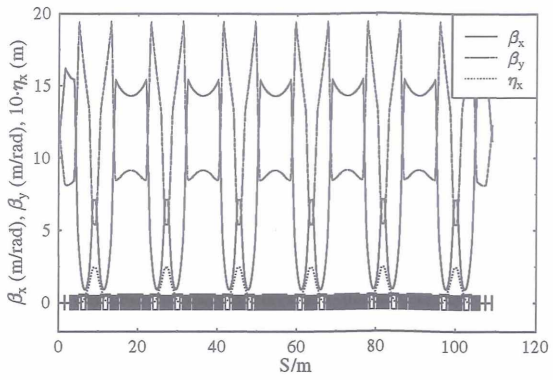

Figure 2: Lattice functions within one superperiod of the SBLC damping ring. Each superperiod consists of the unit cells with wigglers and two matching sections at each side.

The energy acceptance of the DR is larger as 4 %.

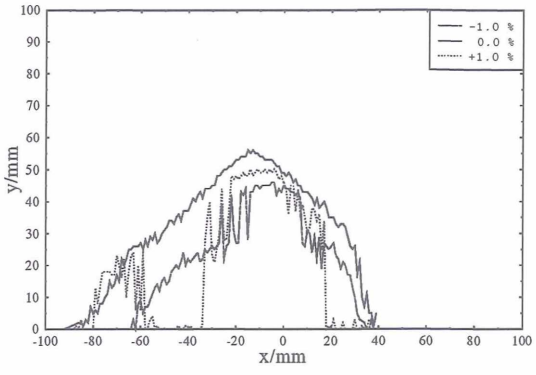

Figure 3: Dynamic aperture of the SBLC-damping ring with field errors $\Delta B/B = 5 \cdot 10^{-4}$ for the bending and $\Delta G/G = 5 \cdot 10^{-3}$ for the quads.

3 ALIGNMENT TOLERANCES AND THE VERTICAL EMITTANCE

The vertical equilibrium emittance is essentially determined by the magnet and beam position monitor (BPM) alignment tolerances and by the orbit correction procedures applied. We used the PETROS computer code to simulate alignment errors and orbit correction procedures. Assuming rms magnet and BPM position tolerances of 50 μm, the MICADO algorithm is applied in several iterations until the quality of the orbit does not improve anymore. From 10 different random seeds of errors we obtain an average vertical normalised emittance of $(1.0 \pm 0.9)10^{-7}\ m \cdot rad$. So the required emittance could just be achieved with the assumed tolerances and standard correction techniques.

4 RF-SYSTEM

The layout of the RF-System is determined by the radiation loss per turn U_0 and the required energy acceptance. For the SBLC-DR U_0 = 3.95 MeV (including the damping wigglers) and the energy acceptance $(\Delta E/E)_{RF}$ should be at least 10 times the energy spread. With an overvoltage factor q = 2 the energy acceptance is 7.2 %. There has to be installed an overall voltage of 7.9 MV with a beam power of P_{beam} = 1.2 MW. The number of cavities is determined by the power which can be fed through the input coupler. Currently, both normal or superconducting cavities are being considered. For the ELETTRA normal conducting cavity [7] as well as the HERA superconducting one [8] it is around 110 kW. Hence overall 10 to 12 cavities have to be installed. The CESR superconducting cavity [9] is designed for an input power up to 250 kW. Already achieved have been 150 kW. This means that 5 to 8 cavities have to be installed. The specifications of the CESR cavity are: G = 6 MV/m, V_{RF} = 1.8 MV, $Q_0 = 10^9$, (R/Q = 89 Ω/cell, $Q_L = 2 \cdot 10^5$ and $l_{eff} = 0.3m$). Taking 5 cavities with a gradient of 1.8 MV/cell the overall RF voltage leads to q = 2.6, with an RF energy acceptance of 7.2 %. By taking the phase ϕ_s = 22.62 degrees, the synchrotron tune results in $\nu_s = 8.92 \cdot 10^{-3}$, $\Omega_s = 2.55 \cdot 10^4$, f_s = 9.724 kHz.

The bunch length is then, with $\sigma_E/E = 2.2 \cdot 10^{-3}$, equal to σ_z = 4.25 mm .

5 INSTABILITIES

5.1 Single Bunch Instabilities

The microwave instability, sometimes referred to as turbulent bunch lengthening, causes an increase in both the momentum spread and the bunch length of a bunched beam. With I_{aver} = 0.8 mA per bunch, $\alpha = 1.64 \cdot 10^{-4}$, $\sigma_z = 4 \cdot 10^{-3}$ m, $(\sigma_E/E) = 2.2 \cdot 10^{-3}$ and R = 104 m one gets for the broad band impedance a maximum allowed value of $[Z_n/n]$ = 0.3 Ω that would avoid the instability. According to some measurements the contribution of the vacuum chamber at ELETTRA has a value of 0.15 Ω [10]. We assume a similar value here as well. From the measured loss factor of the CESR superconducting cavity [9] a broad band impedance of 0.03 - 0.05 Ω could be determined. With 8 cavities the contribution of the RF-system to the broad band impedance is 0.24 - 0.4 Ω. From this we can estimate the impedance as : $[Z_n/n]$ = (0.4 - 0.7) Ω, which is about a factor of two larger than desirable. Taking into account the SPEAR-scaling this value reduces down to 0.06 Ω . So bunch lengthening seems to be avoidable, but not with a large safety margin and further studies of this issue are required.

5.2 Multibunch Instabilities

With 333 stored bunches and a total current of 300 mA, multibunch instabilities are of concern. Stability is guaranteed if $(1/\tau_{||}) < (1/\tau_\varepsilon)$. $1/\tau_{||}$ is the growth rate of the longitudinal coupling bunch instability and τ_ε is the damping time of the synchrotron oscillations. Taking a shunt impedance of $R_{s||}$= 200 $k\Omega$ (which is typical for a normal conducting cavity) results in a maximum current of 136 mA. The shunt impedances of the HOM's within a CESR superconducting cavity are in the range of 0.1 - 0.7 $k\Omega$, leading to an instability threshold of I > 380 mA. Hence the coupled bunch instability are of no importance when using superconducting cavities.

There are coupled bunch instabilities in the transverse direction, too. For a transverse impedance of $R_\perp$= 11 MΩ/m (which is typical for a normal conducting cavity) the maximum stored beam within the DR is 4.0 mA. The transverse impedances of the CESR-SC-cavity are smaller than 0.025 MΩ/m leading to a threshold current of 1760 mA. In this case, however, other contributions to the impedance (in particular the resistive wall impedance) may become dominant. Whether or not a feedback system is required, must be determined by more detailed investigations. In any case it should be noted that the issue of multibunch instabilities is significantly relaxed compared to the B-factory rings presently under construction at SLAC and KEK.

6 REFERENCES

[1] Linear Collider Design Report, DESY-97-048

[2] R. Brinkmann, A Study of Low - Emittance damping ring Lattices, DESY M-90-09, July 1990

[3] ATF, Accelerator Test facility, Design and Study Report, Internal 95-4, June 1995

[4] NCL damping ring, Zeroth-Order Design Report for the next Linear Collider, SLAC, Stanford, 1996

[5] ESRF Foundation Phase Report, February 1987, European Synchrotron Radiation Facility, B.P.220-38043, Grenoble Cedex

[6] J. Murphy, Synchrotron Light Source DATA Book, BNL/NSLS, BNL 42333, Version 4

[7] M.Svandrlik et al. The Cure of Multibunch instability in ELETTRA, Proceedings of the PAC 95, Dallas, Texas, USA

[8] R. Byrns, B.Dwersteg et al., Status of the Superconducting Cavity, Program for HERA, Proceedings of the EPAC 90, Nice, June 12-16, 1990

[9] S.Belomestnyk et al. Wakefield and HOMs Studies of a Superconducting Cavity Mode with the CESR Beam, Proceedings of the PAC 95, Dallas, Texas, USA

[10] J.E. Karantzoulis, The Coupling Impedance of the ELETTRA Storage Ring ST/M-TN-90/14, August, 1990, Sincrotrone Trieste

EMITTANCE DILUTION THROUGH COHERENT ENERGY SPREAD GENERATION IN BENDING SYSTEMS

P. Emma, *SLAC, Stanford, California,* USA*
R. Brinkmann, *DESY, 22603 Hamburg,* GERMANY

Abstract

For a bunched beam, coherent energy spread generated within a bending system may couple to the transverse (bending) plane coordinates through the chromatic transfer functions of the particular beamline—even an achromatic beamline. The resulting transverse emittance dilution is dependent on the magnitude of the energy spread, its generation rate along the beamline, and the beamline's chromatic transfer functions. The coherent energy spread may be due to resistive-wall wakefields or coherent synchrotron radiation. For specific beamlines, such as a periodic arc or wiggler, the longitudinal-to-transverse coupling is minimal and, in ideal cases, completely suppressed resulting in reduction or cancellation of all transverse emittance dilution effects. This is of particular interest for micro-bunch transport or compression systems such as exist in future FEL or linear collider projects.

1 INTRODUCTION

Many FEL and future linear collider projects utilize transport lines which bend high energy bunched electron beams—with bunch lengths in the sub-picosecond range—in order to achieve this bunch compression or, in some cases, simply to transport the micro-bunch [1,2,3]. Unfortunately, several processes exist which may generate significant energy spread as the bunch traverses this beamline, especially for a very short bunch. Along with the well known stochastic process of quantum fluctuations which produce an incoherent, random energy spread within the bunch, several mechanisms produce a coherent energy spread along the bunch such as resistive wall wakefields [4] or coherent synchrotron radiation [5,6,7].

An electron which, for example, looses energy, $\delta(s) \equiv \Delta E(s)/E_0$, at location s within this bending system will be transported to its end through the chromatic transfer functions, $\partial x/\partial\delta \equiv R_{16}(s)$ and $\partial x'/\partial\delta \equiv R_{26}(s)$, which map an off energy particle from the point of energy loss into transverse phase space at the end of the bending system. Since the energy loss can be different for different particles, the resulting energy spread can potentially dilute the transverse emittance in the bending plane depending on the coherence of the process. A random process results in an intrinsic emittance dilution which is not recoverable while a coherent energy spread generates a projected emittance dilution where correlations among the beam coordinates remain. The latter is therefore a reversible process. We present a few idealized bending systems which, depending on the details of the coherent energy spreading process, minimize or cancel this emittance dilution. We do *not* examine the actual energy spreading processes which lead to this dilution and in most cases we use an idealized or simplified model of the process.

* Work supported by Department of Energy contract DE-AC03-76SF00515

2 EMITTANCE DILUTION

The bend plane phase space coordinates of a particle are expressed as the vector $\mathbf{x} = [x\ x']^{\mathrm{T}}$, and the rms emittance, ε, is then taken from the covariance of the particle ensemble.

$$\varepsilon^2 = \det\left\langle \mathbf{x}\cdot\mathbf{x}^{\mathrm{T}} \right\rangle \tag{1}$$

As defined in the previous section, when a particle looses (or gains) energy at a location s within a bending system (even an achromatic system) its final (bending-plane) phase space coordinates at the end of the system will be altered with respect to the on-energy particle as

$$\mathbf{x}_s = \mathbf{x}_0 + \Delta\mathbf{x}(s) = \mathbf{x}_0 + \begin{bmatrix} R_{16}(s) \\ R_{26}(s) \end{bmatrix}\delta(s)\ . \tag{2}$$

(For simplicity we define coordinates such that $\langle\mathbf{x}\rangle = \langle\Delta\mathbf{x}\rangle = 0 = \langle\delta\rangle$). From Eq. (1) and (2) and an input emittance ε_0, the final emittance at bend system end is

$$\varepsilon^2 = \varepsilon_0^2 + \varepsilon_0\left[\beta\left\langle\Delta x'^2\right\rangle + 2\alpha\left\langle\Delta x\Delta x'\right\rangle + \gamma\left\langle\Delta x^2\right\rangle\right] + \left\langle\Delta x^2\right\rangle\left\langle\Delta x'^2\right\rangle - \left\langle\Delta x\Delta x'\right\rangle^2 \tag{3}$$

where β, α and γ are the nominal Twiss parameters at bend system end. The second line of Eq. (3) is an additive emittance even for a zero-emittance input beam.

For an incoherent energy loss process (i.e. δ is random with no correlation to other phase space coordinates) we first calculate the variance of $\Delta\mathbf{x}$ due to the incremental energy spread generated at each location s and sum these in quadrature over the beamline as uncorrelated quantities.

$$\left\langle\Delta x^2\right\rangle_{\mathrm{inc}} = \int R_{16}(s)^2\,\frac{d}{ds}\sigma_\delta^2 ds \tag{4}$$

The square of the generated energy spread is represented by its rate along the beamline (similar relation for $\Delta x'$).

For a coherent process, where a particle's energy deviation is purely a function of its longitudinal position along the bunch, the transverse coordinate shifts, $\Delta\mathbf{x}(s)$, which originate at each s location add linearly, so we first sum $\Delta\mathbf{x}(s)$ over s and then find its total variance.

$$\left\langle\Delta x^2\right\rangle_{\mathrm{coh}} = \left(\int R_{16}(s)\frac{d\sigma_\delta}{ds}ds\right)^2 \tag{5}$$

Here the incremental energy spread generation is expressed as a rate along the beamline (similar relation for $\Delta x'$).

The difference between the incoherent and the coherent process is now clear as Eq. (4), the incoherent process, represents a monotonically increasing summation of positive values, whereas Eq. (5), the coherent process, is a summation of signed quantities which may vanish.

The full emittance dilution for the coherent process is then written from Eq. (3) where, due to coherence, the correlation $\langle \Delta x \Delta x' \rangle^2 = \langle \Delta x^2 \rangle \langle \Delta x'^2 \rangle$, and so the second line (additive emittance) is zero.

$$\varepsilon^2 \approx \varepsilon_0^2 + \varepsilon_0 \frac{1}{\beta}\left[\left\langle \Delta x^2 \right\rangle + \left(\alpha \left\langle \Delta x^2 \right\rangle^{1/2} + \beta \left\langle \Delta x'^2 \right\rangle^{1/2} \right)^2 \right] \quad (6)$$

The variances above are taken from Eq. (5). Here we assume full coherence so that, for example, a particle's energy deviation is solely a function of 1) its longitudinal position within the bunch and 2) a scalar which is equal for all particles at any particular location s along the beamline, but may vary with s (e.g. due to changing bunch length). This assumes particles do not shift with respect to each other in the bunch as will occur with a longitudinal phase space rotation of $>\pi/2$. We, therefore, only consider a functional energy dependence along the bunch whose shape does not vary significantly with s.

3 ARCS, WIGGLERS AND CHICANES

Several bending systems are of interest in future FEL and linear collider designs. We use as examples, a periodic FODO-cell arc, a simple wiggler and a magnetic chicane. There are two cases of interest for each. If we restrict ourselves to processes such as coherent synchrotron radiation (CSR) or resistive wall wakefields, which generate coherent energy spread of a magnitude which depends on the bunch length, then it is worth distinguishing between a simple transport line, where the bunch length is virtually constant, and a compressor, where the bunch length is reduced (or increased) along the beamline. We now describe how Eq.'s (5) and (6) apply to an arc, a wiggler and a chicane.

3.1 Arc

We restrict our analysis to an arc of constant bending radius constructed of FODO cells and which includes appropriate periodic dispersion matching and suppression sections prior to and following the FODO cells.

The chromatic transfer functions, $R_{16}(s)$ and $R_{26}(s)$, which map from locations s within an arc to just beyond the final dispersion suppression bend, can be shown to be periodic functions which oscillate about zero over the arc. Fig. 1 shows the dispersion function, η_x, and the transfer functions, as defined above, for a 36°-arc composed of 15 FODO cells of ψ_x = 108°/cell. Note, η_x maps δ (originating upstream of the first bend) to x at a location s in the arc, whereas the transfer functions map δ (originating at s) to x at a location beyond the last bend.

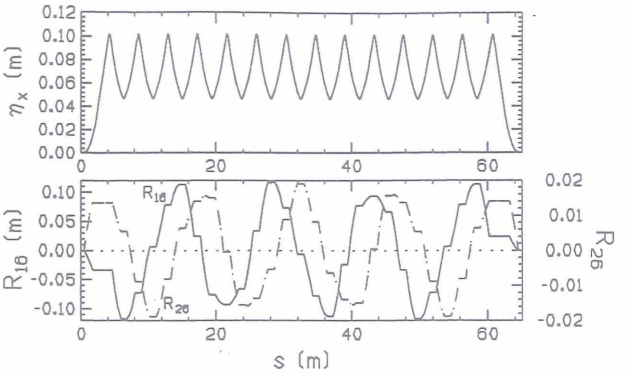

Figure 1. Dispersion function (top) and chromatic transfer functions (bot), for the example FODO-cell arc.

This arc has a 9π total phase advance and the dispersion function is matched to the periodic solution. In this case, the mean $R_{16}(s)$ and $R_{26}(s)$ are nearly zero. Therefore, a constant energy spread generation rate (e.g. constant bunch length) will generate almost no emittance increase. In Eq. (5) this implies extracting the constant energy spread rate from the integral leaving expressions for the mean R_{16} and R_{26}, both of which are nearly zero.

For a compressor-arc (changing bunch length), the energy spread generation rate must be included to evaluate the emittance growth. Fig. 2 shows the CSR emittance growth as a constant length bunch moves through the arc (a) and also for a compressing bunch (b).

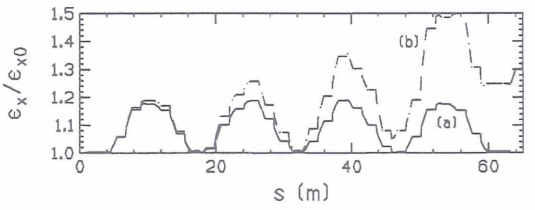

Figure 2. Fractional CSR emittance growth in arc for a constant 25-μm bunch (a) and a compressing bunch of 25-10 μm (b). The charge is 2 nC and input emittance is $\gamma\varepsilon_0 = 1$ μm.

In Fig. 2 the incremental rms coherent energy spread at each dipole magnet slice is generated as 'steady-state' CSR [7], ignoring vacuum chamber shielding, using

$$\Delta\sigma_\delta(s) \approx 0.22 \frac{r_e N \Delta L_B}{\gamma \rho^{2/3} \sigma_z^{4/3}} , \quad (7)$$

where N is the bunch population, ΔL_B is the dipole magnet slice length, ρ is the bend radius, σ_z is the bunch length, r_e is the classical electron radius and γ is the Lorentz energy factor. For a constant bunch length the net arc emittance growth is zero but oscillates by up to 20%. The compressing bunch destroys the symmetry and in this case produces a net 30% growth.

3.2 Wiggler

As an example of a wiggler system [8] we take the TESLA bunch compressor at DESY [9] which compresses a 9 mm rms bunch to 600 μm. The system is composed of eight 16° bends and two 8° bends to introduce an energy

dependent path length. The dispersion function and the transfer functions, as defined above, are shown in Fig. 3. As in the case of the arc, the transfer functions oscillate around zero.

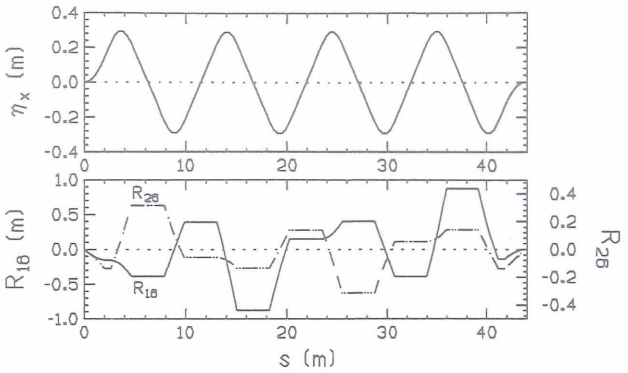

Figure 3. Dispersion function (top) and chromatic transfer functions (bot) of the TESLA bunch compressor wiggler.

The CSR emittance growth across this wiggler is shown in Fig. 4 for a 1-mm constant bunch length (a) and also a compressing bunch from 9 to 0.6 mm (b).

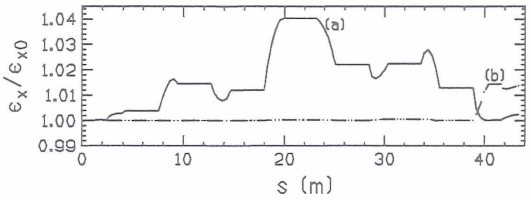

Figure 4. Fractional CSR emittance growth in wiggler of Fig. 3 for a constant 1-mm bunch length (a) and for a compressing bunch of 9-0.6 mm (b). The charge is 6 nC and input emittance is $\gamma\varepsilon_{x0} = 8$ μm.

Although the CSR effects are small, the constant bunch results in nearly full cancellation of emittance dilution whereas the compressing bunch results in a 1.5% dilution.

3.3 Chicane

As an example of a four-dipole magnetic bunch-compressor chicane we take the second compressor of the Linac Coherent Light Source (LCLS) [1] at SLAC. Its function is to compress a 390 μm rms bunch to 20 μm. This is in a regime of significant CSR and potential emittance dilution. A single 13.2-meter chicane with four 3.6°, 1.5-meter long bends can be used to make the compression but CSR calculations show the emittance more than doubles for a 1-nC beam and input emittance of 1 μm (the transfer functions do not oscillate about zero).

To compensate we form a double chicane of twice the length with separating optics (4 quadrupoles) to introduce a $-\mathbf{I}_{2\times2}$ bend plane transfer matrix between chicane centers. The first chicane bend angles are reduced (increasing the bunch length there which reduces the CSR energy spread) and the second chicane is set to complete the 20 μm final bunch compression such that dilution effects of the first chicane cancel with the second. The chicanes may also be empirically adjusted, if necessary, to minimize the observed dilution while maintaining final compression. The dispersion function, bunch length (σ_{z1}=single-chicane, σ_{z2}=double-chicane) and emittance growth are shown in Fig. 5 (top-dash is η_x of the single chicane).

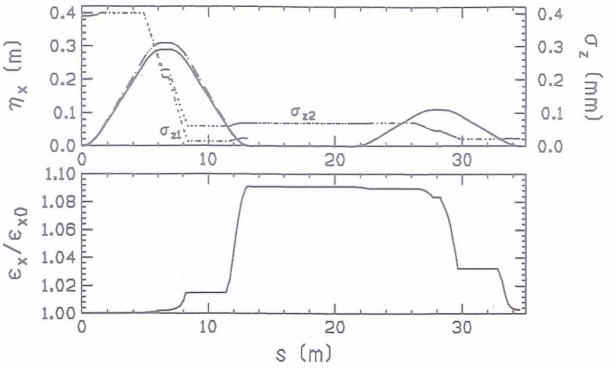

Figure 5. Dispersion (top-solid), bunch length (top-dots) and CSR emittance growth (bot) in single (σ_{z1}) and double (σ_{z2}) chicane for compressing bunch of 390-20 μm (top-dash is η_x of single chicane). The charge is 1 nC and $\gamma\varepsilon_{x0} = 1$ μm. Emittance growth of single-chicane ($\varepsilon/\varepsilon_0 \approx 2.3$) is not shown.

4 CONCLUSIONS

We have demonstrated that for a pure coherent energy spread generated within a bending beamline the resulting transverse emittance dilution can be minimized or canceled by a judicious choice of optics. The inherent periodicity of a FODO-cell arc and a wiggler generate cancellations which, for constant energy spread generation rate, can neutralize emittance growth. Variations on these basic bunch-compressor beamlines (e.g. the double chicane) can also be designed to compensate the emittance, even for a sharply compressing bunch. This compensation may prove useful in future FEL and linear collider projects which transport extremely short bunches.

5 REFERENCES

[1] V.K. Bharadwaj, et al., "Linac Design for the LCLS project at SLAC", these proceedings.

[2] "Zeroth-Order Design Report for the Next Linear Collider", SLAC Report 474, May 1996.

[3] "Conceptual Design of a 500 GeV e^+e^- Linear Collider with Integrated X-ray Laser Facility", DESY 97-048, 1997.

[4] O. Napoly and O. Henry, "The Resistive-Pipe Wake Potentials for Short Bunches", Part. Acc., Vol. 35, pp. 235-247, 1991.

[5] M. Dohlus and T. Limberg, "Wake Fields of a Bunch on a General Trajectory Due to Coherent Synchrotron Radiation", these proceedings.

[6] E.L. Saldin, et al., "On the Coherent Radiation of an Electron Bunch Moving in and Arc of a Circle", TESLA-FEL 96-14 (Nov. 1996).

[7] Ya. S. Derbenev, et al., "Microbunch Radiative Tail-Head Interaction", DESY, Sep. 1995.

[8] T.O. Raubenheimer, et al., "Chicane and Wiggler Based Bunch Compressors for Future Linear Colliders", SLAC-PUB-6119, May 1993.

[9] P. Emma, "Bunch Compressor Beamlines for the TESLA and S-band Linear Colliders", DESY-TESLA 95-17 (July 1995).

ULTRA-SHORT BUNCHES BY USING A QUASI-CONTINUOUS COMPRESSOR SCHEME IN A LONG BEAM TRANSFER LINE

H. Schlarb and R. Brinkmann, DESY, Notkestr.85, D-22603 Hamburg, Germany

Abstract

Integration of an X-Ray Free Electron Laser facility is planned in the TESLA design for a future e^+e^- Linear Collider. In the present scheme, the FEL drive beam is transported to a central user facility in a several km long beamline. In this paper we present how the longitudinal wakefield effect for short bunches in combination with a special beamline magnetic lattice can be used to obtain compression down to an rms-bunch length in the range of a few μm. Peak current of more than 50 kA would enable the X-Ray FEL facility to generate photon wave lengths in the sub-Angstrom regime.

1 DESIGN OF THE TRANSFER LINE

In the current design for a future **T**era **E**lectron Volt **S**uper Conducting **L**inear **A**ccelerator (TESLA) the drive beam for the X-Ray FEL is compressed to a bunch length of σ_z = 25 μm and accelerated in the LINAC to energies of E_0 =15 to 50 GeV. After 3 km the beam is kicked into a 12 km long transfer line and transported to the central user facility, close to the high energy physics laboratories. An intensive study of wakefields, excited in resistive beam pipes and in the TESLA acceleration modules, opens up the possibility to start with an initial bunch length of 50 μmand end with rms-values of 2 μm. In the design proposed here the bunch compression takes place over several stages using the longitudinal properties of the wakefields in combination with compressor modules situated along the beamline. The stages can be decomposed as follows:

- **Pre-compression:** using the LINAC wakefields (σ_z = 50 μm→5 μm)
- **Over-compression:** interchange of the tail and the head of the bunch (σ_z = 5 μm→8 μm)
- **Compensation:** energy correlation from the LINAC wakefields is eliminated by the resistive wall wakefields (σ_z = 5 μm)
- **Correlation:** rebuilding of an energy correlation using again the resistive wall wakefields (σ_z = 5 μm)
- **Final Compression:** using energy correlation of the previous stage (σ_z = 5 μm→2 μm)

In order to simulate the various stages a 1-dimensional numerical code has been written. The initial beam parameters are given in the following table :

Quantity		Units	Value
Energy	E_0	GeV	30.0
Long. Emittance	ϵ_z	keV mm	25.0
Charge	Q_0	nC	1.0
Bunch length	σ_z (rms)	μm	50.0
Peak current	I_{peak}	kA	2.4

Following points are considered:

- Random distribution in the long. phase space
- Wakefields (resistive tube & LINAC)
- Compaction factor in the compressor modules
- Space charge effects.

2 COMPRESSOR MODULES

A special beamline magnetic lattice, 240 m long, with a closed dispersion trajectory and a tuneable positive momentum compaction[1] of α_c = 1-3·10^{-5} is used to compress the bunch. One module consists of three dipoles (bend-radius = 1.2 km, length = 5, 10, 5 m) and FODO-cell structure ($\beta_{x,y}^{aver}$ = 20 m, 22.5 m).

3 WAKEFIELDS

In the present scheme the longitudinal correlation between energy and position inside the bunch is generated by the electromagnetic fields co-travelling with the bunch.

3.1 *Resistive Wall Wakefields*

Wakefields induced in a cylindrically tube of finite conductivity are well understood. Analytical solutions for the delta wake potential in the ultra-relativistic limit, up to any multipole order[2], have been derived in [1, 2, 3]. It has been shown that the short range wakefields can be decomposed in a high frequency ($k_r = \sqrt{3}/\zeta_0$) strongly damped ($\alpha_r = 1/\zeta_0$) oscillator and an additional diffusion term. The characteristic length ζ_0 will be given by

$$\zeta_0 = \left(\frac{2b^2}{Z_0\sigma_0}\right)^{1/3} \quad (1)$$

where b denotes the radius, σ_0 the conductivity of the wall material and Z_0 =120 π the impedance of vacuum. For a stainless steel tube σ_0 =1.4·10^6 Ω^{-1}m^{-1} and a radius of

[1] Definition of α_c is given by $\Delta L/L \equiv \alpha_c \Delta E/E$ where L denotes the length of the module and E the energy of the particles.

[2] In the following only the monopole term is considered. The higher orders ($n > 0$) inherent by the fraction $(r/b)^{2n}$ where r denotes the transverse off-set of the beam from the center of the pipe. They can be neglected for ($r \ll b$).

$b = 5$ cm the characteristic length is $\zeta_0 = 211\mu$m. For two point-like particles the longitudinal monopole wake potential reads[3][4][2]

$$W_{0,\parallel}(\zeta) = -\frac{Z_0 c}{\pi b^2}\left(\frac{4}{3}\, e^{-\alpha_r \zeta}\, \cos(k_r \zeta) - \frac{12\sqrt{2}}{3\pi}\int_0^\infty dx\, \frac{x^2\, e^{-x^2 \alpha_r \zeta}}{x^6+8}\right) \quad (2)$$

with ζ the distance between the source charge and the test charge. For velocities v smaller than the speed of light c the effective bunch length at the wall and the retarded effect of the 'radiated' electromagnetic fields produced by the image current modify the delta wake potential for very short distances $|\zeta| < b/\gamma$, where γ denotes the Lorentz factor. The longitudinal delta wake potential per unit length as a function of ζ is shown in Fig.1. For distances in the range

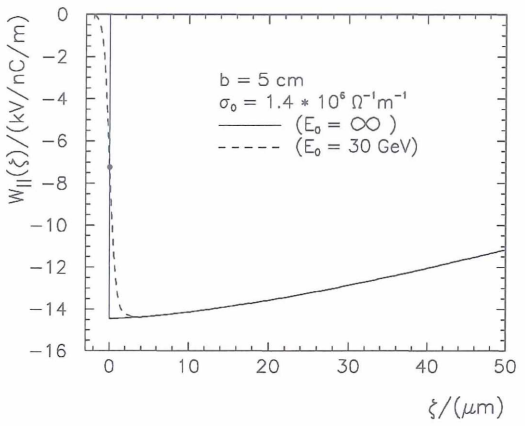

Figure 1: Delta wake potential

$b/\gamma < \zeta \ll \zeta_0$ the short range wakefields act purely capacitive and the forces are independent of ζ. The wake potential for a charge distribution with a rms-bunch length σ_z in the above range will be given by integration of the charge longitudinally. In the special case of a Gaussian charge distribution the longitudinal wake potential will be approximately given by the error-function (see Fig.2). The energy correlation produced by the bunch due to the resistive wall wakefields is linear at the center of the bunch and obeys automatically the desired phase relation. This behavior of **self-regulated** correlation can not be produced by an off-crest phase acceleration of the beam in a LINAC. For very short bunch lengths an off-crest acceleration will fail anyway since the amplitude of the generated wakefields grows quadratically with the resonance frequency of the cavities ($W_\parallel \propto f_{res}^2$), while the resulting compensation will only be proportional to the f_{res} ($dE/dz \propto f_{res}$).

[3] The dc-model of conductivity has been used. In case of $\zeta_0 \approx \tau c$ where τ denotes the relaxation time of the conduction electron ($\tau \sim 10^{-15}\ s^{-1}$) the frequency-dependent Ohm's law has to be used. For ourer parameter set it can be neglected.

[4] The anomalous skin effect has not been taken into account. The assumption is justified for materials of poor conductivity if the penetration-depth $\delta = \sqrt{2c/\omega_c Z_0 \sigma_0}$ at the cut-off frequency $\omega_c = b/\gamma c$ is much larger than the mean free-path $l = v_F \tau$ of the conducting electrons.

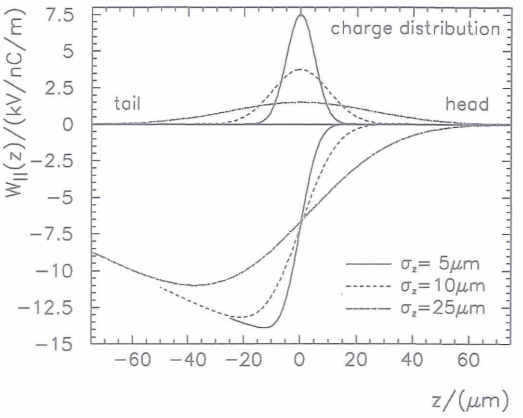

Figure 2: Wake potential for Gaussian charge distr.

3.2 *Wakefields of the TESLA Module*

The longitudinal wakefields for one TESLA module, 10.4 m long, consisting of 8 cavities has been calculated [4]. The results are shown in Fig.3 together with the wake produced by the 8th cavity normalized to one module. It can be seen that both wake potentials can be used for a pre-compression of the bunch coming from the LINAC. The latter, being more linear over the bunch, would lead to a better performance. Since the wakefields for several modules are not yet available the average wake potential (solid curve) is used for numerical simulations. We expect that the LINAC-wakefields of 250 modules (3 km) will look more like the wake of the 8th cavity (dashed curve). This would increase the efficiency of the compressor scheme by 30%.

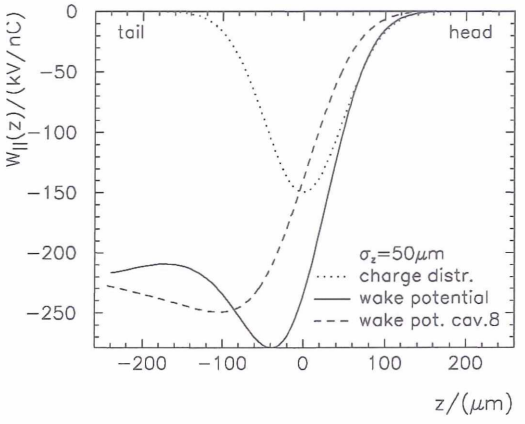

Figure 3: Wake potential of one TESLA module

4 RESULTS

4.1 *Longitudinal Charge and Energy Distribution*

The nonlinearities of the wake potentials at the tails of the bunch reduces the efficiency of such a method. The present simulation shows that approximately 50% of the initial charge can be compressed to extremely small values of less than 2 μm shown in Fig.4(a). The energy distribution of the core of the bunch is shown in Fig.4(b) and reflects essentially the longitudinal emittance of the initial bunch.

The two typical peaks at the edges of the energy distribution are caused by the over-compression in the second stage. This stage is mainly used to increase the efficiency and the stability of the compressor scheme. Note that the LINAC can run with an on-crest acceleration phase, since no compensation of the wakefields is needed. Finally the bunch in

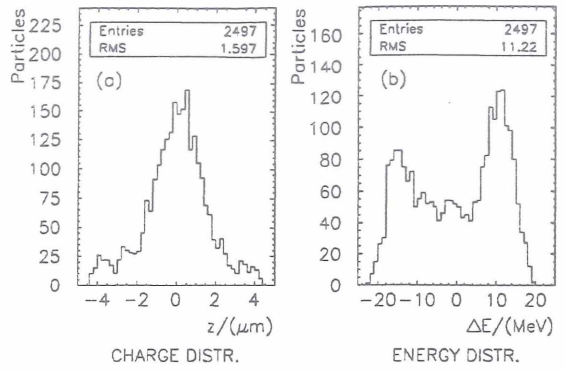

Figure 4: Longitudinal charge distribution (a) and energy distribution (b) for 50% of the initial charge Q_0; the peak current reach $I_{peak} = 50\,\mathrm{kA}$.

the longitudinal phase space at the end of the transfer line is shown in Fig.5. The tails of the bunch have to be removed by collimation.

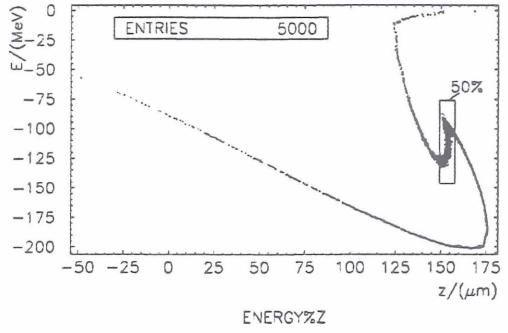

Figure 5: Longitudinal phase space distribution of the particles at the end of the compression scheme; E = 0 corresponds to the initial beam energy $E_0 = 30\,\mathrm{GeV}$.

4.2 *Stability of the Compression scheme*

An important question is the stability of such a scheme for different initial bunch parameters since the energy correlation is generated by the bunch itself. This has been studied in detail for bunch to bunch charge fluctuations up to $\pm 20\%$ while the other parameters have been kept constant. The results are given in Fig.6(a) and (b). The variation is limited to reasonable values for the bunch length, the peak current and the energy spread.

5 OPEN QUESTIONS

The presented values for the peak current are orders above any existing and planned machine so that we expect additional limiting effects for the practical realization of such a compression method. One of these is the coherent synchrotron radiation (CSR)[5] generated in the bending sys-

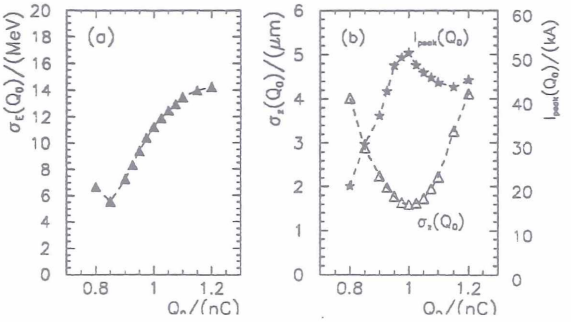

Figure 6: The rms-energy distribution (a) and the rms-bunch length together with peak current (b) for 50% of the initial charge Q_0 as a function of Q_0.

tem of the compressor modules for a bunched beam. This tail-head effect may lead to a coupling between the coherent energy spread generated by the CSR and the transverse (bending) plane coordinates through the chromatic transfer function of the particular beamline. This effect is under study and first estimations shows that this can be the limiting effect for our scheme. It is in principle possible to cancel this effect [6], but the final bunch length will be limited to values somewhat larger than shown above.

6 CONCLUSION

We have presented how the longitudinal wakefield effect can be used to obtain bunch lengths below $2\,\mu\mathrm{m}$ and peak currents above 50 kA with an efficiency of 50%. The concept of over-compression lead to a first order compensation of bunch to bunch charge fluctuations and guarantee the stability of the quasi-continuous compressor scheme up to $\Delta Q_0 \approx \pm 10\%$.

7 ACKNOWLEDGEMENTS

One of the author wishes to thank A. Novokhatski and A. Piwinski for the helpful discussions about the properties of wakefields.

8 REFERENCES

[1] O.Henry & O.Napoly, "The Resistive-Pipe Wake Potentials for Short Bunches", Part. Acc., Vol. 35, pp. 235-247,1991

[2] K. Bane, "The Short Range Resistive Wall Wakefields", SLAC-AP-87, (June 1991)

[3] K. Yokoya, "Resistive Wall Impedance of Beam Pipes of General Cross Section", Part. Acc., Vol. 41, pp. 221-248,1993

[4] A. Novokhatski & A. Mosnier, "Short Range Potentials for a Chain of TESLA cavities", DAPNIA/SEA-96-08, (Nov. 1996)

[5] Ya. S. Derbenev et. al., "Microbunch Radiative Tail-Head Interaction", DESY, (Sep. 1995)

[6] P. Emma & R. Brinkmann, "Emittance Dilution Through Coherent Energy Spread Generation in Bending Systems", contribution to this conference

WAKE FIELDS OF A BUNCH ON A GENERAL TRAJECTORY DUE TO COHERENT SYNCHROTRON RADIATION

M. Dohlus, A. Kabel, T. Limberg
DESY, Notkestr. 85, 22603 Hamburg, Germany

Abstract

If short bunches travel along trajectories with small bending radii a simple geometrical condition permits strong longitudinal and radial wake fields to act: electromagnetic fields emitted by a particle can 'overtake' on a shorter straight trajectory and interact with particles ahead. The bunch then starts to radiate coherently. The electromagnetic fields along the bunch have strong gradients and in general increase emittance. Investigations for the Tesla Test Facility Free Electron Laser have shown that the wrong choice of compressor parameters can increase the emittance by more than a factor of ten when compressing down to 50μm bunch length.

We present a formalism and numerical code to calculate the resulting electromagnetic fields on a general trajectory. Shielding effects of the vacuum chamber have been included. We present first results for the TTF-FEL undulator magnet and calculations of the influence of transition regions (bunch entering and leaving a homogeneous magnetic field).

1 INTRODUCTION

In [1] it has been shown:
1) The 'overtaking length' $L_o = (24\sigma_s R^2)^{1/3}$ is a measure for the interaction length inside of a bending magnet (with the bending radius R and the bunch length σ_s). Usually the overtaking length is large compared to σ_s but not very small compared to the dimensions of the configuration (e.g. R).
2) The longitudinal wake (per length) in the center of the bunch scales as $W_{||} = 1 \Big/ \left(\varepsilon(2\pi)^{3/2}3^{1/3}\sigma_s^{4/3}R^{2/3}\right)$. This leads e. g. to a wake in the order of 1 MV/m for an 1nC bunch with σ =0.1mm on a curvature R=1m.
Additionally in [2] it has been demonstrated:
3) Shielding by horizontal conducting plates in the distance h starts to be effective if the 'shielding length' $L_s = (\sigma_s^2 + h^2)/(2\sigma_s)$ is of the same order as the 'overtaking length'. L_s is the path length for the electromagnetic field emitted by a particle and reflected from the wall to reach the particle one sigma behind it.
4) The length of transient regions (e.g. bunch entering and leaving a homogeneous magnetic field) is of the order of L_o. As the transient lengths may be comparable to magnet lengths their effects have to be taken into account for beam dynamic simulations. An analytical formulation for the longitudinal wake of 1D bunches in an arc has been derived in [3].
5) The wake due to coherent synchrotron radiation (including transient effects) has been taken into account in the calculation of emittance increase for the case of a bunch compressor in the TESLA Test Facility FEL [4].
This approach [2] is not self-consistent: the wake fields are calculated for a source distribution in pre-defined motion $\vec{r}_{s,i}(s)$ (s is length parameter of path, i is index of subbunch). The source bunch has no transversal dimensions (1D bunch) and does not change its longitudinal profile (rigid bunch). Two- or three-dimensional bunches are composed from one-dimensional line charges. The simulation of the shielding effects due to infinitely conducting plates in the horizontal plane is taken into account by mirror charges.
Our *new formulation*, described in chapter two, takes into accont:
1) 2D bunch distributions with longitudinal profile $\lambda(s,t) = \lambda(s - v_s t)$ and profile $\eta(\tilde{z})$ in $\vec{e}_z$ direction. $\vec{e}_z$ is a constant unity vector that is essentially perpendicular to the plane of motion (the motion is not restricted to be exactly in a plane!), $\tilde{z} = z - \vec{r}(s)\cdot\vec{e}_z$ describes the offset to the central path $\vec{r}(s)$ in $\vec{e}_z$ direction;
2) The 2D approach avoids the field singularities of the 1D approach [2] and is therefore better capable of the simulation of fully three dimensional source distributions (using an array of 2D bunches). So called 'space charge forces' are taken into account.
3) The new formulation is better suited for numerical integration (even for 1D bunches).

Chapter three describes the calculation of energy spread increase for the case of a single bending magnet and following drift space for different bunch lengths and bending radii. In chapter four, first results for a micro-bunch entering the TTF-FEL are presented.

2 CALCULATION OF THE LORENTZ FORCE

The action of the electromagnetic field caused by a source (index s) to a charged test particle (index t) is described by the *Lorentz force equation*:

$$\frac{1}{q_t}\vec{F}_t = \vec{E}_s + \vec{v}_t \times \vec{B}_s \ . \tag{1}$$

Using the scalar and vector potentials $\vec{E}_s = -\nabla V_s - \dot{\vec{A}}_s$, $\vec{B}_s = \nabla \times \vec{A}_s$ this force can be split into two terms:

$$\frac{1}{q_t}\vec{F}_t = \underbrace{\nabla\left(\vec{v}_t\cdot\vec{A}_s - V_s\right)}_{\frac{1}{q_t}\vec{F}_{At}} + \underbrace{\left(-\dot{\vec{A}}_s - \vec{A}_s\left(\vec{v}_t\cdot\nabla\right)\right)}_{\frac{1}{q_t}\vec{F}_{Bt}} \ . \tag{2}$$

The first term is a gradient field, the second term vanishes for bunches in linear motion. As the space charge and

current density distributions are determined, the scalar and vector potentials can be directly obtained from the *retarded potential equation*. For a two dimensional bunch with the density $\lambda(s - v_s t)\eta(\tilde{z})$ the scalar and vector potential integrations lead to:

$$\frac{4\pi\varepsilon}{q_t}\vec{F}_{At} = \int \left\{ G_1(s')\vec{R}_{xy} + G_2(s')\vec{e}_z \right\} \left(1 - \vec{\beta}_t \cdot \vec{\beta}_s\right) ds', \tag{3}$$

$$\begin{aligned}\frac{4\pi\varepsilon}{q_t}\vec{F}_{Bt} = {} & \beta_t\beta_s \int \left(\left\{ G_1\vec{R}_{xy} + G_2\vec{e}_z \right\} \cdot (\vec{e}_t - \vec{e}_s) \right) \vec{e}_s\, ds' \\ & - \beta_t\beta_s \int G_3(s') \frac{\partial \vec{e}_s}{\partial s'} ds' \\ & + (\beta_s - \beta_t) \int G_4(s')\vec{e}_s\, ds' \end{aligned} \tag{4}$$

with

$$\begin{aligned} G_1(s) &= \int \left\{ \lambda/R^3 + \dot{\lambda}/(c_0 R^2) \right\} \eta(\tilde{z}) d\tilde{z} \\ G_2(s) &= \int \left\{ \lambda/R^3 + \dot{\lambda}/(c_0 R^2) \right\} \tilde{z}\, \eta(\tilde{z}) d\tilde{z} \\ G_3(s) &= \int \lambda/R\, \eta(\tilde{z}) d\tilde{z} \\ G_4(s) &= \int -\dot{\lambda}/(c_0 R)\, \eta(\tilde{z})\tilde{z} \end{aligned}$$

and $\vec{R} = \vec{r}_t - \vec{r}_s(s') - \tilde{z}\vec{e}_z$, $\vec{R}_{xy} = \vec{R} - (\vec{e}_z \cdot \vec{R})\vec{R}$, $\vec{\beta}_s = \beta_s\vec{e}_s = \vec{v}_s/c_0$, $\vec{\beta}_t = \beta_t\vec{e}_t = \vec{v}_t/c_0$, and $\lambda = \lambda(s' + \beta_s R - v_s t)$. For this derivation we used the chain rule with the boundary conditions $||\vec{r}_s(s = \pm\infty)||^{-1} = 0$. The main contribution to the longitudinal force is given by the integral (3). The last term in (4) vanishes if source and observer particle have the same velocity. The first term vanishes for particles in circular motion if source and observer are on the same orbit. The remaining part (proportional to the curvature $||\partial\vec{e}_s/\partial s||$) gives the so called 'centrifugal space charge force'. In the following calculations, all integrals have been solved numerically without further restrictions.

3 TRANSITIONS FOR LONGITUDINAL WAKES AND ENERGY SPREAD GROWTH IN BENDING MAGNETS

The field calculation simulates the bunch as a set of gaussian sub bunches—each with a different energy, different initial conditiones and an individual path. The trajectories of these sub-bunches are not effected by the calculated fields.

An independent set of bunch slices, initially lined up, is traced through the bending magnet and experiences the energy variations due to the longitudinal fields. Due to the strong longitudinal variation of the fields, the slice centroids follow different paths and a 'centroid emittance' developes.

For the tracking, the bending magnets and drift spaces are cut into slices and the wake fields are calculated and

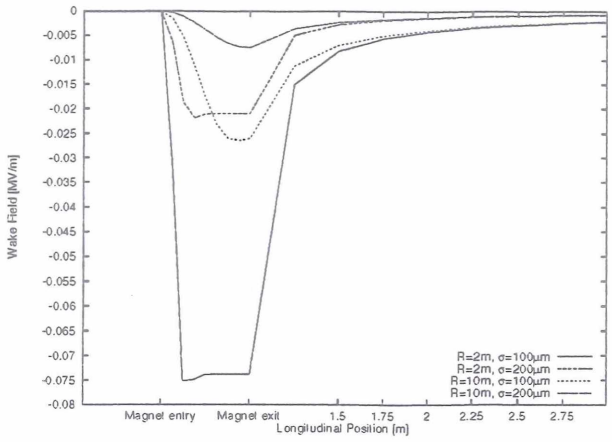

Figure 1: Longitudinal wake field at bunch center vs. longitudinal position.

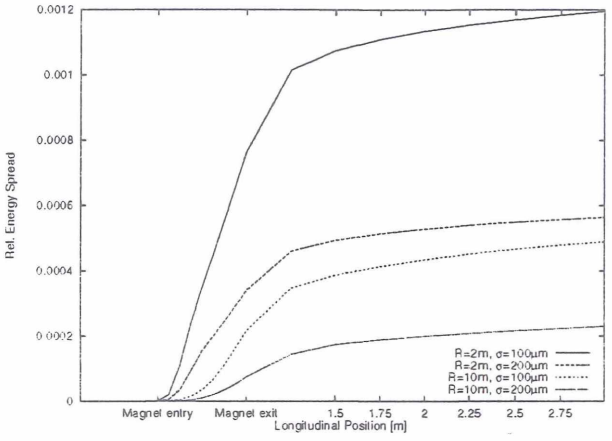

Figure 2: Energy spread vs. longitudinal position.

the consequent energy changes are applied at the end of each slice.

Fig. 1 and 2 show the longitudinal wake field at the bunch center and the resulting energy spread growth for different bunch lengths and bending radii vs. longitudinal position for a very simple set-up, comprising a bending magnet of length .5m and a drift space of length 2.0m. It can be seen that there is no steady-state region for the larger bending radius. The asymptotic behavior of the field past the magnet's exit is independent of the bunch's history and can be shown to be $\lambda/(2\pi\epsilon r)$, where λ is the 1D charge density and r is the distance from the magnet's exit.

4 FIRST CALCULATIONS OF AN UNDULATOR

The longitudinal charge distribution of a bunch traversing an FEL undulator changes drastically due to the microbunching of the SASE process. In the TTF-FEL case, the incoming bunch has a homogeneous peak-shaped distribution with an RMS-length of about 50μm. Micro-bunching along the undulator then produces a chain of microbunches with a periodicity of the wavelength (6.4nm). As first results of undulator field calculations, we present here calculations of the longitudinal wake of a microbunch,

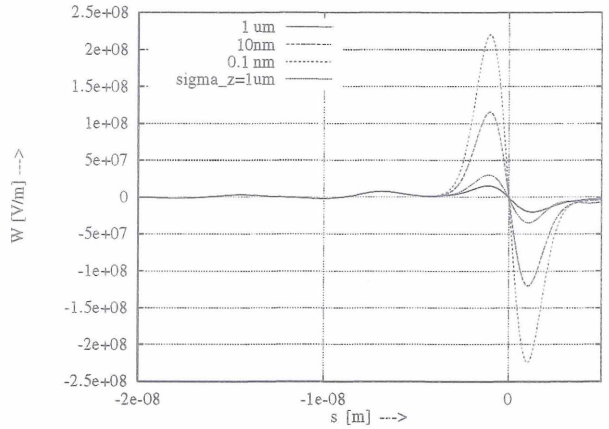

Figure 3: Longitudinal wake for a micro-bunch (3 nm FWHM) in the TTF-FEL undulator for different transverse offsets of the observation point vs. longitudinal position.

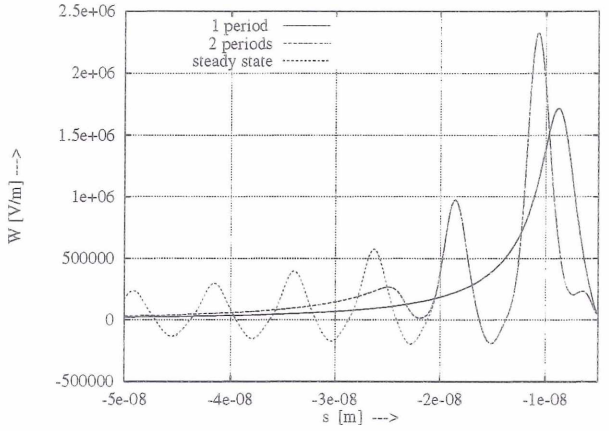

Figure 4: Longitudinal wake for a micro-bunch (3 nm FWHM) in the TTF-FEL undulator for different numbers of periods into the undulator vs. longitudinal position.

modeled as a gaussian distribution with a FWHM of 3.2 nm, half the distance between micro-bunches. The undulator has a period length of 2.7cm and a field strength of 0.5 Tesla. Fig. 3 shows the longitudinal wake field for different transverse offsets in a range between 0.1nm and 1μm. The curve labeled 'σ_z =1μm results from a centered bunch with a non-zero transversal extension. The fields are calculated at a position 20 undulator periods into the undulator, where a steady state regime is reached. The logarithmic dependence indicates a space charge like force to be the cause of the peak around the bunch center (s=0). For an evaluation of bunch energy loss, the transverse bunch distribution has to be folded with these curves.

Fig. 4 shows with higher resolution the region ahead of the bunch, (negative s in these plots means ahead) starting with the second peak, for the bunch being at different numbers of periods into the undulator. There is no significant dependance on vertical offsets in this region.

Fig. 5 then varies the bunch position within an undulator period in the steady state region, the bunch position expressed in degrees of that period. At the zero crossings (90 and 270 degrees), the strength of the focussing field has its maximum.

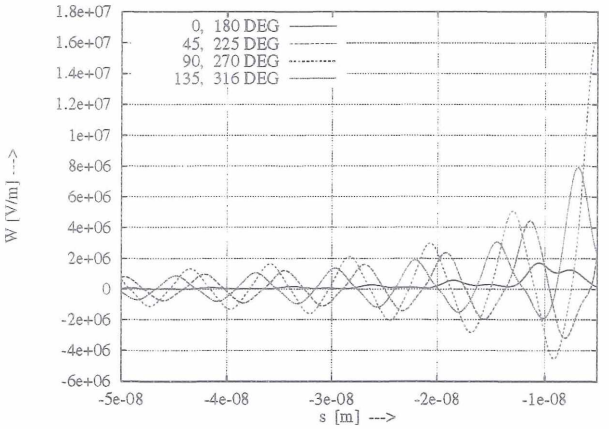

Figure 5: Longitudinal wake for a micro-bunch (3 nm FWHM) in the TTF-FEL undulator for different bunch positions within an undulator period in the steady state regime vs. longitudinal position.

5 SUMMARY

A new formalism for the calculation of wake fields acting on bunches travelling on arbitrarily curved trajectories makes the proper treatment of magnets possible where, unlike in bending magnets, the particle trajectory is not a circle: undulators, quadrupoles etc.. First results for the case of a micro-bunch in the TTF-FEL undulator are shown.

The longitudinal wake fields and the energy spread growth in the transition regimes of a bending magnet are calculated for different bunch lengths and magnet strengths. It can be seen that for bends whose length is considerably shorter than the bending radius no steady-state regime region exists.

6 REFERENCES

[1] *Y. Derbenev, J. Rossbach, E. Saldin, V. Shiltsev: 'Microbunch Radiative Tail-Head Interaction', TESLA-FEL 95-05, September 95.*

[2] *M. Dohlus, T. Limberg: 'Emittance Growth due to Wake Fields on Curved Bunch Trajectories', presented at XVIII International Free Electron Laser Conference (Rome, 1996); DESY print TESLA-FEL 96-13.*

[3] *E. L. Saldin, E. A. Schneidmiller, M. V. Yurkov: 'On The Coherent Radiation of an Electron Bunch Moving in an Arc of a Circle', DESY Print October 1996, TESLA-FEL 96-14.*

[4] *A VUV Free Electron Laser at the TESLA Test Facility at DESY. Conceptual Design Report. DESY Print June 1995, TESLA-FEL 95-03*

THE PROTON SYNCHROTRON DESY III

W.Ebeling, J.R.Maidment,
Deutsches Elektronen Synchrotron DESY,
Notkestrasse 85, 22607 Hamburg,
Germany

Abstract

Desy III is one link in the chain of injectors for HERA, the electron/positron - proton colliding beam storage ring. Because of the relatively low injection (kinetic) energy of 50 MeV space charge plays a significant role in determining the achievable accelerated current. The luminosity in HERA is critically dependent on the transverse beam brightness hence the need to examine, and where possible minimise, emittance blow-up. Measurements of the beam emittance as a function of intensity in Desy III and the derived incoherent space charge tune shift are presented and discussed. Finally some preliminary investigations with regard to upgrading the injection energy via a pre-booster are described.

1 INTRODUCTION

The Desy III synchrotron accelerates protons from a momentum of 0.31 MeV/c to 7.5 GeV/c in approximately 2s. Injection is from a 50 MeV H^- Alvarez linac using charge exchange in a thin ($34\mu g.cm^{-2}$) carbon foil. The linac output current is around 14 mA with a variable pulse length set in normal operation to $33\mu s$ corresponding to ten turns. The RF system consists of a single, ferrite tuned, cavity operating between 3.2 and 10.3 MHz providing harmonic number 11. Transition is not crossed during the acceleration ramp. The original design requirement was for an output intensity of $1 \cdot 10^{11}$ particles per bunch equivalent to some 165 mA circulating in 11 bunches. In routine operation some 10% more current is achieved while the maximum observed current corresponds to 25-30% above the design value. Although the longitudinal bunch area specified in the original proposal[1] is achieved, the assumptions regarding transverse emittance have yet to be met. This is the main topic reported on here.

It should be noted that injection and subsequent acceleration is accompanied by particle loss. The injection efficiency, measured as the ratio of the charge circulating immediately after the n-turn injection compared to that contained within the linac pulse, is 85% to 90%. Thereafter about 55% of this beam survives until full energy with the losses confined to the first 250 ms of the acceleration cycle ie ceasing after a momentum of circa 1 GeV/c. This transmission behaviour does not depend upon the number of injected turns below that required for the maximum achievable intensity.

The occurrence of longitudinal bunch oscillations has been reported elsewhere[2]. A feedback system[3] is installed which damps the dipole modes but is only activated during the magnet flat-top when the revolution frequency is constant. The threshold for the onset of the oscillations is around an intensity equivalent to 60 ma in flat-top Thus during acceleration the observed beam horizontal profile at higher intensities is somewhat influenced by radial synchrotron oscillations and to a much lesser extent by bunch shape oscillations. Although the shape oscillations are not damped by the feedback there is a negligible contribution to longitudinal mismatch at extraction and injection into Petra, the next accelerator in the injector chain.

2 EMITTANCE MEASUREMENTS

Desy III is equipped with residual gas monitors to measure the beam profile in each plane and a single wire scanner to measure the horizontal profile.[4] Both systems produce a beam profile resulting from a time integration. The residual gas monitor is based on the readout of a video camera whilst the wire scanner traverses at $\sim 1\ ms^{-1}$. Comparison of the profiles yielded by each system at peak energy show excellent agreement.[5]

The residual gas monitors, which measure the average profile on 4 consecutive cycles, have been used to acquire profile data over a wide range of beam intensity and momentum. The first conclusion is that there is a blow-up of the emittances in both planes between injection (flat bottom) and full energy (flat top). This is shown in Figures 1 and 2, where the horizontal and vertical emittances are plotted as a function of accelerated current. Due to the transmission losses already mentioned even if no blow-up occurred there would be a factor of ~ 2 reduction in the phase plane density.

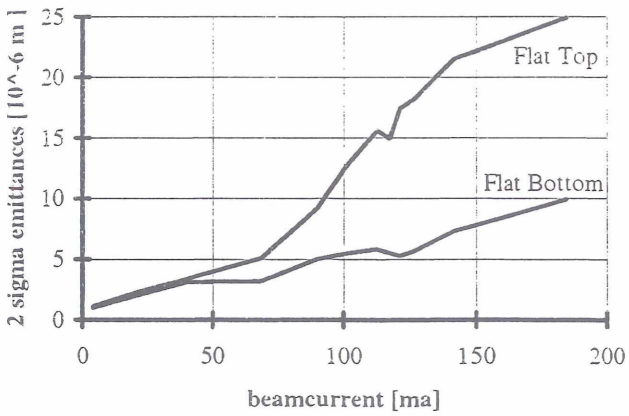

Figure 1: Horizontal emittance vs accelerated current.

Measurements of the emittances at the exit of the linac, using charge deposition on wire harps, yield ε_h = $3.2 \cdot 10^{-6}$m and ε_v = $2.5 \cdot 10^{-6}$m for the horizontal and ver-

tical *normalised*, 2σ emittances respectively. To within the measurement errors, which may be of the order of 25%, the same values are recorded in flat bottom for at most 2-turn injection. No increase in emittance could be detected for 2-turns with up to an additional 20 passages of the proton beam through the stripping foil. At this low intensity there is no evidence of emittance blow-up between injection and top energy.

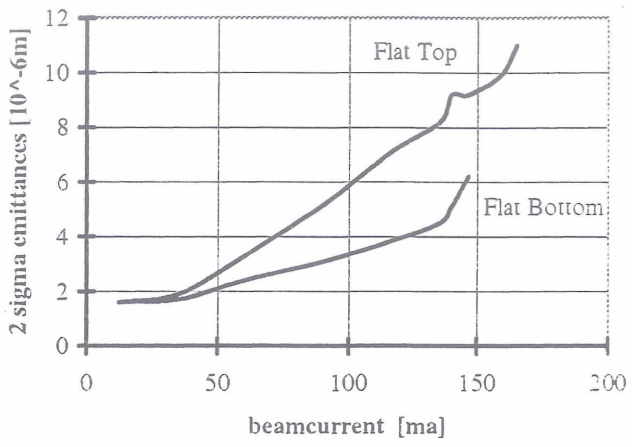

Figure 2: Vertical emittance vs accelerated current.

The injection of further linac turns leads to a recorded emittance at injection which increases approximately linearly with current. There is an additional blow-up during acceleration which also shows an approximately linear increase with intensity, rising to a factor of ~2 under standard operational intensities.

3 TRANSVERSE SPACE CHARGE

Space charge is considered to be the most significant effect limiting the maximum achievable beam brightness. We may write the expression for the vertical detuning as:

$$\Delta Q_v = \frac{N r_p F G}{\pi \varepsilon_v \left(1 + \sqrt{\frac{\varepsilon_h}{\varepsilon_v}}\right) B_f \beta \gamma^2} \qquad (1)$$

Where N is the total number of circulating protons, r_p = classical proton radius, F ($\sim$ 1) takes account of the image forces, G ($\geq$ 1) is a transverse distribution factor, B_f is the bunching factor (average/peak current) and ε is the transverse *normalised*, 2σ emittance. The subscripts h and v refer to the two transverse planes.

Measurements of the (vertical) emittance as a function of time/momentum during the cycle together with the the bunch length allow the derivation of the tune shift. The bunch length is measured using a resistive wall monitor with bandwidth of order 1GHz. To evaluate ΔQ_v we have used F=G=1 in equation1 and for the bunching factor have assumed a parabolic line density which is in good agreement with measurements.

Figure 3 shows typical results for the vertical emittance versus time during acceleration for two different end intensities while figure 4 is a plot of the derived variation of the vertical tune shift for an end intensity of 180 ma. Although ΔQ_v has a maximum value of ~0.6 at the start of acceleration it is not clear that incoherent space charge effects are responsible for the blow-up observed during the whole cycle for high intensity beams. The initial phase space density of low current beams yields similar large tune shifts.

We have not observed coherent betatron oscillations during the acceleration cycle. We may speculate that the radial synchrotron oscillations, whose amplitude increases with increasing intensity and which are not damped until flattop, impose additional good field requirements to maintain transverse emittance. Desy III is equipped with the minimum number of multipole magnets required to independently influence/compensate all 3^{rd} and 4^{th} order betatron sum resonances spanned by a space charge tune spread of 0.4. Skew quadrupoles are incorporated to correct the coupling. To date studies with these systems have been confined to achieving increased accelerated intensity. They are not activated in standard operation. Further studies of their influence on emittance are planned.

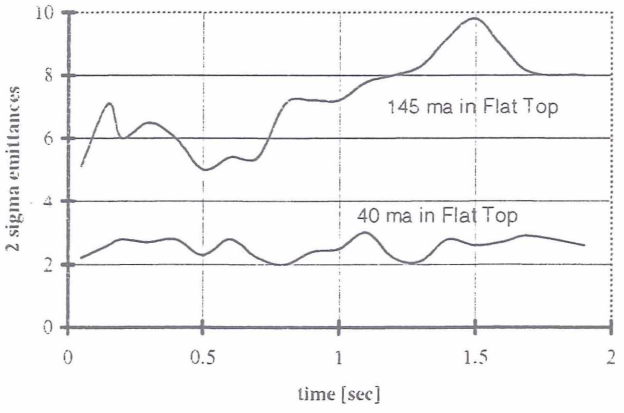

Figure 3: Vertical emittance vs time during acceleration.

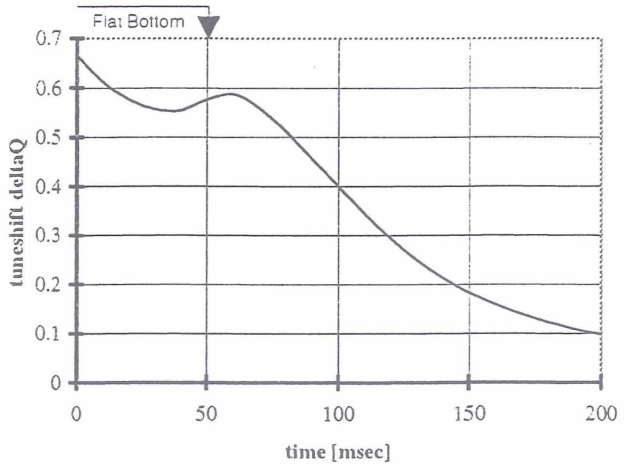

Figure 4: Derived (vertical) tune shift vs time.

4 UPGRADE OPTIONS

Short term improvements concentrate on reducing the observed losses. At present orbit correction is via dc-powered elements. It may be advantageous to incorporate time dependent correctors. We observe a systematic increase of the orbit radius shortly after the start of acceleration indicative of a dipole field tracking error. Improved read-out electronics for the position monitors are essential and system tests are underway.[6]

A study has been made of increasing the injection energy using additional linear accelerator structures in the space between the present Alvarez linac and the synchrotron tunnel.[7] An increase of injection energy to 170 MeV is considered feasible. This would theoretically reduce the space charge tune shift, at constant phase space density, by a factor of 2.

Somewhat more promising is a study in progress based on the use of an intermediate booster.[8]. Sited in the existing building alongside the present linac this would accelerate 2 bunches to 800 MeV kinetic energy using a 1 Hz magnet cycle which is the maximum repetition rate of the linac. The space charge tune shift in the booster would be moderate and that in Desy III reduced by a factor of 3 to 5 depending on the chosen bunch intensity.

Use of such a booster requires bunch to bucket transfer to Desy III using fast (ca. 70 ns risetime) kickers. The ten bunches would be boxcar accumulated using 5 booster transfers. Measurements have been made on an 800 MeV flat-top in Desy III which gave a beam lifetime of 270 s and no observable emittance increase over 2.7 s. The additional accumulation time produces a negligible increase in the overall Hera filling time.

5 ACKNOWLEDGEMENTS

We would like to thank K.Wittenburg and J Schwarz for their assistance in obtaining the profile measurements.

6 REFERENCES

[1] E.Bakewicz et al, "Desy III: Design Report", Internal report DESY HERA 1986-11, 1986.

[2] W.Ebeling et al, "Improvements in performance of Desy III",Proc. XVth Int. Conf. on High Energy Accelerators, p112, Hamburg, 1992.

[3] R.D.Kohaupt, "Feedback Systems at Desy", Proc. 5th Europ. Part. Accel. Conf., p180, Sitges, 1996.

[4] W.Hain et al "Beam Profile Monitors for the Hera Proton Accelerators", Proc. 2nd Europ. Part. Accel. Conf. p759, Nice, 1990.

[5] K.Wittenburg, "Emittance measurement in the proton accelerators at Desy", Proc. Int. wkshp. on Particle Dynamics in Accelerators, Tsukuba, 1994.

[6] M.Wendt. Private Communication

[7] S.K.Esin et al "Desy Linac III Upgrade Study", Proc. XVIIIth Int. Linear Accel. Conf., p190, Geneva, 1996.

[8] V.Balbekov et al. "Desy III Booster Design Study", To be published

Failure Statistics of DESY Power Supplies in 1996

Hans-Joerg Eckoldt, DESY Hamburg, Germany

Abstract

The HERA machine delivered good results in 1996. This was possible due to a higher availability of the technical subsystems than in the years before. Here the failures of the power supplies during 1996 will be analysed and a statistic of the failures of the accelerators will be shown. This will be compared to the failures of the last years to see what improvements had the most succes. A preview onto the next changes will be given and the introduction of new tools (software and hardware) will be explained.

1 INTRODUCTION

One of the subsystems in particle accelerators are the magnet power supplies. Due to the large number of components a high reliability is required. This is not only the availability which is the number of failures multiplied by the repair time of the sub-system, but also the number of failures is important in machines with long filling times. In DORIS the beam is filled within a few minutes after the end of repair whereby in HERA not only the repair time of the power supply is important but also the time of refilling the beams and optimisation for the luminosity run. A failure that is repaired in 10 minutes will have a down time of the machine and the experiments of several hours. To detect systematical errors an analysis of the failures of the power supplies at DESY is made annually and will be presented here. By this systematic errors have been detected and eliminated.

2 SOURCE OF INFORMATION

Beside the machine control room operators a technical shift crew of two persons is working in three shifts when the machines are running. This shift crew is responsible for the repair of the power supplies, part of the water cooling system and the rf-high voltage supplies. Each failure that occurs is written into a log book with time, the assumed reason of failure and with a description of the repair action. This material was used as data base. Additional information about the machine status can be found in computer archives and the control room log books. The HERA machine coordinator tracks down the trips as well in combination with beam loss and down time.

3 NUMBERS OF FAILURES

Over the time period from May 15th till December 23rd the shift crew was called 574 times to solve a problem. This is the actual time when the HERA electron machine was commissioned till it was turned off for the winter shut down. The problems to be solved are from simple reset of an electronic up to a several hours lasting repair of the power parts, which is luckily not very often.

The first statistic of this type was made in 1993. That result and the numbers of the last years is shown in table 1

Table 1: Number of events when technical shift crew had to react.

	1996	1995	1993
HERA	238	248	252
PETRA	114	165	143
DORIS	87	81	184
DESY II / III	43	113	n.n.
transport lines preaccelerators	92	131	n.n.
analysed period	5304 hrs	6720 hrs	n.n.

4 STATISTICS

The availabilty of the subsystem power supply can be calculated by

$$AV = \frac{MT - (NOF * TOR)}{MT} * 100\%$$

with AV = availability
MT = machine time
NOF = number of failures
TOR = time of repair

The average repair time for the power supplies is assumed as 45 min per failure. Pushing a reset button is much shorter whereby the repair in the power parts takes much longer.

The MTBF mean time between failure of the machines is given by the formula:

$$MTBF\_M = \frac{MT}{NOF}$$

The failure distribution of power supply failures at DESY can be seen in table 2. P and e indicate the proton or electron machine of HERA whereby the e + p is the sum of both.

Table 2: Power supply failures in the machines, Mean TimeBetweenFailure, AVailability

	problems	MTBF_M hrs	AV
HERA e+p	238*	22.3	96.6%
HERA p	163	32.5	97.6%
HERA e	84	63.1	98.8%
PETRA	114	46.5	98.3%
DORIS	87	61	98.7%
DESY II / III	43	123.3	99.4%
transport lines preaccelerators	92	57.6	98.6%
entire DESY	574	9.2	91.9%
analysed period	5304 hrs		

The availability in table 2 includes all failures that appeared and is just the availability of one subsystem. It does not give the number for the performance of the machine. In comparison the actual time between two beam costing failures due to power supplies in HERA is 56 hours.

MTBF of the power supplies in the machines

$$MTBF = \frac{MT * NOPS}{NOF}$$

with NOPS = number of power supplies

Here two numbers are calculated. One is the overall value including every fault that appeared and the power supply was turned off. The second value is with only the problems of the power supply. External interlocks and failures as grid disturbances have been substracted.

* Please note that the sum of failures of HERA e + HERA p is higher than the value of HERA e+p. Grid disturbances were conted for both machines. In the sum only one event is counted per machine

Table 3: MTBF of the power supplies

	Number of PS	MTBF_PS overall	MTBF no external failures
HERA e+p	1166	25985	29310
PETRA	269	12515	13988
DORIS	93	5669	8968

5 KATEGORIES OF FAILURES

The data material was sorted to the failures of the machines and categorised. The categories are:

1) unknown -failures that could not be sourced down
2) work induced -due to work a failure was produced
3) single interlocks -interlocks from exterior eg. thermoswitch of magnet. (not really failure but turn off of the supply)
4) Electronic malfunction -error that is due to a malfunction of electronic without a physical failure in the electronic
5) Electronic component -a physical failure in the electronic or survey elements
6) ELS -electronic protection in the choppers. The voltage drop over the MOSFET transistors in the switched mode supplies is monitored. In case of short circuit or break down of a transistors this turns the power supply off. (one of the major problems in HERAe in 1995)
7) Shorts to ground -low impedance to ground within the magnets or the power supplies
8) Semiconductors, fuses -failure of the power semiconductors eg. SCRs, diodes and power fuses. A 100 mA fuse would be an electronic component.
9) mechanical switches - contactors, circuit breakers and polarity switchers
10) PSC, controles -power supply controllers, programmable logical controllers, main computer in the control room
11) transformers -transformers, chokes etc. also the circuit breakers for the transformer protection
12) connections -bad connections of circuitboards, plugs up, bad soldering points, bad screwing of copper bars
13) water cooling plant - failures in the cooling system. An error causes several power supplies to trip
14) water/air cooling in the supplies - only the supplies of one water circuit trip. One to maximum four supplies of the choppers.

6 FAILURES IN THE MACHINES

When looking at the failures each machine has it´s own pattern of failure due to the different types of supplies

and also the age of the units. The failures can be seen in table 4.

HERA p

Still a systematic failure is in the system. The problem is the mechanical polarity switcher of the chopper supplies. The auxiliary contacts of the contactors become high resistive. During polarity switching the magnet is shorted by the switch. A build in electronic waits for this status to continue which due to the bad contacts will not be detected. The polarity switcher stops in the middle of the action.

Table 4: Failures in the machines

	HERA e	HERA p	PETRA	DORIS
unknown	1	4	0	1
work	0	4	1	2
Single interlocks	11	8	3	21
Electronic malfunction	11	21	21	22
Electronic component	2	6	24	5
ELS	14	5		0
Short to ground	0	4	2	0
Semiconductor, fuses	0	0	3	0
mech. switches	9	71	4	0
grid disturbances	9	9	9	9
PSC, controls	4	22	8	4
Transformers	0	0	0	0
connections	7	4	14	5
Water cooling plant	1	2	1	2
Water, cooling	4	3	10	6
correctors	12	0	14	8
sum	85	163	114	84

HERA e

No really overwhelming problem is seen in these statistics. Systematic errors appear to have been eliminated, leaving random errors to be dealt with. The largest problem of the last year, the aging of MOSFETs, has been eleminated by exchanging the MOSFETs.

PETRA

The year was good. The major problems of the previous year been eliminated. Still the number of damaged electronic components might be a sign for the aging of the power supplies.

DORIS

The power supplies worked well this year. The number of failures is constant to the previous year, whereby one quarter of the failures were turn offs by external interlocks. The electronics problem was mainly to one power supply where the failure was extremly hard to find.

DESY II / III

The number of failures decreased rapidly. In 1995 it was a problem with a bad contact of a high voltage switch. The problem was fixed.

BEAM TRANSPORT LINES

Here the number of failures decreased with only routine maintenance.

7 NEW TOOLS FOR MAINTENANCE

When looking at the investment and operating costs of accelerators the demand for short maintainance period and long runs gets stronger. This is usually in contradiction to the technicians view who wants to maintain the power supplies for a failure free next run. Therefore new methods and tools have to be found to decrease the time of working at the units with the same amount off quality.

One fairly simple attempt was made to control the accuracy of the supplies. By a computer program a group of power supplies is driven with a slow ramp procedure and the data of the monitored current is stored. With an EXCEL-spreadsheet this data is visualized. Errors in the Digital/Analog Converter (DAC) or the DigitalVoltMeter (DVM) can easily be detected. This program is used also to control suspicious power supplies during ramping of HERA .

In 1997 an infrared thermo camera will be taken to supervise the power supplies. By this it is possible to check connections and operation of power parts during normal run conditions of the accelerator. On a vendors presentation of such a camera some bad connections where found. This promises good results.

8 SUMMARY

When comparing the numbers of the events the last year did not look much better than the 1995 year though the impact of the failures to the machine run time was smaller. The supplies had more failures during turning on time or massage times than during the actual run time. These failures have to be solved in the next shut down. For several machines the obvious systematic errors seem to be eliminated. The consequence is that the future failures have to be investigated even closer to guarantee a better run.

UPGRADE OF THE H⁻-INJECTION SYSTEM AT THE DESY PROTON LINAC III

C.-M. Kleffner, G. Jacobs, N. Holtkamp, M. Nagl, I. Peperkorn, J. Peters
Deutsches Elektronen Synchrotron DESY, Germany,
A. Schempp, IAP, Universität Frankfurt, Germany
and V. Paramonov, INR Moscow, Russia

Abstract

In the near future the injection system of the proton linac at DESY will be upgraded. Two different types of H⁻-sources are operated at DESY. The new rf-driven volume source is free of cesium. On a long-term basis this source is planned to replace the present operating magnetron source.

For reasons of reliability of the proton linac and for further developments of ion sources a parallel operation of two sources should be possible at the Alvarez linac. Each source has a separate RFQ to accelerate the ions to an energy of 750 keV. A new transport line with one dipole, 8 quadrupoles and one intermediate buncher was designed to match the beam between both RFQs and the Alvarez linac.

The codes COPPOC and TRANSPORT were used to determine the length of the transport line and the parameters of the dipole and the buncher. Because of the high current of 20 mA and above the estimation of the space charge forces is of special interest. The macro-particle-code PARMTRA takes into account the particle-to-particle electric forces among all particles. The properties of the beam line have been studied in connection with the effects on the final beam quality after acceleration with the 50 MeV Alvarez linac.

1 INTRODUCTION

At present the H⁻-ion accelerator facility LINAC III at DESY consists of a magnetron ion source followed by a RFQ (Radio-Frequency-Quadrupole)-accelerator in front of a 50 MeV Alvarez linac [1].

The H⁻-injection system upgrade program which is under development at present will enable parallel operation of two ion sources at the Alvarez linac. The proposed MEBT (Medium Energy Beam Transfer) between the two RFQs and the Alvarez linac has a twofold goal: i) it is designed to match the beam of both ion sources to the acceptance of the Alvarez linac. ii) the mechanical construction of the upgrade will facilitate further developments of ion sources and tests at the Alvarez linac.

Concerning the reliability of the H⁻-injector for HERA operation in the near future, it is essential that the time necessary to switch from the new volume source to the magnetron ion source will become as short as possible. The MEBT between the two ion sources and RFQs and the Alvarez was therefore designed to operate in two modes without the need of altering the mechanical structure.

The new volume source will be installed on the axis of the Alvarez linac, whereas the beam coming from the magnetron source will be bent by a 60°-magnet to this axis. A rebuncher is needed for the longitudinal dynamics in the MEBT.

The optical design of the MEBT is important insofar as the beam quality in the low energy part determines the characteristic of the beam in the high energy part of the linac.

2 DESIGN OF THE MEBT

The design procedure for determing the parameters of the MEBT is as follows:

The space charge force at the high current of 20 mA at the energy of 750 keV finally limit the overall length of the MEBT due to the strong debunching of the ion beam.

As part of the design calculations for the new MEBT a number of options were investigated. Various combinations of one or two dipole magnets with 30°, 45° or 60° and different edge angles were tested in simulations. It was found that the effect of the dispersion generated by a 60° sector magnet on the beam quality can be minimized. A MEBT with only one short dipole gives the possibility to reduce the distance between both RFQs and the rebuncher to less than 60 cm.

The number of quadrupoles was kept small to save space. Since there is no space to install steering magnets the quadrupoles can be displaced transversally in order to align the beam in horizontal and vertical direction.

Eight quadrupoles – 6 for each transport line – arranged in doublets are used to focus the beam transversally. The parameters of the rebuncher cavity have been estimated by calculating the phase and energy spread at its position and the optimized drift length from rebuncher to the first Alvarez tank. A sketch of the layout of the MEBT is shown in figure 1.

3 PARAMETERS OF THE MEBT COMPONENTS

3.1 Magnets

For the beam focusing only one standard Alvarez type of quadrupole is employed. Steering angles of up to 10 mrad will be realized by transverse displacements of the quadrupoles of up to 1 mm. The 60°-bending magnet is a pulsed sector dipole magnet. The manufacturing of the magnets was given to industry. All magnets will be powered with the same type of DESY-developed pulsed power

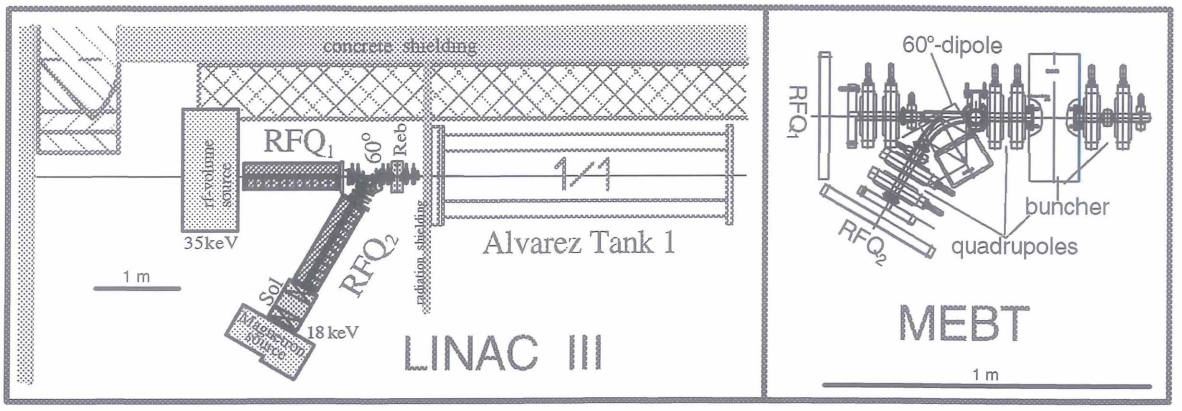

Figure 1: Layout of the MEBT.

supplies. Due to the small duty factor of the proton linac of 1:4000 at a repetition rate of 0.25 Hz air-cooling is sufficient.

3.2 *RFQ accelerator*

The new RFQ accelerator is based on the design of the operating 4-ROD RFQ [2] at LINAC III and was delivered by the IAP Frankfurt. The design input energy has been increased from 18 keV to 35 keV in order to permit the operation of the volume source with higher extraction voltage.

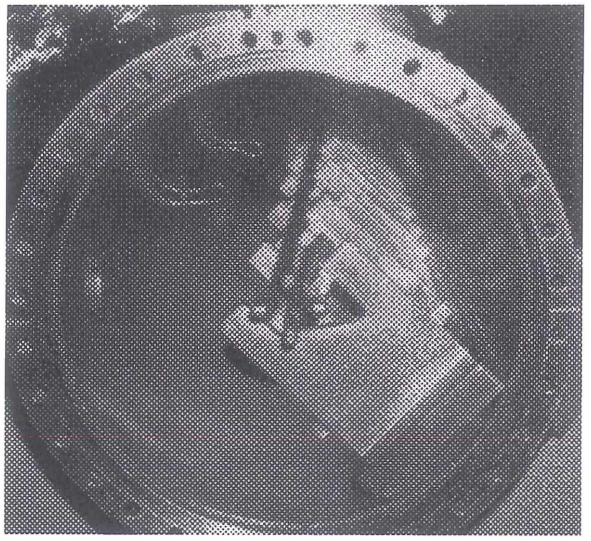

Figure 2: View of the RFQ accelerator.

Figure 2 shows the low energy part of the RFQ. Both RFQs will be powered by the same rf-amplifier.

3.3 *Rebuncher cavity*

A new rebuncher cavity is under construction at the IAP Frankfurt. It is a two gap spiral loaded resonator operating at 202 MHz. The design values are as follows:

A rf-amplifier for the rebuncher cavity is under construction at DESY.

f_0	202 MHz
U_{eff}	58 kV
U_{gap}	45 kV
P	5 kW
length	12 cm

Table 1: Main parameters of the rebuncher cavity for the MEBT.

3.4 *The Ion Sources*

Currently a 18 keV magnetron source is operating as the H^--ion source for LINAC III. To reduce the work functions for the electrons the magnetron source must be operated with cesium. The rf-driven volume source [3] at DESY makes a cesium-free operation possible with high currents and smaller emittances compared to the magnetron source.

3.5 *Beam diagnostic*

The measurement of the beam parameters will be performed by DESY standard devices. At the exit of the RFQs and in front of the Alvarez tank the current will be measured by commercially available current transformers. Screen monitors at two different places in the MEBT will be used to optimize the beam alignment and the focusing strengths of the quadrupoles. The bunch length at the entrance of the Alvarez tank will be derived from signals of a capacitive pick-up and of the new BSM monitors inside the Alvarez linac [4]. As an alternative an additional BSM [5] can be installed between MEBT and the Alvarez linac.

4 BEAM DYNAMICS CALCULATIONS

The beam optic was developed using the codes COPPOC [6] and PARMTRA [7]. The first order code COPPOC was used because of its powerful optimizer and the intuitive interface. PARMTRA is a particle tracking code for ions that takes into account the space charge forces and the rf-defocusing in the rebuncher cavity.

The transversal and longitudinal envelopes in the MEBT are shown in figure 3 to figure 5. The parameters of the H^--beam behind the RFQs differ according to the different

electrode design. Following parameters have been assumed in the calculation:

	MEBT 1: rf-source & RFQ_1 $\rightarrow$ Alvarez	MEBT 2: magnetron source & RFQ_2 $\rightarrow$ Alvarez
$\epsilon_{x,y}$	36 π mm mrad	36 π mm mrad
$\Delta\phi$	$\pm$ 19°	$\pm$ 29°
ΔW	$\pm$ 10 keV	$\pm$ 14 keV

Table 2: Beam properties (at 750 keV) at the exit of the RFQ.

The quadrupole strengths and the gap voltage of the buncher were optimized with the code PARMTRA. The equivalent defocusing force of the rebuncher amounts to 40% of that of the following quadrupole magnet. Thus, it cannot be neglected in finding the matching parameters of the beam line.

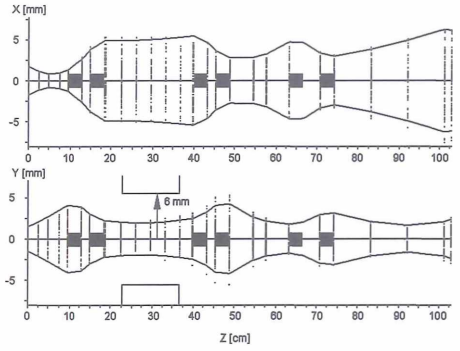

Figure 3: Transversal beam envelopes (2σ) for the MEBT 1 transport line with 20 mA.

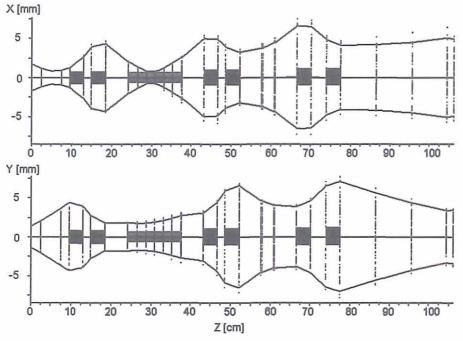

Figure 4: Transversal beam envelopes (2σ) for the MEBT 2 transport line with 20 mA.

There is some enlargement in the emittances (table 3). The rf-defocusing inside the buncher causes a transverse emittance growth due to the nonlinear forces. The dispersion induced by the bending magnet cannot be fully compensated but was minimized due to the small horizontal β-function inside the dipole magnet.

The calculated beam properties with currents of up to 30 mA are suitable for further acceleration with the Alvarez. Compared to the present situation the beam matching to the Alvarez linac can be improved and compensates

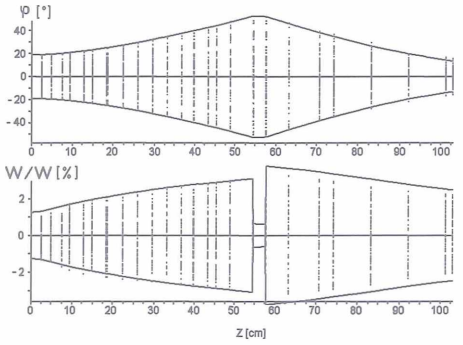

Figure 5: Longitudinal beam envelopes (2σ) for the MEBT 1 transport line with 20 mA.

I/[mA]	$\epsilon_x/\epsilon_{x,0}$	$\epsilon_y/\epsilon_{y,0}$	$\epsilon_z/\epsilon_{z,0}$
0	1.1	1.0	1.0
10	1.3	1.2	1.1
20	1.4	1.3	1.2
25	1.6	1.4	1.2
30	1.7	1.6	1.3

Table 3: Emittance growth factors at different currents in the MEBT 2 transport line.

the influence of emittance growth within the MEBT on the final beam quality. Tracking calculations of the Alvarez linac with and without the MEBT are still in progress and show that a reduction of the emittance at the high energy end should be possible with the usage of the MEBT.

5 SCHEDULE

The modifications of the accelerator system are planned to be made during the HERA shutdown in winter 1997/98. First tests are scheduled for March 1998.

6 ACKNOWLEDGMENTS

The authors are grateful to the technical groups at DESY for their support.

7 REFERENCES

[1] LINAC III collaboration, Rev. Sci. Instruments **62** (4), April 1991.

[2] M. Ferch, Dissertation, IAP Frankfurt, 1984.

[3] J. Peters, **The status of DESY H^- sources**, LINAC96, p199-201.

[4] A.V. Feschenko, A.V. Liiou, A.N. Mirzojan, A.A. Menshov, P.N. Ostroumov, N. Holtkamp, C.-M. Kleffner, M. Nagl, I. Peperkorn, **Bunch Shape Monitors for the DESY H^--Linac**, this conference.

[5] A.V. Feschenko, private communication.

[6] **COPPOC**, I. Borchardt, U. Naujokat, H. Ruge, DESY 1985.

[7] **PARMTRA**, J. Struckmeier, GSI Darmstadt, Germany, private communication.

Petra Bunch Rotation

Wilhelm Kriens

Deutsches Elektronen-Synchrotron, DESY
Hamburg, Germany

Abstract

The upgrade of the Petra *bunch rotation* scheme for protons will be described. Bunch compression in Petra is necessary for stable longitudinal transfer matching with Hera. The influence of beam loading in Petra has to be taken into account for currents above 50 mA even though a strong fast rf feedback system is installed. Amplitude modulation in a short push-pull cycle is chosen for *bunch rotation* and a bunch length compression factor of 0.7 is established with tolerable distortion.

1 INTRODUCTION

Proton transfer from Petra to Hera at 40 Gev/c with regard to longitudinal phase space matching using a 52 MHz rf system in both machines is somewhat critical [1].
Even with an optical change in Petra [2] ($\gamma_{tr} = 6.6 \nearrow 7.9$) the rf voltage ratio for matching is rather unfavourable.

$$\frac{(\, h\,|\eta|\,)_{Petra}}{(\, h\,|\eta|\,)_{Hera}} = 7.4 \qquad (1)$$

The voltage in Petra is limited to 150 kV for short term operation. Therefore the voltage in Hera for matching (20 kV) is too low for stable beam injection.
Choosing to operate Hera at 100 kV during injection, requires longitudinal bunch compression by a factor of 0.67.

2 BUNCH COMPRESSION

The first scheme for *bunch rotation* comprised a 180 degree phase jump, a dwell period during which the bunch lengthens, a jump back to the original stable phase followed by about a quarter synchrotron period before beam transfer [3]. Since the transfer is determined from synchronization with Hera, the start trigger for the phase jump is prepared a fixed number of revolution turns before transfer. Although the procedure could be optimized to achieve adequate compression at moderate beam currents, above 50 mA (some 40 % of design) beam loading effects degraded the ideal behaviour. In particular the bunches became distorted during the phase jump.
In order to reduce beam loading effects, amplitude modulation was applied to the rf system inducing quadrupole mode oscillation for bunch compression. For this purpose a voltage controlled attenuator device with small phase deviation is used at low power input. Additionally the time constant of the transmitter gain control had to be increased to pass the modulation. The choice for the modulation cycle depends on the ability of the rf system and was optimized in relation to beam dynamics. The result can be seen from figure 1. A typical bunch in Petra is measured just before *rotation* and in the last turn at transfer.

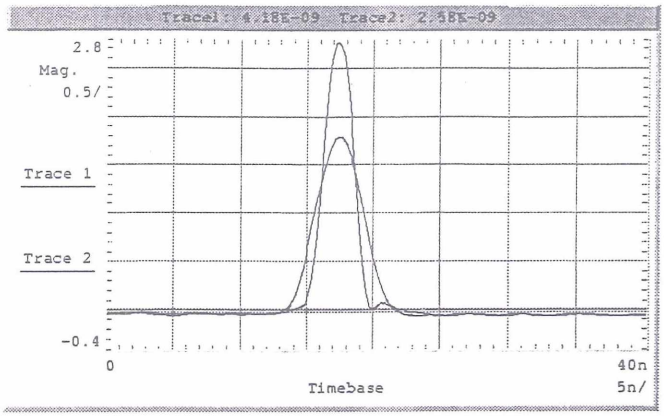

Figure 1: Bunch display just before *bunch rotation* (Trace 1) and the same bunch at extraction time (Trace 2).

2.1 PETRA RF System

Two 52 MHz cavities of the same type with independent power transmitters are installed [4]. Therefore careful phasing for power balancing is necessary to get the required circumferential voltage. In this case the total rf system can be simplified as shown in figure 2 to calculate the beam loading effects.
The transmitter forward voltage $\underline{V}_G$ can be expressed in terms of the cavity voltage $\underline{V}_C$ and the beam voltage $\underline{V}_B = \frac{R_0}{2}\underline{I}_0$. From figure 2 we get the relation between the low level input voltage $\underline{V}_S$ and $\underline{V}_C$ directly.

$$\begin{aligned} \underline{V}_G &= \underline{V}_C + i\Omega\underline{V}_C + \underline{V}_B \\ &= (\underline{V}_S - F\underline{V}_C)G \end{aligned} \qquad (2)$$

The detuning value $\Omega = Q_0\frac{\Delta\omega}{\omega}$ has settled prior to *bunch rotation* i.e.
$\underline{V}_B = -i\Omega\underline{V}_{C0}$ and $\underline{V}_{C0} = \underline{V}_{G0}$ with $\varphi_B = 0$.
Introducing the modulation index $\underline{m} = \frac{\underline{V}_S}{\underline{V}_{S0}}$ and assuming $FG \gg \Omega$ ($FG \approx 100$) we get

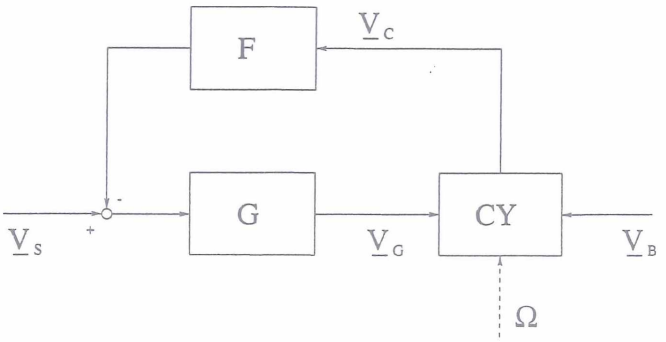

Figure 2: Block diagram of the Petra rf system with G the transmitter gain and F the feedback factor. Voltages $\underline{V}$ are in complex notation. Ω is the detuning value of the cavity CY.

$$\frac{\underline{V}_C}{\underline{V}_{C0}} = \frac{\underline{m}(1+FG)+i\Omega}{1+FG+i\Omega} \approx \underline{m} \qquad (3)$$

$$\frac{\underline{V}_G}{\underline{V}_{G0}} = \frac{\underline{V}_C}{\underline{V}_{C0}}(1+i\Omega) - i\Omega \approx \underline{m}(1+i\Omega) - i\Omega \qquad (4)$$

From equation 3 we can see that the cavity voltage is proportional to the input voltage due to the strong fast feedback. Therefore the low level modulator directly controls the cavity voltage as desired but the power transmitter is disturbed by beam loading corresponding to equation 4.
With $V_{C0} = 140\ kV$, $R_0 = 2\ M\Omega$ and 70 mA of average beam current the detuning value is $\Omega = 1$.
If we suppose that the transmitter could deliver a factor of two more power for short term modulation, then 35 mA for phase jump ($\underline{m} = -1$) and 130 mA for amplitude modulation ($\underline{m} = 1.3$) are the beam current limits for operation. Both computer simulations and the reality in Petra has shown that $\underline{m} = 1.3$ is sufficient for bunch compression via amplitude modulation.

2.2 *ESME Simulation*

The ESME computer program [5] was used to optimize the operation mode for amplitude modulation of the cavity voltage. The aim was to get a minimum compression factor for the bunch length with tolerable distortion of the emittance.
Due to the ability of the rf transmitter the simulation is done with a modulation cycle as shown in figure 6. It can be seen that fast ramping of the voltage up and down with twice the synchrotron frequency is the best way to quickly induce shape oscillation. The maximum voltage corresponds to $\underline{m} = 1.3$ and the minimum voltage is found to be symmetric with respect to the starting value.
For the special case of 0.1 eVs emittance and a bigaussian distribution (see figure 3) we get the evolution of the bunch length and the distortion of the emittance turn by turn as seen in figure 7 and figure 8. The optimum timing for beam transfer is at turn 440 after three quarter synchrotron oscillations. Only for rather low emittance more *rotation* cycles are useful. Figure 4 displays the phase space at turn 440 in our special case.
To illustrate the bunch oscillation more impressively a mountain range display of the bunch length is shown in figure 5.
Table 1 shows the influence of the initial emittance on the *bunch rotation* based on a bigaussian phase space distribution. Bunch compression fulfills the Hera requirement for stable injection with less than 5 % of distortion.
Furthermore it can be seen from the simulation that the modulation parameters are not very sensitive. Therefore a tuning of these values is not foreseen in the operation control.

Table 1: Compression and Distortion vs initial Emittance

Emittance	Bunch length	Compression	Distortion
[eVs]	FWHM [ns]	[ ]	[%]
0.04	1.74	0.652	0.2
0.06	2.15	0.646	0.6
0.08	2.49	0.647	1.2
0.10	2.80	0.653	2.1
0.12	3.09	0.668	3.4
0.14	3.33	0.686	5.0
0.16	3.61	0.717	7.4

3 ACKNOWLEDGEMENT

The author would like to thank U.Hurdelbrink, P.Schmidt and G.Weiberg for technical support and J.R.Maidment for comments regarding the manuscript.

4 REFERENCES

[1] J.R. Maidment, HERA-p: Longitudinal Miscellany Internal Paper, DESY, August 10, 1992

[2] B. Parker, Neue Optiken fuer PETRA und PR-Weg, Betriebsseminar, St.Englmar 1996 DESY HERA 96-05

[3] G. Wiesenfeldt, Untersuchungen zur longitudinalen Strahlanpassung beim Protonentransfer von PETRA nach HERA, Diplomarbeit, Universitaet Hamburg, March 1995

[4] A. Gamp, Servo Control of RF Cavities under Beam Loading, DESY HERA 91-09, May 1991

[5] J. MacLachlan, User's Guide to ESME v. 8.13, June 30, 1995.

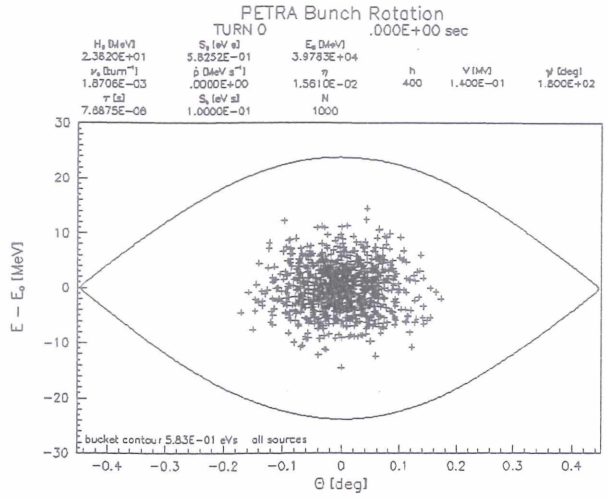

Figure 3: Initial bigaussian Phase Space Distribution

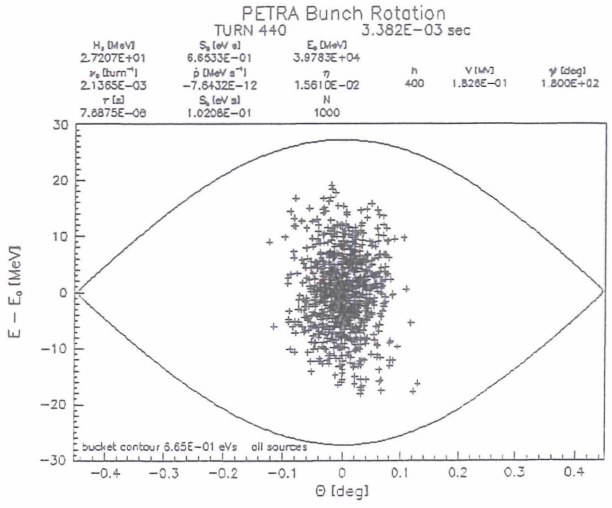

Figure 4: Distribution at Transfer (turn 440)

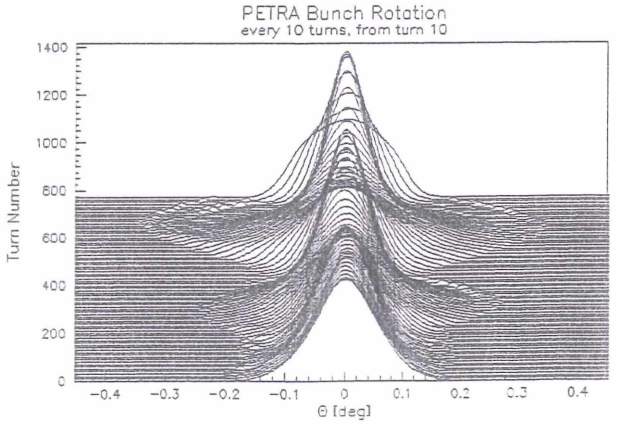

Figure 5: Mountain Range Display of the Bunch length

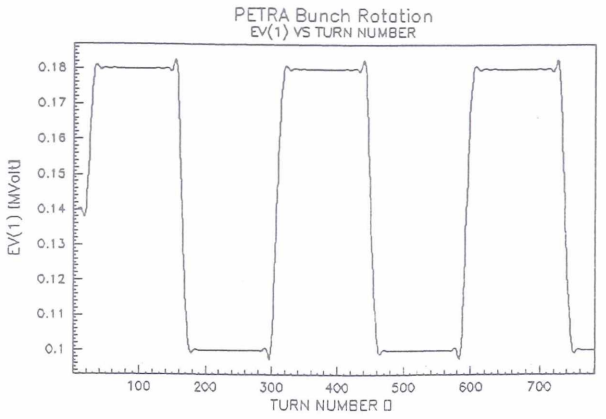

Figure 6: Cavity Voltage Modulation

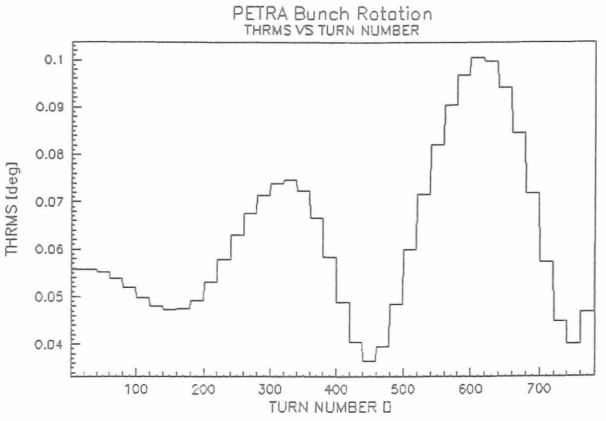

Figure 7: Bunch length ($THRMS \times 50\ ns \approx FWHM$)

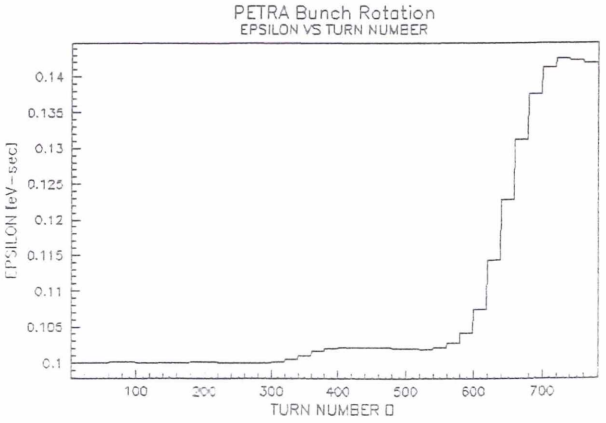

Figure 8: Emittance growth

NUMERICAL SOLUTION FOR FOKKER-PLANCK EQUATIONS IN ACCELERATORS

M.P. Zorzano, H. Mais, DESY, D-22607 Hamburg, Germany and
L. Vazquez, Universidad Complutense, 28040 Madrid, Spain

Abstract

A finite difference scheme is presented to solve the Fokker-Planck equation in (2+1) variables numerically. This scheme is applied to study stochastic beam dynamics in two-dimensional phase space.

1 INTRODUCTION

One important problem of accelerator physics is to investigate the particle motion under the influence of noise [1]. There are various sources of noise: rf noise, random power supply ripple, random ground motion, restgas scattering, and quantum fluctuations due to radiation. The physical questions one wants to answer are: what is the longtime behaviour of the dynamics, what is the probability for the particle to hit the vacuum chamber (and then be lost) (mean first passage time), what are the average fluctuations of the particle around the periodic design orbit of the accelerator (moments), and what is the time evolution of the probability density (transient and stationary behaviour).

Mathematically stochastic systems can be modelled by stochastic maps (in the time discrete case) and by stochastic differential equations (s.d.e.) in the time continuous case. In the following we will restrict our considerations to s.d.e. with Gaussian white noise. Gaussian white noise is a very good approximation in many accelerator problems [1]. The solution of these s.d.e. are Markovian diffusion processes which can be described by the Fokker-Planck equation [2]. The Fokker-Planck equation is a partial differential equation for the probability density and the transition probability of these stochastic processes.

In general, the stochastic equations of motion of a particle in an accelerator are very complicated and can not be solved analytically, therefore one has to use numerical schemes. One way is to consider the s.d.e. directly. An alternative way is to investigate and solve the Fokker-Planck equation.

In this paper we study stochastic beam dynamics in two-dimensional phase space. We describe a finite difference scheme to solve the corresponding Fokker-Planck equation with two phase space variables plus time. Extensive numerical simulations for this kind of problem have been performed in [3] using finite elements for the partial differential equation and Monte Carlo simulations for the s.d.e.. Here we concentrate on the finite difference scheme because of its simple implementation, its flexibility with respect to different boundary conditions, the straightforward extension to higher dimensional problems, its efficiency concerning CPU time and because it is easy to understand the physical meaning of each term in the scheme.

The paper is organized as follows: in section 2 we present the numerical scheme for solving the Fokker-Planck equation in (2+1) variables and in section 3 we present some examples and applications to accelerator physics. Section 4 summarizes the main results and gives a list of open questions for future studies.

2 NUMERICAL SCHEME FOR SOLVING THE FOKKER-PLANCK EQUATION

We restrict our investigation to stochastic dynamics in two-dimensional phase space. The general equations of motion we want to study are of the form

$$\frac{d}{ds}x_1 = x_2 \tag{1}$$

$$\frac{d}{ds}x_2 = -a_1(x_1) - a_2(x_1, x_2) + a_3(x_1)\eta_1 + a_4\eta_2 \tag{2}$$

with η_1, η_2 a Gaussian white noise vector process. $a_1(x_1)$ can be an arbitrary nonlinear potential (field), $a_2(x_1, x_2)$ can include van der Pol-like damping terms, $a_3(x_1)\eta_1$ describes random parameters and $a_4\eta_2$ represents an additive noise term. The corresponding (Ito) Fokker-Planck equation for the probability density reads [2]

$$\begin{aligned}\frac{\partial}{\partial s}p(x_1, x_2, s) &= \\ &= -\frac{\partial}{\partial x_1}[x_2 \cdot p(x_1, x_2, s)] + \\ &+\frac{\partial}{\partial x_2}[(a_1(x_1) + a_2(x_1, x_2)) \cdot p(x_1, x_2, s)] + \\ &+\frac{1}{2}\frac{\partial^2}{\partial x_2^2}[(a_3^2(x_1) + a_4^2) \cdot p(x_1, x_2, s)]\,.\end{aligned} \tag{3}$$

Equation (3) can be written in the form of two fluxes, one in x_1 and one in x_2 such that

$$\frac{\partial p}{\partial s} = \frac{\partial A}{\partial x_1} + \frac{\partial B}{\partial x_2} \tag{4}$$

a form which suggests to use an operator splitting method [4]. First we evaluate implicitly the x_2 derivative and then - also implicitly - the x_1 derivative with a tridiagonal scheme

$$\frac{p_{i,j}^{n+\frac{1}{2}} - p_{i,j}^{n}}{\Delta s} = \frac{F_{i,j+\frac{1}{2}}^{n+\frac{1}{2}} - F_{i,j-\frac{1}{2}}^{n+\frac{1}{2}}}{\Delta x_2} \tag{5}$$

$$\frac{p_{i,j}^{n+1} - p_{i,j}^{n+\frac{1}{2}}}{\Delta s} = -x_2\ \frac{p_{i+1,j}^{n+1} - p_{i-1,j}^{n+1}}{2\Delta x_1} \tag{6}$$

with

$$F_{i,j+\frac{1}{2}} = D\ \frac{p_{i,j+1} - p_{i,j}}{\Delta x_2} + \\ +[a_1(x_1) + a_2(x_1, x_2 + \Delta x_2)]\frac{p_{i,j+1} - p_{i,j}}{2} \quad (7)$$

where we have set $2D = [a_3^2(x_1) + a_4^2]$. Making the von Neumann analysis of stability it turns out that the scheme is unconditionally stable. For more information see [5],[6].

3 RESULTS AND EXAMPLES

3.1 *Harmonic oscillator*

The first example we have studied is the damped harmonic oscillator with strong diffusion i.e. $a_1(x_1) = Kx_1$, $a_2(x_1, x_2) = \gamma x_2$, $a_3(x_1) = 0$ and $a_4 = \sigma$. K, γ, σ are constants. Since this problem can be studied analytically [7] it served to check our numerical scheme. With the parameter set $K = 1$, $\gamma = 2.1$, $\sigma = 0.8$, a 80×80 grid, $\Delta x_1 = \Delta x_2 = 0.1$, $\Delta s = \pi/1000$ and the exact solution at $s = 0.95$ as initial condition we obtained the time evolution of the probability density depicted in figure 1.

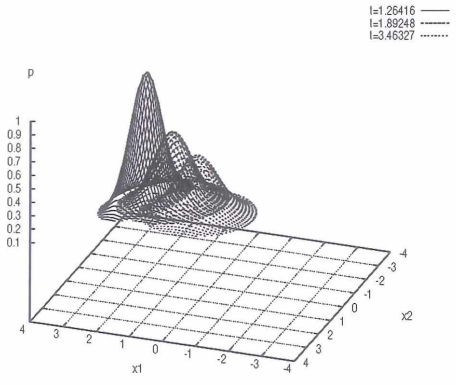

Figure 1: Density evolution in the damped linear harmonic oscillator equation, drift and diffusion resulting from the stochastic excitation.

3.2 *Duffing oscillator*

As a second example we have investigated the Duffing oscillator with damping, multiplicative and additive Gaussian white noise. In this case $a_1(x_1) = \omega^2[\alpha x_1 + \epsilon x_1^3]$, $a_2(x_1, x_2) = 2\tau\omega x_2$, $a_3(x_1) = -\omega^2\sqrt{2D_{11}}x_1$, and $a_4 = \sqrt{2D_{22}}$. $\omega = 1, \alpha = -1, \tau = 0.2, \epsilon = 0.1$ are constants. For two different sets of noise intensities D_{11}, D_{22} we obtained the results shown in figure 2 and figure 3.

In this nonlinear system with multiplicative noise one can observe a noise induced transition [8]. In the additive noise case the system has two stable points just like the deterministic system. Under the influence of multiplicative noise the probability density at the origin grows. Further increasing of the strength of the multiplicative noise

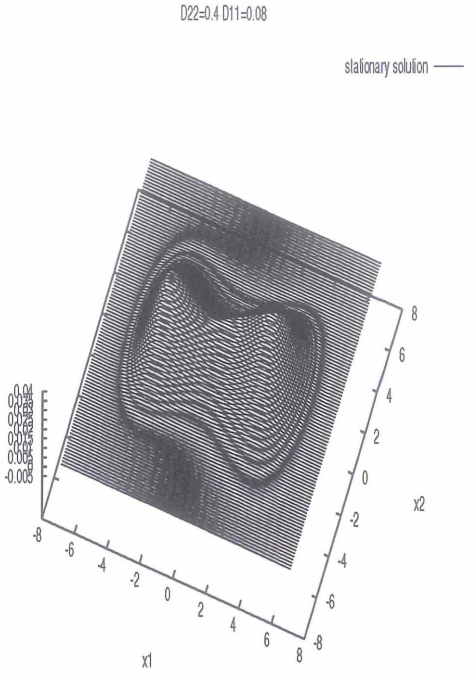

Figure 2: $D_{22} = 0.4$, D_{11}=0.08, view of the stationary density in phase space. dt=π/1000 Finite difference integration.

changes the stability of the origin - the origin becomes a stable point.

3.3 *Beam-beam interaction in storage rings under the influence of noise*

We have made a preliminary study of the the beam-beam interaction in storage rings under the influence of noise. The model we have chosen was defined by

$$\frac{\partial p}{\partial s} = -\frac{\partial(x_2 p)}{\partial x_1} + \\ \frac{\partial}{\partial x_2}[(\alpha x_2 + w^2 x_1 + f(x_1, s))p] + \frac{1}{2}\frac{\partial^2}{\partial x_2^2}(dp). \quad (8)$$

with $f(x_1, s) = \sum_{n=1} -8\pi\xi_{bb}(\frac{1-e^{-\frac{1}{2}x_1^2}}{x_1})\delta_(s = nL)$. We set the parameters to $\frac{d}{2} = 0.000147, \tau = 0.0000310, w = 0.7, \xi_{bb} = 0.07$ (see figure 4).

4 SUMMARY AND CONCLUSIONS

In this paper we have presented a robust finite difference scheme for the numerical solution of the Fokker-Planck equation in (2+1) variables. The scheme has been checked with finite element calculations and with direct numerical simulations of the underlying s.d.e. It seems to be a good candidate for solving more complicated and more realistic accelerator models such as higher dimensional problems

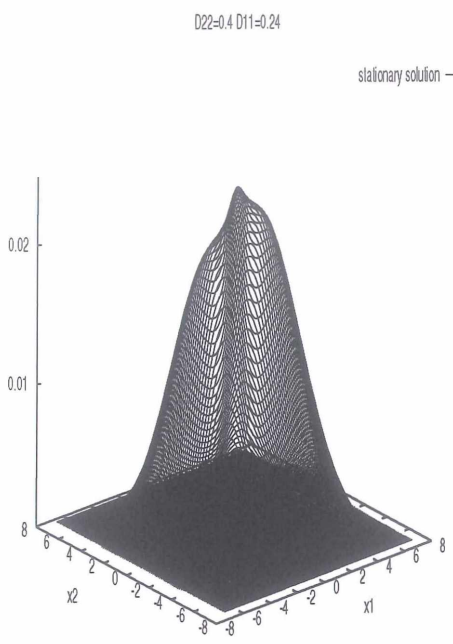

Figure 3: $D_{22} = 0.4$, D_{11}=0.24, view of the stationary density in phase space. dt=π/1000 Finite difference integration.

(coupled betatron motion), non- Gaussian white noise perturbations of Ornstein-Uhlenbeck type and explicitly time dependent coefficients $a_i(..., s)$.

5 ACKNOWLEDGEMENT

This research was partly supported by the EC Human Capital and Mobility grant no: ERBCHRXCT940480, and by a DESY PhD scholarship. L.V. thanks the support of the Comision Interministerial de Ciencia y Tecnologia of Spain under grant PB95-0426. The authors want to thank L. A.Bergman, B.F.Spencer, S.F.Wojtkiewicz, E.Johnson for information about their work.

6 REFERENCES

[1] A.Pauluhn. Thesis: *Stochastic Beam Dynamics in Storage Rings* DESY 93-198 December 1993

[2] H.Risken *The Fokker-Planck Equation,Methods of Solutions and Applications.* Springer-Verlag 1984

[3] B.F.Spencer, L. A.Bergman Nonlinear Dynamics, 4 (1993) 357-372

[4] W.Press,S.Teukolsky, W.Vetterling, B.Flannery. *Numerical Recipes in C* Cambridge Univerity Press 1994.

[5] R.D.Richtmyer, K.W.Morton. *Difference Methods for Initial-Value Problems.* Interscience Publishers. 1967.

[6] M.P.Zorzano,H.Mais,L.Vazquez. *"Numerical solution of two dimensional Fokker-Planck equations"* to be published.

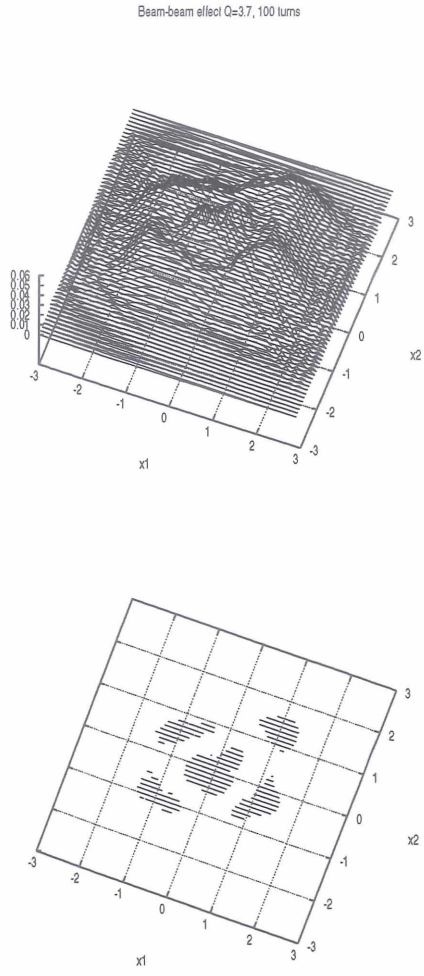

Figure 4: Electron case. Density for the beam-beam effect with Q=3.7, $\xi = 0.07$, damping time 250 turns. The lower figure is the projection onto the phase space of the areas of highest probability.

[7] S. Chandrashekar. *Stochastic Problems in Physics and Astronomy.* Reviews of Modern Physics. Vol. 15. (1943) 1-44.

[8] W.Horsthemke, R.Lefever *Noise-Induced Transitions* Theory and Applications in Physics, Chemistry, and Biology. Springer-Verlag Heidelberg New York Tokyo 1984.

NOTE ON THE SC LINEAR COLLIDER TESLA CAVITY DESIGN

J. Sekutowicz, D. Proch, C. Tang , DESY-MHF, 22603 Hamburg, FRG

Abstract

The experience we have gained over the last few years from experiments with superconducting cavities for the TESLA test facility, justifies a revision of the design proposed almost five years ago [1,2]. The proposed new design, presented here, takes the advantage of the high quality factor $Q_o > 10^{10}$ and low electron emission at the specified accelerating field of 25 MV/m, as demonstrated by some tested cavities. The main aim of the design is to simplify production and preparation of superconducting (sc) cavities and thus to reduce the cost of the linear collider. The new cavity shape has an enlarged iris diameter with the following advantages: significantly lower loss factors, a simplified and less expensive scheme for the HOM damping and the suitability of hydroforming and higher stability of the field profile.

1 INTRODUCTION

The quality factor, Q_o, vs. E_{acc} of two 1.3 GHz, 9-cell TESLA cavities is shown in Fig. 1. The Q_o reaches a very high value ~ $5 \cdot 10^{10}$ at low field region and stays above $1.7 \cdot 10^{10}$ for one cavity and above $3 \cdot 10^{10}$ for the second one, for the accelerating field of E_{acc}=25 MV/m, the specified value for the sc linear collider [3]. The power dissipated in the cavity wall P_{diss}, cooled by 2 K

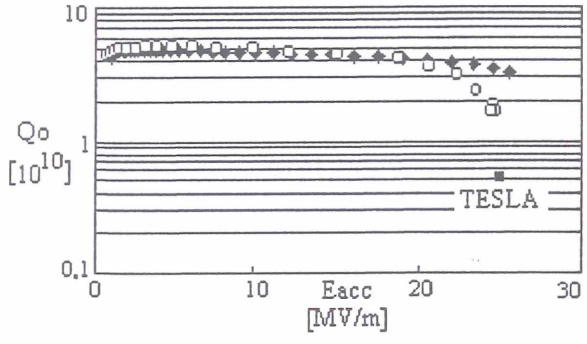

Fig. 1 Q_o vs. E_{acc} as measured in a vertical cryostat

LHe, is inverse proportional to $(R/Q) \cdot Q_o$, where (R/Q) is the characteristic impedance of a cavity. For cavities with quality factors depicted in Fig. 1, the P_{diss} at 25 MV/m is 3.4 and 6 times respectively, lower than for a cavity with the specified value of $Q_o = 5 \cdot 10^9$ [3]. The small slope of both curves demonstrates the important feature that cavities have low electron emission. It results from careful cleaning during the cavity preparation and the low field enhancement factor E_{peak}/E_{acc}. The shape of the TESLA structure, proposed almost five years ago, has been chosen to minimize: E_{peak}/E_{acc} to keep electron emission loading low and H_{peak}/E_{acc} to shift quench level towards higher E_{acc} and to maximize (R/Q) to provide low cryogenic load. Final values of these parameters (see Table 1) have been achieved by means of a small iris diameter, but there are few negative consequences of the small aperture.

2 WEAK POINTS OF THE CURRENT DESIGN

The error of the field amplitude in an individual cell for the accelerating π mode is proportional to $(N)^2/k$, where N is the number of cells in the structure and k is the coupling. Since the cell-to-cell coupling k is small, the profile of the accelerating field is sensitive to the frequency perturbation of an individual cell. Any mechanical, chemical or thermal preparation of TESLA structures causes a perturbation of the field configuration. Many TTF cavities from the first production had to be re-tuned several times to keep the field unflatness below the specified level of 5 %. Since tuning had to be performed outside the clean room, each re-tuning required that the cavity must be re-cleaned. This makes the preparation more expensive and more time-consuming to an unacceptable level for 20000 sc cavities. After the helium vessel is welded, no access to the cells is possible and therefore re-tuning, even when necessary, is impossible.
Field unflatness decreases the effective accelerating field. Since the energy of colliding beams has been fixed, a compensation must be made for the lower effective gradient, either with additional length of the collider or by an operation of some cavities at E_{acc} above 25 MV/m. This requires only negligible additional RF power but the operation at a higher gradient may lead to an increased γ-radiation and a higher probability of quenches.
The second complication coming from the field unflatness is a difference in Q_{ext}. The acceleration process in the TESLA collider is performed during the transient. This requires all cavities to be at 25 MV/m at the same time, 533 μs after the RF pulse is switched on. As the cavity fill time depends on the loaded Q (in case of sc cavities mainly on Q_{ext}) differences in Q_{ext} yield to differences in the accelerating gradient during acceleration. This means that the energy gain, in cavities with non nominal Q_{ext}, changes from the beginning to the end of the pulse. To avoid this source of energy spread two adjustable fundamental mode (fm) coupler designs, based on a coaxial line technique, have been proposed [4,5]. In both designs, the adjustment of Q_{ext} is performed by a change of penetration of the inner conductor in the beam tube. The adjustment unfortunately makes the design more complicated and expensive. Additionally, a fast voltage control loop will be used to reduce the energy spread, but this will require more RF power.

A third problem resulting from the field unflatness is an increase of characteristic impedance of other modes, belonging to the fm passband. If the cavity is well tuned, then the characteristic impedances of these modes are negligible. Perturbation of an individual cell causes that especially the impedance of the mode $8\pi/9$ increases. The damping of these parasitic modes is possible only by fm coupler. So, it is expected that the external Q's of these modes are in the range of the nominal value of Q_{ext} of the fm. A typically observed field unflatness of 15 % increases (R/Q) of the $8\pi/9$ mode from almost 0 to 5 Ω. In this case the impedance of this mode is 15 MΩ, as high as the impedance of monopole modes from the TM_{011} passband with the highest (R/Q) ≅150 Ω.

In the present design, neighboring cavities in a cryomodule are separated by a 3/2 λ long beam tube. Therefore the ratio of the active length to the total length of the TESLA structure is only 0.75. Thus one quarter of both linacs length, 7 km, is not used for the acceleration. The effective average accelerating field is then reduced from 25 MV/m to almost 19 MV/m. One can improve the fill factor by increasing the number of cells per cavity and by shortening the interconnections between the cavities. Since the field profile of the present TESLA structures is already sensitive to frequency errors, an increase of N is impossible, so only interconnections could be made shorter to improve the fill factor.

The cost of the electron beam welding is a significant part of the cavity fabrication cost. Eighteen half cells and two beam tubes per cavity must be specially prepared to provide nineteen high quality welds. Alternative fabrication methods are under consideration to lower the production costs. Two of them hydroforming [6] and spinning [7], show a strong potential. The hydroforming of Nb cavities needs still more R&D, but the experience with Cu cavities proofs that the required shape can be obtained with high precision and good reproducibility. The hydroforming process becomes simpler when the ratio of the maximum radius (equator) to the minimum radius (iris) of a cavity is 2 or less. In the current design this ratio is almost equal to 3. The shape of the cavity plays also an important role. Also here, the tests performed on copper cavities showed that any narrow or small curvature, especially in the iris region, makes hydroforming more complicated. Unfortunately this is the case for the current cavity design.

The very high intensity FEL (λ= 1 Å) is one of the proposed new applications of the 3 km part of the TESLA e-linac. This operation requires very short bunches with σ_z = 25 μm, which can excite wake fields to the THz region. Since the longitudinal loss factor $k_{\parallel}$ and thus the energy loss scale approximately with $(\sigma_z)^{-1/2}$, the total energy deposited by single bunch will be big. This will influence the beam. Additionally, the high energy photons may brake Cooper pairs in the superconducting material and increase the wall losses of the fm. As a remedy, to keep the energy deposition low, one can decrease $k_{\parallel}$ by enlarging the iris opening.

3 NEW SHAPE

We expect that the improved cavity shape should :
-increase cell-to-cell coupling,
-simplify hydroforming or spinning of the structure,
-reduce the loss factor $k_{\parallel}$,
-simplify HOM mode damping,
- simplify the design of the fm coupler (not variable),
-increase the ratio of the active length to the total length.
Besides, the new design should keep, as much as possible, the advantages of the current shape. These advantages are parameters like: (R/Q), E_{peak}/E_{acc} and H_{peak}/E_{acc}. Some of the disadvantages we have pointed out can be overcome with an increase of the iris diameter [2]. The proposed new shape (Fig. 2) has an iris aperture of 102 mm The iris is circularly formed with r = 17 mm. The parameters of the old and the new shape are listed in Table 1.

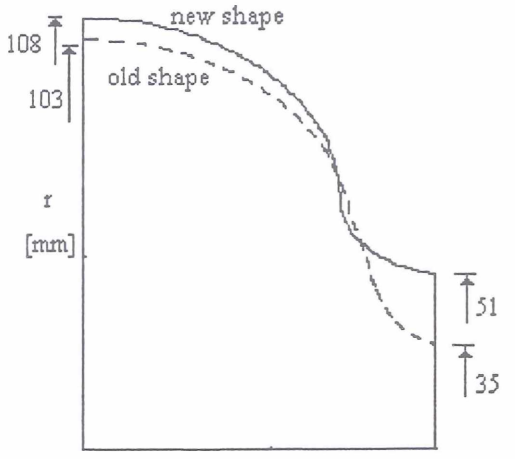

Figure 2 The new and the old shape of the inner cell (not in scale)

Table 1 Parameters of the old and the new cavity shape

Parameter	Old	New	Change [%]
(R/Q) [Ω]	1035	695	- 33
k [%]	1.84	5.51	200
E_{peak}/E_{acc}	2.0	2.34	17.0
H_{peak}/E_{acc} [Oe/(MV/m)]	42.6	50.2	17.8
$k_{\perp}$ (σ=1mm) [V/(pCm)]	18	6.7	- 63
$k_{\parallel}$ (σ=1mm) [V/pC]	8.7	5.5	- 37
iris diameter [mm]	70	102	46
iris shape h./v. axis, radius [mm]	ellip. 12/19	circle 17	
r_{equ}/r_{iris} inner /end cell	3 / 2.7	2 / 1.9	- 29 / -27

4 DISCUSSION

The cell-to-cell coupling increased by a factor of three as compared to the current design. This makes the structure less sensitive to any machining tolerances and provides room to increase the number of cells per cavity. The new geometry is more suitable for hydroforming or spinning. The ratio of the equator radius to the iris radius is near 2 for the inner cell and even below 2 for the end cell. The iris region is now wider and the wall can be made thicker in this region. Hereby stiffening rings, used in the current design to reduce the Lorentz force detuning, can be avoided [6].

The loss factors of the new geometry are significantly lower. The single passage deposited energy is reduced by 37 % for the monopole modes and by 63 % for the dipole modes. The decrease of the loss factors indicates a decrease of HOMs characteristic impedances, too. Therefore the energy deposited in the resonantly excited parasitic modes will be reduced. This gives more relaxed requirements for the damping of these modes.

The enlarged iris of the new end cell enables an increase in diameter of the beam tube. We have fixed this diameter to 0.11 m. It is the smallest size that allows propagation of all monopole modes in the tube. The first eight dipole modes stay under cutoff but their field in the beam tube seems to be high enough for damping to the BBU limit. Two HOM couplers shifted angularly by 90° and attached at every second beam tube may be used for the damping of parasitic modes excited in two neighboring cavities. This damping scheme requires only one HOM coupler per cavity. Due to the HOM propagation the distance between HOM coupler and end cells can be much larger than for the current design. Since the fundamental mode is under cutoff and the distance to end cells is large, a very little fm rejection, achievable without any additional filter, is needed to prevent output cables and feedthroughs from overheating. This simplifies the design of the HOM coupler.

As the field pattern is stable, variable couplers are not necessary. If operation of the collider should differ from the nominal one, Q_{ext} can be changed by means of a 3-stub waveguide transformer installed in the input line of each cavity. The transformer also makes the RF distribution system more flexible for phase adjustment and gives more freedom in the length of intersections.

There are mainly two negative consequences of the larger iris aperture. As predicted, a larger aperture lowers (R/Q) of the fm. The reduction is compensated by a high Q_o and finally the cryogenic loss is smaller. In order to keep cavities matched for the nominal operation: U=26 MV/cavity and the I_b=8 mA, Q_{ext} should be increased by 33 %, and fill time will therefore be longer by 240 µs. When Q_{ext} has still its previous nominal value, 2 % of the RF power will be reflected but fill time will be longer by 180 µs. This problem should be investigated in more detail. The ratios of E_{peak}/E_{acc} and H_{peak}/E_{acc} have increased by 17 %. This means more γ-radiation at the specified E_{acc} and higher quench probability. Surface cleaning methods (BCP, high pressure water rinsing) and assembling methods are still in an optimization phase. Also inspection methods of the Nb material, which help to eliminate Nb sheets with defects leading to quenches, are under development. It is the hope that further progress in the fabrication, the assembly and the cleaning methods can compensate for the increase of these parameters.

5 CONCLUSION

Table 2 Summary of features of the new shape

k , cell-to-cell coupling	+
$k_{\parallel}$, longitudinal loss factor	+
$k_{\perp}$, transversal loss factor	+
r_{equ}/r_{iris} inner cell and end cell	+
fill factor of both linacs	+
simplified scheme for HOM damping	+
simplified fm coupler	+
(R/Q) fm characteristic impedance	-
E_{peak}/E_{acc} , H_{peak}/E_{acc}	-

A summary of the positive and the negative features of the new cavity shape is given in Table 2. We plan to build copper models of the new structure to prove experimentally the stability of the accelerating field, the proposed scheme of the HOM damping and the coupling between structures for the fm and the HOMs. As a next step, Nb prototypes should be fabricated to investigate the hydroforming method, the Lorentz detuning and to check new limitations in the accelerating field.

6 ACKNOWLEDGMENTS

We would like to express our gratitude to the TESLA collaboration group for many helpful discussions.

7 REFERENCES

[1] E. Haebel, A. Mosnier, J.Sekutowicz, „Cavity Shape Optimization for Superconducting Linear Collider", Proc.of HEACC'92, Hamburg, 1992.

[2] E. Haebel, A. Mosnier, „Large or Small Iris Aperture in SC Multicell Cavities", Proc. of The 5th SRF Work.,Hamburg, 1991.

[3] D. A. Edwards, „TESLA TEST FACILITY LINAC-Design Report", TESLA Rep. 95-01.

[4] B. Dwersteg, „Mechanical Concept of TESLA Main Coupler Development at DESY",TESLA Rep 93-15

[5] M.Champion, „RF Input Coupler and Windows: Performances, Limitations and Recent Developments", Proc. of 7th Work. on S RF, Gif sur Yvette, 1995.

[6] H. Kaiser, DESY; private communication.

[7] V. Palmieri et al., „Recent Experience with the Spinning of 1.5 GHz Seamless Copper Monocells", Proc. of 7th Work. on SRF, Gif sur Yvette, 1995.

EXPERIMENTAL MEASUREMENT OF HIGH-GRADIENT STANDING WAVE ACCELERATOR TRANSPORT MATRIX

S. Reiche, DESY, Hamburg, Germany
J.B. Rosenzweig, University of California, Los Angeles, USA
L. Serafini, INFN-Milano, Milan, Italy

Abstract

This paper presents an experimental study of the transverse beam dynamics of an electron beam in a high-gradient, standing wave linear accelerator. A 3.6 MeV beam from the UCLA RF Photoinjector (SATURNUS) is injected at various phases and rf field amplitudes into the plane wave transformer (PWT) linac (peak acceleration 40 MeV/m), and its transverse dynamics measured by a corrector magnet sweeping method. This method allows us to reconstruct the transverse matrix elements, which are compared to analytical predictions(J.B. Rosenzweig and L.Serafini, Physical Review E 49, 1599 (1994)). The determinant of the experimentally derived matrix is found to be the ratio of the initial to final momentum, verifying the theory, and providing direct evidence of adiabatic damping of transverse trace space.

1 INTRODUCTION

With the rise in use of high gradient radio-frequency linear accelerators (rf linacs), in devices such as rf photoinjectors[1] and linear collider test facilities[2], there has been increased attention placed on the strong transverse focusing effects present in these devices. These effects, which are due both to first order transient effects at the entrance and exit of a linac, and to second order ponderomotive (alternating gradient) effects in the body of the periodic linac structure, are of primary importance in understanding the beam transport in moderate energy sections ($5 < \gamma = E/m_e c^2 < 100$) of electron accelerators. While theoretical analyses of the focusing properties of linacs date back to the 1960's[3, 4], recent work has produced a more detailed understanding of the ponderomotive force[5], and analytical solutions of these equations for arbitrary acceleration phase and spatial harmonic content of the rf fields have been found[6], which led to a matrix description of the trace space transport.

This matrix treatment of beam dynamics in high gradient rf linacs, as well as the underlying analytical model for the averaged (over an rf period) transverse forces, have formed the underpinning of much recent work, from the optics of linear collider test facilities[2], to the full theory of space-charge dominated beam dynamics in rf photoinjectors[7]. While these implementations of the theory have been compared positively with computer simulation, there has, however, been no effort to date to verify the theoretical advances with experiment. This paper therefore presents a first such verification.

2 THEORY

The trace space transport matrix corresponding to a rf linac, which upon multiplication of a transverse trace space vector, *e.g.* (x, x') , gives the mapping of this vector through the linac, has recently been derived for arbitrary rf phase, amplitude, and spatial harmonic content in the linac. Including all terms to second order in the average accelerating gradient $eE_0 \cos(\phi) \equiv \gamma' m_e c^2$, where E_0 is the amplitude of the synchronous ($\nu_\phi \cong c$) spatial harmonic wave component of the rf field, and $\phi = \omega t - kz$ is the phase defined with respect to the maximum acceleration in this wave, the action of a ponderomotive force can obtained to second order by averaging over the fast alternating gradient first order forces and the induced lowest order oscillatory motion, as[5, 6]

$$\overline{F_r} = \eta(\phi) \frac{(qE_0)^2}{8\gamma m_0 c^2} r \tag{1}$$

with

$$\eta(\phi) \equiv \sum_{n=1}^{\infty} b_n^2 + b_{-n}^2 + 2 b_n b_{-n} \cos(2\phi). \tag{2}$$

The coefficients b_n are the Floquet amplitudes of the spatial harmonics, defined by the expression, valid for an ultra-relativistic ($\nu_b \cong c$) electron

$$E_z \equiv E_0 \mathrm{Re}\left[\sum_{n=-\infty}^{\infty} b_n e^{i(2k_0 n z + \phi)} \right] \tag{3}$$

where $k_0 = \psi/d = \omega/c$ and ψ is the rf phase shift per period of the linac, with $\psi = \pi$ in the structure considered here.

From the averaged force, the differential equation governing the *seculat* trajectory of the electron, about which the fast oscillations induced in first order are performed, is derived. Its general solutions, given in matrix form, can be found in Ref. 6. At the ends of an rf structure, there are first order transient angular kicks associated with entering and exiting the fringing field which are not immediately cancelled in first order by a nearby kick. These kicks, again valid when considering the secular trajectory, are given by $\pm\gamma'/2\gamma$, for the exit and entrance regions, respectively. Multiplying the matrices associated with the entrance, interior, and exit of the linac, we have the full trace space transport matrix,

$$M = \tag{4}$$

$$\begin{bmatrix} \cos(\alpha) - \sqrt{\frac{2}{\eta(\phi)}} \cos(\phi)\sin(\alpha) & \sqrt{\frac{8}{\eta(\phi)}} \frac{\gamma_i}{\gamma'} \cos(\phi)\sin(\alpha) \\ -\frac{\gamma'}{\gamma_f}\left[\frac{\sin(\phi)}{\sqrt{2\eta(\phi)}} + \frac{\sqrt{\eta(\phi)}}{\sqrt{8}\cos(\phi)}\right]\sin(\alpha) & \frac{\gamma_i}{\gamma_f}\left[\cos(\alpha) + \sqrt{\frac{2}{\eta(\phi)}}\cos(\phi)\sin(\alpha)\right] \end{bmatrix}$$

Here $\alpha = \frac{\sqrt{\eta(\phi)}}{\sqrt{8}\cos(\phi)} \ln(\gamma_f/\gamma_i)$, with γ_i and γ_f the initial and final Lorentz factors of the electron, respectively, which are simply related by $\gamma_f = \gamma_i + \gamma' L$, with L equal to the length of the linac section, with $\gamma' m_e c^2$ equal to the averaged (over a period of the linac) acceleration gradient.

3 THE EXPERIMENT

The linac used for the present experiments is a component of the UCLA Photoinjector, a rf accelerating section which boosts the energy of a 3.6 MeV photoelectron beam extracted from a high gradient 1.5 cell π-mode rf gun to approximately 12.8 MeV at maximum in these experiments. This linac is constructed of a novel, high shunt impedance design known as a plane-wave transformer[8] (PWT), and has non-negligible spatial harmonic content (*e.g.* $\eta(0) = 1.23$). The experimental arrangement is nearly ideal for observing the focusing and adiabatic damping predicted by the matrix given in Eq. 4. This is due to a number of advantages, the first being that the beam can be viewed as essentially point-like for the purpose of centroid measurements, as it has a short rms phase extent, $\sigma_\phi \cong 1°$ (as determined by coherent transition radiation[9] measurements), it has a low rms normalized emittance, measured as $\epsilon_n < 10^{-5}$ m-rad, and moderately large charge per bunch, $Q \cong 200$ pC. This charge is large enough to clearly observe the photoelectrons over the dark-current background, yet small enough that collective effects on the centroid motion, such as transverse wake-fields, can be neglected.

The additional advantage this arrangement offers is that the matrix elements to be measured are most strongly dependent on the ratio γ_f/γ_i, and on γ'. The PWT is by nature a high gradient linac ($\gamma' \leq 50$ m^{-1}), with moderate length $L = 42$ cm, and thus to obtain a large value γ_f/γ_i one only need inject with a relatively small initial energy $\gamma_i m_e c^2$. This energy cannot, however, be made arbitrarily small due to the constraint that $\nu_b \cong c$, and a related requirement that the relative energy gain per period of the linac be much smaller than unity, both of which are required in order to guarantee the validity of Eq. 4. Thus the injection energy given by the rf gun (which must in fact produce a relativistic beam due to its extraction dynamics) is nearly ideal for maximizing the matrix elements given in Eq. 4.

In order to determine the transfer matrix of the PWT linac, the centroid of the photo-electron beam is measured using a differential steering technique originally developed to calibrate the beam energy after the gun. For this measurement, the current I of steering (or kicker) magnet K1 is swept while monitoring the centroid position of the electron beam on the downstream phosphor screen P1. The momentum of the beam is determined from the differential change of the centroid position dx_c/dI with current I. The near-axis field $\int B_y(I,z)dz$ of the horizontally-deflecting steering magnets was determined with Hall probe measurements, and the phosphor screens and related video calibrations performed before the experiments.

This method of the momentum determination helps establish the initial conditions of the beam, and also forms the technical basis for the matrix element measurements. As it is difficult to determine the actual electromagnetic center of the linac with respect to the insertable phosphor diagnostics, we were forced to use a differential steering technique. In this case, one of the low energy magnets previous to the linac (K1 or K2) was swept, while observing the centroid motion of the beam downstream of the linac (P2 or P3). The four combinations of the steering magnets and observation points, along with knowledge of the drift lengths, integrated field of the steering magnets, and precise calibration of the video images of the phosphor screens, give four measured quantities which allow reconstruction of the linac transport matrix.

4 RESULTS

In the initial round to experiments, the dependence of the matrix elements on linac injection phase was measured. For each phase, we swept through eight different currents in the steering magnets, and obtained a linear fit to the resulting centroid motion at the phosphor screens. Three noticeable effects were the source of small errors in this method: (1) a large amount of dark current emitted from the gun, (2) transverse centroid injection errors arising from cathode drive laser pointing jitter, and (3) a slow drift in the photocathode drive laser injection phase. This third effect allowed data to be taken over only a limited time span, with all data taken in a single session to ensure the reproducibility of conditions.

The data resulting from these measurements give the calculated values of the centroid sweep rate using the transport derived from the M-matrix and the relevant drift matrices. There is fairly good agreement for all four measurement sets between the predictions and data over all phases where reliable measurements could be made, with a slightly larger sensitivity on phase offsets from the crest displayed by the data. Note that there are larger errors associated with two measurements made at screen P3 for phases of -2.2 and +10 degrees. The P3 data was inherently more difficult to obtain, because the photoelectron beam was much larger in size than at P2, and the two more uncertain points suffered from large interference from the dark current background at their specific running conditions.

The data are inverted to give the elements of the M-matrix, with the results shown in Figs. 1. The relative experimental uncertainty shown by the error bars is larger than for the data sets due to the higher order sensitivity introduced by the inversion process. Also shown in Figs. 1 are the theoretical predictions for the M-matrix. Since the matrix elements were more sensitive to the experimental noise in the data, we also fit the data to a quadratic in ϕ, and then used the resulting filtered data function in the inversion routine to generate a smooth fit in ϕ for the matrix elements. As can be seen, this fit agrees quite well with theoretical predictions.

As a final check on the validity of these data sets, and to independently verify the adiabatic damping component of

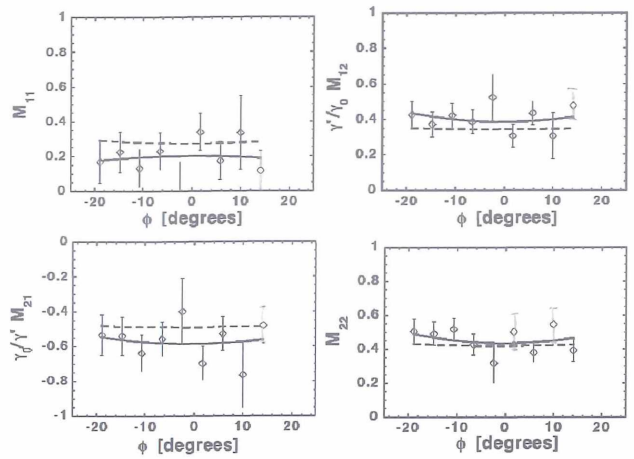

Figure 1: Matrix elements of the transverse trace space map M of the PWT linac as a function of phase ϕ. The values obtained from inverting a quadratic fit to the raw data are drawn by a solid line, the theoretical values by a dashed line. The matrix elements M_{12} and M_{21} are weighted by the factors γ'/γ_0 and γ_0/γ', respectively, to normalize all matrix elements.

the transformation, in Fig. 2 (left) we display the experimentally derived values of det(M), as well as the predicted values, γ_i/γ_f. Because of the form of the algebraic relation between the determinant and the matrix elements, the relative experimental uncertainty in det(M) is no larger than for the elements themselves. We have also plotted the values of det(M) obtained from the quadratic fit to the raw data. Not too surprisingly, this produces agreement with theory as consistent as the agreement found for the matrix elements.

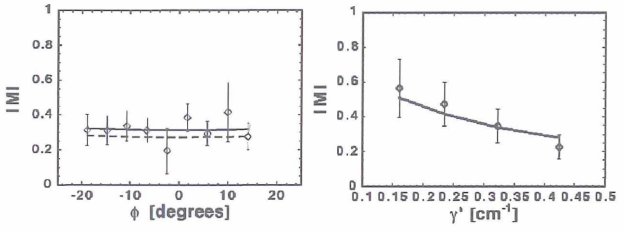

Figure 2: Determinant of the transverse trace space map for different acceleration phases ϕ (left) and gradients γ' (right). The values for the inverted fit to the data for the phase dependency are represented by a solid line, and for the theoretical predictions by a dashed line.

In order to complete a parametric study of the predictions of Eq. 4, and explore the adiabatic damping effects in more detail, we undertook a set of measurements of the matrix elements' dependence on E_0. In this case the rf attenuator was used to lessen the power fed into the linac, yielding, after resetting the phase to optimal acceleration, final beam energies of 7.1, 8.7, 10.6 and 12.8 MeV, or average accelerating fields of E_o =8.3, 12.1, 16.6, and 21.9 MV/m, respectively. This data can then be inverted as before to give the matrix elements. These experimentally derived determinants are plotted in Fig. 2 (right), along with the predicted values of γ_i/γ_f. This plot, which shows the expected behavior quite well is, taken along with Fig. 2 (left), convincing direct evidence for the adiabatic damping of transverse "action", or area, in trace space.

5 CONCLUSION

In conclusion, these sets of measurements have provided a first verification of the theoretical model developed in Refs. 5 and 6 of linear transverse dynamics of electrons undergoing simultaneous strong acceleration as well as first and second order transverse focusing in an rf linac. The matrix treatment of the dynamics predicted by this model has been directly tested, with the experimentally derived matrix elements in fairly close agreement with the model derived elements. The determinants of the matrices obtained in this manner have been shown to display the expected dependence, det(M) = γ_i/γ_f, giving direct evidence for the adiabatic damping of trace space area. Some deviations from theoretically predicted matrix elements themselves were noticeable, however, especially in the data obtained at lower acceleration gradient.

6 ACKNOWLEDGMENTS

This work performed with partial support from U.S. Dept. of Energy grants DE-FG03-90ER40796 and DE-FG03-92ER40693, the Sloan Foundation grant BR-3225 and the Deutscher Akademischer Austauschdienst (German academic exchange program).

7 REFERENCES

[1] K.J. Kim, *Nucl. Instruments and Methods A* **275**, 201 (1989).

[2] TESLA Test Facility Linac Conceptual Design Report, Ed.D. Edwards (DESY, Hamburg, 1995).

[3] E. Chambers, Stanford High Energy Physics Laboratory Report (Stanford, 1965).

[4] R. Helm and R. Miller, in *Linear Accelerators*, Eds. Pierre M. Lapostolle and Albert L. Septier (North-Holland, Amsterdam, 1969).

[5] S.C. Hartman and J.B. Rosenzweig, *Phys. Rev. E* **47**, 2031 (1993).

[6] J.B. Rosenzweig and L. Serafini, *Phys. Rev. E* **49**,1599 (1994).

[7] L. Serafini and J.B. Rosenzweig, TESLA report 96-12 (DESY, Hamburg, 1996), also submitted to *Phys. Rev. E.*

[8] R. Zhang, *et. al., Proc. of the 1995 Part. Accel. Conference*, 1102 (IEEE, 1995); D. Swenson, in *Proc. of the 1988 European Part. Accel. Conf.* p.1418 (World Scientific, 1989).

[9] U. Happek, A.J. Sievers, and E.B. Blum, *Phys. Rev. Lett.* **67**, 2962 (1991).

THE S-BAND LINEAR COLLIDER TEST FACILITY AT DESY

M. Schmitz for the SBLC study group
Deutsches Elektronen Synchrotron (DESY), Notkestraße 85, D-22603 Hamburg, GERMANY

The S-Band Linear Collider Test Facility under construction at DESY serves as a test bed for the essentiell hardware to build a large scale e^+e^- linear collider based on a 3GHz accelerating rf and having a center of mass energy of at least 500GeV. Besides the injection system at the beginning and a beam analysis area at the downstream end, the central part of the test facility consists of two modular units similar to those to be installed in a S-Band Linear Collider (SBLC) tunnel. The key-questions of Higher Order Mode (HOM) excitation, measurement, damping and feedback on the alignment of the accelerating structure as well as the quadrupole position have to be answered in order to manage the most crucial aspect of a 15km linear accelerator, namely the beam stability. The final layout of this test facility and the performance of the present setup including the first accelerating section fed by a 150MW klystron will be presented.

I. INTRODUCTION

Since 1991 a study group investigates the feasibility of a large S-Band Linear Collider (SBLC). Although S-Band accelerators are used in a lot of laboratories, the demands for a SBLC are not simple extrapolation from any existing accelerator. Therefore a R&D program started in 1992 to build up a S-Band Test Facility at DESY, in which the crucial aspects for a SBLC design can be investigated experimentally:

- Design, construction and operation of an injection system that is capable to produce bunchtrains that fulfill the SBLC demands (see section II).
- Development, operation and improvement of a high peak power rf-source, i.e. klystron and modulator as well as other high power components, like rf-windows and loads (see section III).
- Elaboration of a reliable concept to keep the HOM-effects below a tolerable limit determined by emittance growth. In this context measurement and damping of HOM's as well as straightness and alignment of the accelerating structure has to be mentioned (see section IV).
- Development of suppression techniques fighting ground motion and vibration (see section V).

The general layout of this test facility is shown in figure 1 and its main parameters are listed in table 1. Delivered by an injector the beam will be accelerated by 2 modular units similar to those as being proposed for the SBLC. One module consists of 2 travelling wave sections (β=1, $2\pi/3$-mode, 17MV/m) of 6m length each, that are driven by one 150MW/3µs klystron connected to a 375MW peak power modulator. In addition the downstream end of each accelerating section is completed with correctors, one screen and a focussing triplet accomodating a stripline type beam position monitor. Before being dumped at the end of the 40m long test facility the quality of the 400MeV beam will be analyzed using a spectrometer beamline including an OTR screen.

energy at full current	400	MeV
injector energy	≈4	MeV
length of bunchtrain	≥2	µs
number of bunches	1-250	
bunch to bunch separation	8, 16 or 24	ns
particles per bunch	1.5, 3.0 or 4.5	$10^{10}e^-$
current in bunchtrain	≥300	mA
normalized rms-emittance	$\approx 100 \cdot 10^{-6}$	π m rad

Table 1: Main parameters of the S-Band test linac

In the present status the beamline ends downstream of the 1. acc. section behind the focussing triplett. Except for a 4-cell travelling wave structure (TWB1), which is quite important for the process of bunching the injector is completely built up and delivers beam to the first acc. section. Since the first half of this section is surrounded by solenoids, it can not be mounted on the regular girder containing the micro-movers (see section IV). Therefore the concept of beam-based-alignment is not applicable for this section anyhow and thus a 5.2m long section similar to the regular 6m section (see table 3) has been placed there. The additional space will accomodate a kicker by which means the excitation of HOM's can be provoked in the following 3 regular 6m sections. From this point of view the 1.acc. section can also be regarded as belonging to the injection system. Results of the beam operation with this present setup are described in the next section.

II. INJECTOR AND BEAM OPERATION

The injector, combining high bunchcharge with short interbunch spacing, was designed by means of EGUN and PARMELA calculations [1]. The pulses of desired charge in a train of adequate timestructure are generated at a 90kV thermionic gun and compressed by means of two standing wave subharmonic bunchers SHB1 (125MHz/34kV) and SHB2 (500MHz/36kV) as well as two S-Band travelling wave structures TWB1 (β=0.6, 4cells, $2\pi/3$, 7MV/m) and TWB2 (β=0.95, 16cells, $8\pi/9$, 12MV/m). Two 5MW klystrons will be used to supply TWB1 and TWB2 individually. In order to achieve a gradient of 12MV/m at the available power of 5MW while maintaining a large iris aperture, the group velocity of TWB2 is only 0.4%·c. Therefore the $8\pi/9$-mode was

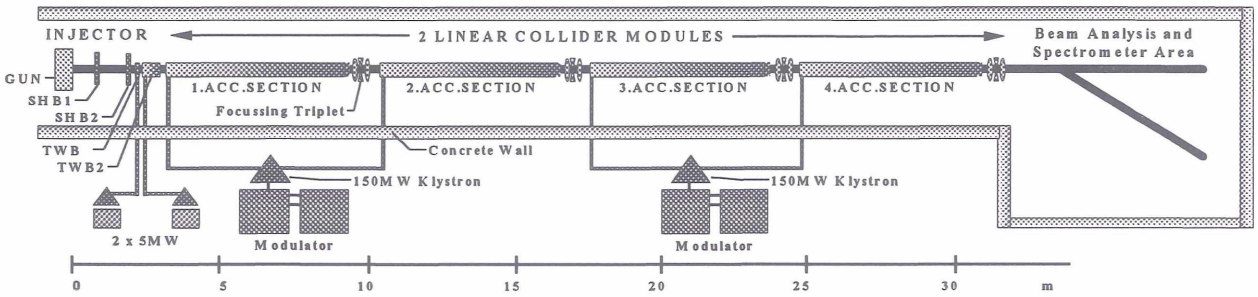

Figure 1: General Layout of the S-Band Test Facility

chosen. Starting with a 90kV gunpulse carrying 12nC ($7.5 \cdot 10^{10} e^-$) in a FWHM-bunchlength of 2.5ns, PARMELA simulation predicts an overall compression to a pulselength shorter than 10ps with more than 95% transmission. Since both TWB's also serve for acceleration the kinetic energy at the output of the injector is expected to be about 4MeV.

Starting in april 1995 with a short beamline dedicated for commissioning of the bunchtrain production at the gun, a longer beamline including both SHB's investigated their bunching performance from autumn 1995 to end of june 1996 [2]. The present setup started its operation in autumn 1996. It includes the first accelerating section and the whole injector complex except for TWB1.

The gun produces 2μs long bunchtrains with 8ns, 16ns or 24ns interbunch spacing. The gunpulses carry at least 7nC ($4.4 \cdot 10^{10} e^-$) in a FWHM length of typically 2.2ns. Their normalized rms-emittance measured 60cm downstream of the gun was $3\pi \cdot$mm·mrad compared to the PARMELA prediction of $6.8\pi \cdot$mm·mrad. From the same simulations 200ps long pulses are expected after compression with both SHB's. Bandwidth limited by the wallcurrent monitor 300ps long signals and a transmission better than 85% were observed. This is valid for every bunch of the train, since a feedforward-system compensates beamloading effects at both SHB's. In the final stage TWB1 sitting at the longitudinal focal point determined by the operation of both SHB's and having a phase velocity of 0.6·c will guarantee a clean capture of these pulses.

However TWB1 is still missing while TWB2 is already at its final position. In order to be captured at TWB2 having a phase velocity of 0.95·c, the 90keV pulses have to be accelerated at SHB2 while SHB1 still operates around zero crossing. From a 6.8nC ($4.25 \cdot 10^{10} e^-$) gunpulse about 5nC ($3.12 \cdot 10^{10} e^-$) can be found downstream of TWB2. In that optimized case SHB2 raises the average beamenergy by 36keV while its amplitude was 52kV which gives a phase of about 50° wrt. the beam. Finally 4.8nC ($3 \cdot 10^{10} e^-$) have been accelerated through the 1. acc. section of 5.2m length. From a 8μm-Al foil mounted ≈1.5m behind this section Optical Transmission Radiation (OTR) has been detected and a profile of the beam can be seen. Measuring the displacement of the beam at the OTR-screen introduced by a correction coil results in a beam momentum of 100MeV/c (±15%), corresponding to an accelerating gradient of 19MV/m. Taking the 5.2m section parameters from table 3 this gradient compares fairly well with the measured input power of 58MW.

Besides the information on the beam profile, the OTR will be used for energy and bunchlength measurement. In the first case its angular distribution has to be analyzed, while in the second case the frequency spectrum of the infra-red part of the coherent OTR needs to be measured. Both experiments just started commissioning their setup.

III. MODULATOR AND KLYSTRON

Since modulators and klystrons contribute significantly to the total cost of a linear collider, as much peak power as possible has to be produced with a single device.

	Design	#1	#2	
beam voltage	535	527	508	kV
μ-perveance	1.79	1.78	1.80	$A/V^{1.5}$
output power	150	153	150	MW
pulse length	3.0	≥ 3.0	≥3.0	μs
efficiency	40	43	45	%
gain	≥50	56	57	dB

Table 2: Parameters of both 150MW klystrons

In 1993 a R&D program together with SLAC, the Technical University of Darmstadt, PHILIPS (Hamburg) and DESY started to construct and operate two 150MW/3μs/50Hz klystrons. Accompanied by 2D and 3D simulations [3] to optimize the overall layout, in 1994 the first and in 1995 the second klystron having a slightly modified output circuit geometry and improved HOM damping in the drift tube was built and tested at SLAC meeting the requirements as can be seen in table 2.

Similar to the one at SLAC to test the 150MW klystron at full power and 60Hz, two PFN-type modulators for the test facility are built at DESY. They consist of 4 lines in parallel resonantly charged up to 50kV within 17ms via a charging choke. A current of 16kA is supplied into the primary of a 1:23 pulse transformer when discharging the PFN by switching two thyratrons. Maximum ratings of the modulator are 535kV and 700A [4].

The first unit of modulator and klystron has been installed in the test facility and was successfully commissioned at 150MW/3μs/50Hz with the same performance as during the SLAC tests (see table 2). The second unit will be commissioned soon.

Since November 1996 one output arm of the 150MW klystron#1 has been connected to the 1. acc. section while the other still works on a load. Presently, after about 400h of beam operation and conditioning, the section can be operated with an 1.5μs long rf-pulse of 60MW (i.e. 120MW of klystron power) at 25Hz repetition.

IV. ACC. SECTION AND HOM-HANDLING

The accelerating section is of constant gradient type operating in $2\pi/3$-mode, with a continuous taper of the group velocity along its whole length of 6m. HOM handling to avoid emittance dilution due to single- and multibunch instabilities together with simple construction techniques to reduce the costs for mass production are the main topics to be investigated. The HOM handling concept requires HOM-damping, adequate section detuning as well as a certain straightness and alignment of the section. Assuming an average Q-value of the HOM's of 4000 (natural ≈13000) and the SBLC bunchcharge of 1.8nC (6ns interbunch spacing) the total accuracy of alignment and straightness of the 6m section has to be ≤50μm rms. In that case beam dynamics calculations predict an emittance growth of about 20% for a 15km long linac.

Since there are a lot of trapped modes in long travelling wave structures, external dampers would have to be coupled to the section at many positions, which is neither reasonable nor cost saving. Instead of that internal damping by sputtering a thin (20μm) steel layer onto the iris showed a Q-reduction of the HOM by a factor of 5, while the fundamental Q changes only by 5%. This layer withstood an iris tip field of 28MV/m in a high power standing wave test resonator without any degradation.

Nevertheless one or two cells will be equipped with HOM couplers to measure the beam induced power which is correlated to the average excentricity of the beam axis wrt. the section. This signal has to be minimized (beam based alignment) when driving the micro-movers that are mounted below the section girder. The girder as shown in figure 2 must not deteriorate the straightness of the section, mounted on top of it, even with temperature transient around it. Therefore it is constructed from a tube (448mm dia.) that is totally thermal insulated. The movers, one on each end of the girder can operate between ±1.5mm with a step size of 150nm (see figure 2).

In the process of replacing old sections of the LINAC II (the e^+e^- injector linac at DESY) 5.2m long sections having comparable parameters (see table 3) were built at DESY. While the straightness tolerance is easily met after the vertical inductive brazing of typically 1m long

	Linac II	SBLC	
length of section	5.2	6	m
attenuation	0.5-0.6	0.55	neper
group velocity	3.3-1.2	4.1-1.3	%·c
filling time	750	790	nsec

Table 3: Parameters of the accelerating sections for LINAC II and SBLC

pieces, which have a measured rms deviation of typically 20μm, the horizontal braze of the complete 5.2m section has shown deviations of up to 1mm. They have been decreased down to 100μm rms by a recently developed straightening procedure, and will achieve the target value of 30μm after commissioning of an improved straightening device constructed for this reason.

Up to now five 5.2m sections have been assembled, tuned and high power tested at DESY. One of them is installed in the test facility as 1. acc. section and 3 are operating in the LINAC II continuously without difficulties.

Other major technical developments being made so far are a very compact symmetric high power input coupler [5] and the collinear load [6]. The collinear load absorbs the remaining rf-power over the last eight cells of the section while still accelerating the beam. Such a load avoids a second high power coupler (costs), represents no obstacle for the inductive brazing coil, is perfectly symmetric (no transverse kicks due to field asymmetries) and absorbs any higher order mode touching the end of the section.

The first 6m section equipped with symetric high power couplers, iris coating, internal load and 2 HOM couplers (one at the front end and one almost at 2/3 of the section length) will be installed on the regular girder in the test linac end of May this year.

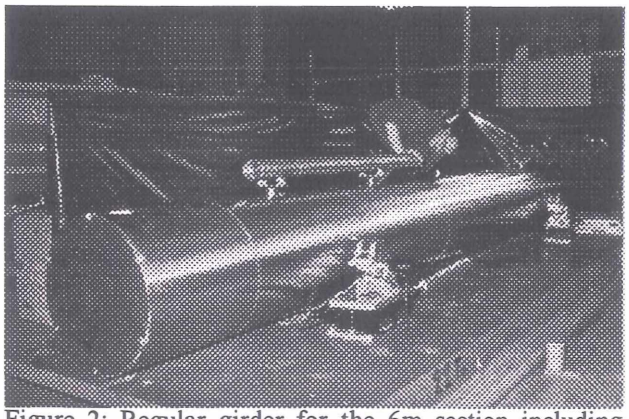

Figure 2: Regular girder for the 6m section including micro movers (short piece of structure on top to demonstrate the full assembly)

V. GROUND MOTION AND VIBRATION

Any kind of quadrupole motion within the frequency range of 2-30 Hz can hardly be damped either in a passive manner or with beam based feedback techniques. Therefore ground motion detectors (geophones and accelerometers) have been tested and further developed [7]. Each quadrupole in the test facility will be equipped with such a detector to feed back on the vertical quadrupole position via piezo movers. Attenuation of amplitudes up to 14dB within this frequency range has been achieved and corrects the vertical rms quadrupole motion down to the 20 nm range.

In addition a simple and stiff concrete support with mechanical resonances well beyond 100 Hz has been built for the quadrupole to avoid any externally driven excitation. To decouple the vibration introduced by water flow within the coil windings of the quadrupole, the coils are mounted on a separate aluminium support within the quadrupole yoke. This support can be mounted separately to the floor.

VI. ACKNOWLEDGEMENT

I would like to thank all the members of the collaboration from the different institutes and countries for their contributions. The significant progress which has been made during the last 5 years is based on the enthusiasm of the people involved and the willingness of the management to encourage this work.

VII. REFERENCES

[1] M. Schmitz, A.D. Yeremian, "The Injector for the S-Band Test Linac at DESY", Proc. of the 1994 International Linac Conference, Tsukuba, Japan, 21-26 August 1994

[2] M. Schmitz, "Performance of the first Part of the Injector for the S-Band Test Facility at DESY", Proc. of the 1996 International Linac Conference, Geneva, Switzerland, 26-30 August 1996

[3] M. Dohlus et al, "Comparison of CONDOR, FCI and MAFIA Calculations for a 150 MW S-Band Klystron with Measurements", Proc. of the 1995 P.A.C., Dallas, Texas, 1-5 May 1995

[4] S. Choroba et al., "A 375MW Modulator for a 150MW Klystron at the S-Band Linar Collider Test Facility at DESY", Proc. of the 1996 International Linac Conference, Geneva, Switzerland, 26-30 August 1996

[5] V.E. Kaljuzhny et al, "Design and Performance of a Symmetric High Power Coupler..", DESY-M-94-11, 1994, Internal Report

[6] J. Haimson, "Collinear Termination for High-Energy Particle Linear Accelerators", PATENT-US-3264515, Aug 1966. 7pp.

[7] C. Montag, "An active mechanical Stabilization System for Linear Collider Quadrupoles to compensate fast Ground Motion", Proc. of the 1996 International Linac Conference, Geneva, Switzerland, 26-30 August 1996

HERA Status and Upgrade Plans

F. Willeke, Deutsches Elektronen-Synchrotron, Notkestr.85, 22603 Hamburg, Germany

Abstract

The HERA electron-proton collider at Hamburg Germany, designed for collisions of $820 GeV$ protons with $30 GeV$ electrons is now in its 6th year of operation. It delivers luminosity for the colliding beam detectors H1 and ZEUS and longitudinally polarized positrons for the internal target experiment HERMES. HERA is operated close to the design luminosity with peak values of $1.2 \times 10^{31} cm^{-2} sec{-}1$. While the beam currents still fall short of expectations, the luminosity was increased by focusing the beams very tightly at the interaction points at the expense of using up most of the margins on aperture, chromaticity and beam-beam tuneshift. In 1996, an integrated luminosity of $\int \mathcal{L} dt = 17.2 pb^{-1}$ has been delivered. Despite the strong beam-beam interactions, the degree of longitudinal polarization of the positron beam is, with $(50 - 60)\%$, larger than expected.

Despite the good results of HERA, more luminosity is needed for the physics program in the next decade. Preparations are underway to increase the luminosity by rebuilding the low-β insertions. With unconventional new types of magnets, it seems to be possible to increase the luminosity substantially. The expected value is $\mathcal{L}_{peak} = 7.5 \cdot 10^{31} cm^{-2} sec^{-1}$ which is five times larger than the design value.

1 INTRODUCTION

The HERA collider [1] for $820 GeV$ protons (p-beam) and $30 GeV$ electrons or positrons (e-beam) in Hamburg is the only high-energy accelerator in which two completely different species of particles are brought into collision. The double ring collider has a length of $6.3 km$. The proton ring has a superconducting magnet structure with $4.6 T$ magnets. The electron ring has conventional magnets but needs, besides 84 room temperature rf cavities, a superconducting cavity system to reach at the current top-energy of $27.5 GeV$. HERA has two interaction regions for the colliding beam experiments H1 and ZEUS. In addition it hosts two fixed target experiments, the gas target experiment HERMES which needs a longitudinally polarized electron or positron beam and the new HERA-B experiment which is going to analyze the interactions of halo protons with a wire target.

The collider has been providing luminosity for more than five years now. It is operated close to the design values for luminosity and spin polarization. The recent incorporation of the HERA-B target operation in HERA operations was a success. At this point four different experiments with very different demands on the accelerator performance are running simultaneously without much detrimental interference.

The results from the HERA experiments open up a rich future physics programme. It is therefore highly desirable to produce luminosity in excess of what the present design can deliver. Therefore, plans are underway to rebuild the collider interaction regions (IR) to allow stronger focusing of both beams.

2 HERA LUMINOSITY OPERATION

HERA luminosity operation has made steady progress. The machine is now operated close to design conditions. Since 1994 HERA has been operated with $27.5 GeV$ positrons which collide with $820 GeV$ protons. At this point the peak luminosity is $1.2 \cdot 10^{31} cm^{-2} sec^{-1}$, the number of protons per bunch is up to $6 \cdot 10^{10}$, the total beam current of the positrons reaches values of up to $44 mA$. The normalized emittance of the p-beam is in the order of $4 \mu m$ in collisions. The beam-beam tune shift of the positrons of $\Delta \nu_{ye} \simeq 0.03$ exceeds already the design value by a factor of 1.5. While the beam currents quoted above are still below expectations, the matched beam cross section at the interaction point is reduced by more than a factor compared to the design value. Thus high luminosity in HERA is achieved by cutting into the margins of aperture, chromaticity of the protons and of beam-beam tune-shift of the leptons.

Great progress has been made in the last two years on overall reliability. In 1997, HERA is delivering luminosity to the experiments for nearly 50% of the scheduled time. The minimum time needed to re-inject, to accelerate and to tune the two beams amounts to about 20% of the scheduled time. The remaining 30% are still needed at this point for optimizations or recovery from failures. The recent progress is the result of preventive maintenance on the more than thousand magnet power supplies [3] and regular reconditioning of the superconducting rf cavities. Furthermore a large effort is underway to store accelerator data in circular buffers to ease trouble shooting on the numerous components[2].

In 1996, HERA delivered an integrated luminosity of $17.2 pb^{-1}$ to the colliding beam experiments H1 and ZEUS. At present, luminosity is produced at a monthly rate of $4.5 pb^{-1}$. The continuous improvement of HERA operations is reflected in figure 2 which shows the integrated luminosity versus the running time for the years 1992-1997.

Since 1995, the HERMES experiment investigates the reactions of high energy longitudinally spin-polarized

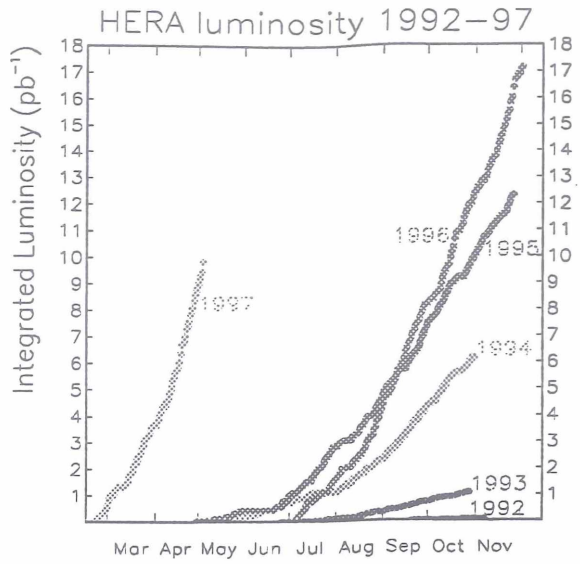

Figure 1: Accumulation of HERA Luminosities 1992-1997

positrons with a polarized gas target. HERA has a pair of spin rotator magnets installed around the experiment, which rotate the vertically oriented spin into the longitudinal direction and back into the vertical direction. The polarization is usually between 50% and 60% in routine operation. Peak values of up to 70% have been observed. The polarization is remarkably stable. Major tuning with harmonic orbit bumps [7] is performed only once or twice per year. High polarization can then be maintained by occasional orbit corrections. There is some indication, that high polarization is more difficult to obtain with strong beam-beam interactions. In 1996, there was some correlation was observed between beam-beam tune-shift of the positron beam and spin polarization. The tuneshift reached values of $\Delta\nu = 0.035$ and sometimes the polarization approached a level of 50% only after many hours of slow growth (The polarization time in HERA at $27.5GeV$ is less than 37 minutes). More careful control of the tunes inside a very narrow window reduced this problem. Recently the vertical β function of the positron beam has been reduced at the interaction point (IP). Since then no correlation between proton beam intensity and positron spin polarization has been observed.

3 HERA ELECTRON OPERATION

A very unpleasant surprise was that the lifetime of intense electron beams in HERA is not determined by bremsstrahlung at desorbed gas molecules as expected but by effects which have been explained by dust trapped inside the beam. The present understanding is that dust particles are emitted from the chamber of the integrated ion getter pumps by an unknown mechanism. This effect makes the operation with electrons virtually impossible. Since 1994 HERA has been operated with positrons and there are no anomalies in the beam lifetime. The dust or microparticles hypothesis has been supported by many experiments [5, 4, 6]. All efforts to overcome this problem have failed so far. It has been attempted to lower the voltage of the integrated pumps. This was not successful. Turning off the pumps completely seems to suppress the effect. This leads however to unsatisfactory lifetime due to increased pressure of desorbed gas. It has been attempted to drive out trapped particles by kicking the beam. This provides relief only for a period of several minutes. Then the lifetime breaks down again. BPM monitors have been used as clearing electrodes. But this did not solve the problem. The last attempt to resolve the problem, without major changes in the pumping system, was to equip all integrated pumps with pre-resistors of $5M\Omega$. This did not improve the situation.

In the winter shutdown period 1995-1996, an $\simeq 120m$ long section of HERA has been equipped with passive non-evaporating getter pumps (NEG [8]). These pumps have been operated without any problems in the 1996 and 1997 luminosity operation. Pumping speed and required generation are within expectations. Experiments with electron beams indicate, that in this vacuum section, the local beam losses due to bremsstrahlung events have been drastically reduced after the NEG pumps have been installed. Electron beam experiments with all getter pumps turned off have been performed in December 1996. They seem also to indicate that the lifetime degradation is removed if there are no getter pumps present and electrons behave the same as positrons. Therefore, the pumping system in the HERA e-ring is planned to be replaced by NEG pumps in the winter shut-down 1997/1998.

4 HERA LUMINOSITY LIMITATIONS

The Luminosity of HERA is best written as

$$\mathcal{L} = \frac{N_p I_e}{4\pi e \sigma_x \sigma_y} \qquad (1)$$

(N_p is the number of protons per bunch, I_e is the total beam current of the lepton beam, e is the elementary charge, $\sigma_{x,y}$ are the rms beam sizes of the p-beam or e-beam with $\sigma^p_{x,y} = \sigma^e_{xy}$).

With a bunch spacing of $96ns$ HERA luminosity is limited by the total lepton beam current and the beam current is limited by the available rf power. At present, the rf power is sufficient to store $45mA$ reliably at $27.5GeV$, the lowest possible energy which allows longitudinal spin polarization. An eighth rf station is under construction to raise this limit above $50mA$. The total available rf power will be $12MW$ which will allow the design beam current of $58mA$ to be stored at $27.5GeV$.

The bunch intensity of the protons is limited by space charge effects at injection into the booster. The incoherent space charge tuneshift at 50MeV injection into the synchrotron DESYIII is $\Delta Q_{incoh} = 0.4$ (see also [10]), which corresponds to about $1.2 \cdot 10^{11}$ protons per bunch at extraction into the PETRA injector ring. Tight aperture in the